Studies of potential applications of peptide ligands for the parathyroid hormone/parathyroid hormone-related protein type 1 receptor for therapeutic options of bone and calcium metabolic diseases

I 型副甲状腺ホルモン受容体に対するペプチドリガンドの

骨とカルシウム代謝疾患への適用可能性に関する研究

Hiroshi Noda

Contents

Abbreviation used in this thesis

$1,25(OH)_2D_3$	1α,25-dihydroxyvitamin D_3
AAALAC	Association for Assessment and Accreditation of Laboratory Animal Care
Aib	α-aminoisobutyric acid
AUC	Area under the curve
B.Ar	Bone area
B.Pm	Bone perimeter
BFR	Bone formation rate
BID	Twice daily
BMD	Bone mineral density
BS	Bone surface
BV	Bone volume
C1HR	Collagen1a1-PTHR1-H223R
Ca	Calcium
cAMP	3',5'-cyclic adenosine monophosphate
CKD	Chronic kidney disease
cryo-EM	Cryogenic electron microscopy
CTX1	C-terminal telopeptides of type I collagen
DMP1	Dentin matrix protein 1
EC_{50}	Median effective concentration
ECD	Extracellular domain
ELISA	Enzyme-Linked Immunosorbent Assay
E_{max}	Equal maximum effects
ERK1/2	Extracellular signal-regulated kinase 1/2
Fb.Ar.	Fibrosis area
FGF23	Fibroblast growth factor 23
GPCR	G protein-coupled receptor
Har	Homoarginine
i.v.	Intravenous
IC_{50}	Median inhibitory concentration
iCa^{2+}	Ionized Ca
Ihh	Indian hedgehog
JMC	Jansen's metaphyseal chondrodysplasia
LA-PTH	Long-acting PTH
Ma.BA	Medullary bone area

Ma.TA	Medullary total area
MAR	Mineral apposition rate
M-PTH	Modified PTH
MSC	Mesenchymal stem cells
N.D.	Not detected
N.Ob	Number of osteoblast
N.Oc	Number of osteoclasts
N.Ot	Number of osteocytes
Nle	Norleucine
Ob.Pm	Osteoblast perimeter
Oc.Pm	Osteoclast perimeter
OPG	Osteoprotegerin
Pi	Phosphate
PKA	Protein kinase A
PKC	Protein kinase C
PLC	Phospholipase C
PTH	Parathyroid hormone
PTHR1	PTH/PTHrP type 1 receptor
PTHrP	Parathyroid hormone-related protein
QOL	Quality of life
RANKL	Receptor activator of nuclear factor-κB ligand
Runx2	Runt-related gene 2
s.c.	Subcutaneous
sCa	Serum Ca
SD	Standard deviation
SEM	Standard error of the mean
sPi	Serum Pi
T.Ar	Tissue area
TMD	Transmembrane helical domain
TPTX	Thyroparathyroidectomized
TRAP	Tartrate-resistant acid phosphatase
TV	Total volume
uCa	Urinary Ca
uCre	Urinary creatinine
uDpD	Urinary deoxypyridinoline
uPi	Urinary Pi

Veh	Vehicle
WT	Wild-type
μCT	Microcomputed tomography

Preface

Parathyroid hormone/parathyroid hormone-related protein receptor (PTH/PTHrP type 1 receptor; commonly known as PTHR1) is a family B G protein-coupled receptor (GPCR) that binds two distinct polypeptide ligands (Alexander et al., 2013), parathyroid hormone (PTH) and parathyroid hormone-related protein (PTHrP), and thereby plays two distinct and critical biological roles: the maintenance of calcium (Ca) and phosphate (Pi) homeostasis and the control of bone and tissue development (Potts, 2005). These functional roles place the PTHR1 in a position of prominence for a number of high-impact diseases, including osteoporosis, hypoparathyroidism and Jansen's metaphyseal chondrodysplasia (JMC), and also as a key drug-discovery target.

PTH is a peptide hormone composed of 84 amino acids secreted by the parathyroid gland. The molecular weight is about 9400 daltons (Brewer and Ronan, 1970; Niall et al., 1970). The amino acid sequence of PTH in different species has been identified and especially its N-terminal portion shows high homology between species (Gensure et al., 2004; Guerreiro et al., 2007; Papasani et al., 2004; Power et al., 2000; Trivett et al., 2005). The N-terminal fragment of PTH, PTH (1–34), is known as potent as the intact native hormone, PTH(1–84), for binding to the receptor and inducing biologic responses *in vitro* and *in vivo* (Potts et al., 1971).

The physiological role of the parathyroid grands in Ca regulation was first established by James Bertram Collip in a definitive series of experiments (Collip, 1925). PTH plays a key role in maintaining the levels of Ca in the blood and extracellular fluids. The hormone is secreted from the parathyroid gland with sensing the blood Ca levels falling down, and then acts on the bone and kidney to mobilize Ca into the blood (Brown et al., 1983; Shoback et al., 1983). In the bone, PTH acts on

osteoblasts to produce the receptor activator of nuclear factor-κB ligand (RANKL), which acts on osteoclasts to stimulate their bone resorption activity (Boyce et al., 2012; Saini et al., 2013; Silva et al., 2011). In the kidney, PTH acts on cells of the distal tubules to increase their reabsorption of Ca (de Groot et al., 2009; van Abel et al., 2005). PTH also acts on cells of renal proximal tubule to decrease their reabsorption inorganic Pi, resulting in lower blood Pi levels (Biber et al., 2009; Miyamoto et al., 2004; Nagai et al., 2011; Picard et al., 2010). PTH also activates the mitochondrial 25-hydroxyvitamin D_3-1-α-hydroxylase in renal proximal tubule cells; this leads to transform vitamin D_3 to active form, which, in turn, is a potent inducer of intestinal Ca and Pi absorption (Martin et al., 2008; Miao et al., 2004). Regarding the regulation of Pi metabolism by PTH, PTH promotes the production of fibroblast growth factor 23 (FGF23) in osteocytes which are differentiated from osteoblast lineage cells and embedded into bone matrix (Rhee et al., 2011). FGF23 is mainly produced by osteocytes and acts on the kidney as a hormone to decrease serum Pi (Shimada et al., 2001). FGF23 suppresses Pi reabsorption in the renal proximal tubule and decreases serum 1α,25-dihydroxyvitamin D_3 [$1,25(OH)_2D_3$] resulting in suppression of intestinal Pi absorption (Shimada et al., 2004). On the other hand, $1,25(OH)_2D_3$ upregulates FGF23 production in osteocytes (Saito et al., 2005). FGF23 also suppresses the production and secretion of PTH in the parathyroid glands (Ben-Dov et al., 2007). In this way, PTH, $1,25(OH)_2D_3$, and FGF23 coordinately regulate Pi metabolism. In patients with chronic kidney disease (CKD), it has been reported that serum FGF23 levels increase prior to PTH elevation during early stages of CKD (Isakova et al., 2011). Abnormally high serum FGF23 levels in late stage of CKD appear to exert unwarranted off-target effects, including left ventricular hypertrophy (Gutierrez et al., 2009), faster CKD progression, and premature mortality (Nasrallah et al., 2010). Based on these current insights regarding FG23 in CKD, a concept has been proposed in which kidney-specific PTH action in the early stage of CKD could lower serum FGF23 levels through lowering serum Pi resulting in improvement of the prognosis of patients with CKD (Juppner, 2011).

In regulation of bone metabolism, bone remodeling occurs through life after growing phase; that is osteoclasts derived from hematopoietic stem cell precursors resorb the bone and then osteoblasts derived from the differentiation of mesenchymal stem cells (MSC) form the new bone to renew the organ resulting in maintaining the bone structure strength. Runt-related gene 2 (Runx2) of transcription factors, known as a master regulator, expresses from early differentiation stage such as osteoprogenitor cells, followed by osterix and alkaline phosphatase from pre-osteoblasts (Komori, 2006). In osteoblasts, which are more differentiated, abundant bone matrix proteins such as type I collagen are expressed early in the differentiation stage of osteoblasts and osteocalcin are expressed in mature stage (Aubin, 2001). Pre-osteoblasts are proliferative cells but does not synthesize bone matrix actively, and mature osteoblasts are known as cells that synthesize a large amount of bone matrix (Franceschi et al., 2007). A fraction of osteoblasts become lining cells that are resting on the surface of bone (Khosla et al., 2008), and then as osteoblast differentiation progresses further, they are embedded into the bone matrix and differentiate into osteocytes that extend dendrites toward the osteoblast layer and form a network between osteocytes. Dentin matrix protein 1 (DMP1) is expressed in osteocytes (Aubin, 2001).

The PTHR1 is expressed in MSC linage such as osteoblasts and osteocytes but not in osteoclasts (Amizuka et al., 1996; Divieti et al., 2001; Ishizuya et al., 1997). Mechanisms of bone anabolic action induced by intermittent PTH treatment via the MSC lineage cells expressing the PTHR1 include 1) accelerating differentiation of osteoprogenitor cells or pre-osteoblasts into osteoblasts, 2) to enhancing production of bone matrix such as type-1 collagen in mature osteoblast, 3) activating resting osteoblasts which are bone lining cells, and 4) inhibiting mature osteoblast apoptosis (Jilka, 2007). More, it has also been reported that PTH activates osteocytes which act on osteoblasts on the bone surface through osteocyte networks embedded in bone matrix (Silva et al., 2011).

PTH thus plays a role in the bone-remodeling process that goes on continuously and involves coordinated actions of osteoblasts and osteoclasts (Baron and Hesse, 2012). Outcomes *in vivo* for PTH-based ligands are generally well known to vary widely, depending on the temporal profile of ligand action/exposure; hence the dogma: continuous PTH results in net bone catabolism with potentially adverse hypercalcemia, while pulsatile PTH results in net bone anabolism (McCauley and Martin, 2012). It has recently been reported that the Wnt signaling is related to the bone anabolic action of PTH (Krishnan et al., 2006; Kulkarni et al., 2005). PTH(1–34) treatment reduces the expression level of sclerostin, a Wnt signaling inhibitory protein, in the bone, and consequently activates the Wnt signaling in the bone (Bellido et al., 2005; Keller and Kneissel, 2005). Sclerostin is known as a matrix protein specifically expressed in the bone. The effect of PTH(1–34) on the bone is reduced in mice osteocyte-specific overexpressing sclerostin and is abolished in sclerostin knockout mice (Kramer et al., 2010). These results indicate that inhibition of the expression of sclerostin might be one of the components of the bone anabolic effect of PTH, although there is a limitation that excess bone volume in sclerostin knockout mice would mask the bone anabolic effect of PTH.

It is well known that PTH stimulates the bone catabolism as well as the bone anabolism, and that the injection of PTH by the continuous infusion shows the lowering of the bone mineral density (BMD) (Martin et al., 2008). Renal osteodystrophy, especially accompanied with secondary hyperparathyroidism associated with chronic renal failure, is a typical disease demonstrating the relationship between a persistent PTH stimulation and bone effects (Fraser, 2009). In an experiment to compare the effects of intermittent and sustained injection of PTH (1–34) on the bone in rats, the BMD increased by daily intermittent injections or up to 2 hours per day infusion for 4 weeks, while the efficacy on the bone was not observed by continuous infusion for 4 hours per day with a sustained increase in bone resorption-related factors such as RANKL as well as bone formation (Shimizu et al., 2016b). Continuous PTH-administration induces RANKL by acting on osteoblasts expressing PTHR1

and indirectly induces osteoclast-mediated bone catabolic action resulting in releasing Ca and Pi.

Based on these characteristics of PTH actions, therefore, PTH drug with the pulsate pharmacokinetics is desirable for the osteoporosis in which the increase of BMD is required, while the continuous type of PTH drug is expected for the hypoparathyroidism in which the stable calcemic action is required.

PTHrP, which in total is 141 amino acids in length, was identified as the cause of hypercalcemia of malignancy (Suva et al., 1987) and has been known to act as an agonist for PTHR1 at the N-terminal 36 amino acids of PTHrP (Nissenson et al., 1988). Consistent with a key role in the receptor activation (Horwitz et al., 2003; Juppner et al., 1991), the N-terminal portion of PTHrP exhibits the highest homology with PTH, because 8 of the first 13 amino acids are identical. PTHrP is secreted locally from various organs, including cartilages and smooth muscles, breast, hair follicles, and placentae, and is known to act in local autocrine and/or paracrine regulation (Strewler, 2000). In the growth plate, PTHrP is synthesized and secreted by perichondrial cells and chondrocytes at the ends of the growing bones. As chondrocytes go through a program of proliferation and then further differentiation into hypertrophic chondrocytes in the process of the skeletal development, PTHrP acts to delay the endochondral ossification; that is, PTHrP has a role to keep chondrocytes proliferating and delays their further differentiation with suppressing chondrocyte hypertrophy. Indian hedgehog (Ihh) is synthesized by chondrocytes that have just stopped proliferating and is required for synthesis of PTHrP. The feedback loop between PTHrP and Ihh serves to regulate the pace of chondrocyte differentiation resulting in normal bone development (Kronenberg, 2006). The importance of many of these actions of PTHrP has been established by a series of the phenotype analyses in mice missing the *PTHrP* gene (Karaplis et al., 1994), the *PTH/PTHrP* receptor gene (Lanske et al., 1996), and the *PTH* gene (Miao et al., 2002), and also in chondrocyte-specific PTHrP-transgenic mice (Weir et al., 1996).

Blocking the activity of excess circulating PTH or PTHrP at PTHR1 should ameliorate the pathological consequences of hyperparathyroidism and humoral hypercalcemia of malignancy. Based on this objective, N-terminal truncated PTH/PTHrP ligands which bind to the PTHR1 as an antagonist with competitive antagonism against PTH(1–34) *in vitro* and *in vivo* were identified (Goltzman et al., 1975; Horiuchi et al., 1983; Rosenblatt et al., 1977). As a result, further modification of the PTH(7–34) scaffold produced more potent antagonists including an analog of dTrp^{12}-PTH(7–34) (Chorev et al., 1990; Dresner-Pollak et al., 1996). However, clinical trials in patients with hypercalcemia due to primary hyperparathyroidism provided a complete failed results for such a dTrp^{12}-PTH(7–34) analog (Rosen et al., 1997). Although reasons for why the antagonist failed in patients is unclear, the concentration of the peptide in blood would not probably have reached to sufficient levels to block agonistic signaling stimulated by excessive endogenous PTH(1–84).

PTHR1 is shared and activated by both PTH and PTHrP via a two-site mechanism (Bergwitz et al., 1996). This mechanism involves an initial binding of the C-terminal portion of the PTH(1–34) fragment, PTH(15–34), to the N-terminal extracellular domain (ECD) portion of the receptor and a subsequent engagement of the N-terminal portion of the ligand (Lee et al., 1994), PTH(1–14), with the extracellular loop and seven-transmembrane helical domain (TMD) region of the receptor, that leads to receptor activation (Caulfield et al., 1990; Luck et al., 1999). The recent high-resolution X-ray crystal and cryogenic electron microscopy (cryo-EM) structures of the PTHR1, each in complex with a PTH(1–34) or PTHrP(1–36) analog ligand, confirm and extend this model of ligand binding (Ehrenmann et al., 2018; Zhao et al., 2019). These structures thus show the peptide to be bound as a linear α-helix with its C-terminal portion docked to the ECD and its N-terminal portion projecting into the core of the TMD bundle. This binding mode is similar to that seen in the high-resolution structures

reported for several other family B GPCRs (Sutkeviciute and Vilardaga, 2020), including the receptors for glucagon, GLP-1, and calcitonin, in each complex with a bound peptide ligand, thus supporting a common basic mechanism of ligand-induced activation is useful for each of the family B GPCR.

PTH (1–14), an N-terminal fragment of PTH, or its analogs, has been reported to exhibit 3',5'-cyclic adenosine monophosphate (cAMP) and phospholipase C (PLC)-activity (Luck et al., 1999). It has also been reported that the most active [$Aib^{1,3}$,A^{12},Q^{10},Har^{11},W^{14}]-PTH(1–14) in this PTH(1–14) analog, modified "M"-PTH(1–14) (Shimizu et al., 2000a; Shimizu et al., 2001a; Shimizu et al., 2000b; Shimizu et al., 2001b), can be used to characterize ligands such as small-molecule compounds that specifically bind to TMD region of the PTHR1 as a tracer (Carter et al., 2015; Tamura et al., 2016). As a downstream signal of PTHR1, $G\alpha_s$ which activates cAMP/protein kinase A (PKA) and $G\alpha_q$ which activates PLC/protein kinase C (PKC) are known to be coupled in the cells of the target organ (Abou-Samra et al., 1992; Huang et al., 1996; Iida-Klein et al., 1997). In addition, extracellular signal-regulated kinase 1/2 (ERK1/2) signals via $G\alpha_{12/13}$/RhoA/ phospholipase D (Singh et al., 2005) and β-arrestin have also been reported (Gesty-Palmer et al., 2006; Syme et al., 2005). There are seven Ser phosphorylation sites in the intracellular C-terminal sites of PTHR1 that are phosphorylated through stimulation by the agonist (Malecz et al., 1998; Qian et al., 1998). The modified serine residues promote recruitment of β-arrestin, which destabilize the interactions with G proteins, induce the dissociation of agonist, and initiate internalization of the receptor from cell surface (Tawfeek et al., 2002; Vilardaga et al., 2002). It has, therefore, been recognized that this receptor internalization process correlates temporally with the termination of G-protein signaling in a classical model for the GPCRs based on the research in other GPCRs, such as β2 adrenoreceptor (Luttrell and Lefkowitz, 2002).

Consistent with current GPCR theory, the PTHR1 is thought to cause a variety of receptor

conformational changes by a certain ligand analog which bound and may stabilize each conformation. Classical GPCR theory holds that G protein docking shifts the receptor into a high-affinity conformation for agonist binding-the R^G state (De Lean et al., 1980). For the PTHR1, this R^G state is bound by all potent peptide agonists but is particularly crucial to the binding of certain ligands such as PTHrP(1–36) (Dean et al., 2008), M-PTH(1–14) and abaloparatide, which exhibit only weak affinity for G protein-uncoupled PTHR1 conformations (Hattersley et al., 2016; Okazaki et al., 2008). Other ligands, however, such as PTH(1–34), can bind with high affinity to such uncoupled receptors, and thus define a novel and distinct high affinity conformation, called R^0. This R^0 appears a G protein independent state as the binding is observed in the presence of excessive GTPγS which displaces $G\alpha_s$ protein (Dean et al., 2008). The mechanistic basis by which a given G protein – $G\alpha_s$, $G\alpha_q$, etc. – reciprocally modulates the extracellular orthosteric ligand-binding pocket is not well understood, but is likely of biological and medical relevance, given the potential impact on ligand/drug affinity. In general, the duration of the cAMP responses observed in the cell-based studies correlate with the different affinities that PTH(1–34) and PTHrP(1–36) exhibit for the R^0 state, rather than with their affinities for the R^G state, as assessed in membrane assays. PTH(1–34) forms more stable complexes with PTHR1 at the R^0 state than PTHrP(1–36) and accompanies with a prolonged cAMP signaling (Dean et al., 2008). The correlation between PTHR1 R^0 affinity and the duration of intracellular cAMP responses observed for PTH and PTHrP analogs led to the hypothesis that PTHR1 ligands with improved R^0 affinity might stimulate an even longer cAMP response than PTH(1–34). A number of such ligands were identified in a series of PTH analogs containing A number of such ligands were identified in a series of PTH analogs containing "M" substitutions which are known to enhance the affinity with the receptor. (Shimizu et al., 2000a; Shimizu et al., 2001a; Shimizu et al., 2000b; Shimizu et al., 2001b). Interestingly, these analogs induced markedly prolonged calcemic and hypophosphatemic responses not accompanied by altered pharmacokinetics in mice (Okazaki et al.,

2008). In contrast to acting effectively on osteoporosis by a short-acting PTHrP analog (abaloparatide) that selectively binds to the R^G state of PTHR1, to pursue a ligand with high affinity on the R^0 state of PTHR1 may therefore generate a long-acting PTH (LA-PTH) analog, whose prolonged calcemic and hypophosphatemic action would effectively work as a novel treatment option for hypoparathyroidism.

Novel mode of prolonged cAMP signaling by R^0 selective ligands for the PTHR1 has recently been established with endosomal signaling after internalization of the complex of ligands bound to the receptor (Feinstein et al., 2011; Ferrandon et al., 2009; Wehbi et al., 2013). As mentioned before, it has been widely recognized that the cAMP signaling is mediated by the cell surface GPCR and its termination is regulated by internalization of the receptor from cell surface. Recent a series of studies reveal that GPCRs do not always follow this conventional paradigm; that is, some of GPCRs including PTHR1 mediate cAMP signaling not only from the cell surface but also from endosome after internalization (Calebiro et al., 2009; Feinstein et al., 2013; Nguyen et al., 2019; Thomsen et al., 2016). For the PTHR1, it was first pointed out that R^0 selective ligand with prolonged signaling clearly does induce internalization of PTHR1 accompanying with the ligand in the report of efficacy of M-PTH *in vitro* and *in vivo* (Okazaki et al., 2008). Further experiments revealed that the prolonged cAMP signaling in the PTHR1 mediated by R^0 selective ligands requires the internalization occurred subsequent to recruitment of β-arrestin (Ferrandon et al., 2009).

Gain-of-function activating mutations have been identified in patients with JMC (Schipani et al., 1996). All of identified point mutations occur at one of three residue positions in PTHR1, each of which is located at the cytosolic base of a TMD helix: His223 in TM helix 2 (TM2), Thr410 in TM6, and Ile458 in TM7 (Calvi and Schipani, 2000). The residues at these positions are highly conserved in the family B GPCRs (Cordomi et al., 2015). Despite different shapes and sizes of the TM pockets and the different peptide sequences, it is recently reported that family B GPCRs share a common

mechanism of ligand-mediated receptor activation through key conserved residues that stabilize the sharp kink at the middle of TM6 based on the cryo-EM structure analysis (Zhao et al., 2019). The PTHR1 mutations of JMC can thus be predicted to perturb a critical component of the receptor located in the lower portion of the TMD bundle that controls receptor activation and deactivation.

Inverse agonists were first discovered in β-carbolines acting on the GABA/benzodiazepine receptors and have been reported for a number of GPCR (Braestrup et al., 1982). Such kind of ligands are classified as a subclass of antagonists that can bind to an active-state receptor and revert it to an inactive conformation (Bond et al., 1995). PTH analogs deleted of residues 1–6 from the PTH(1–34) scaffold represent no longer activate signaling via the cAMP–PKA pathway, but instead, function as competitive antagonists for the PTHR1 (Goltzman et al., 1975; Horiuchi et al., 1983; Rosenblatt et al., 1977). In the process of screening of PTH(7–34) scaffold, the substitution of Gly to dTrp at the position of 12 was identified as a key residue for an inverse agonist (Gardella et al., 1996). Further modification of the inverse agonist, a number of PTH and PTHrP analogs including [Leu^{11},$dTrp^{12}$,Trp^{23},Tyr^{36}]-PTHrP(7–34)NH_2, was produced (Carter et al., 2001).

Osteoporosis is a metabolic disease characterized by reduced bone strength resulting in fractures (Unnanuntana et al., 2010; Vestergaard et al., 2007). Primary osteoporosis is subclassified into postmenopausal osteoporosis, male osteoporosis, and idiopathic osteoporosis. Especially, there are many patients with postmenopausal osteoporosis, and it is estimated that worldwide 1 in 3 women and 1 in 5 men aged 50 years or older will experience osteoporosis fractures in the rest of their lives (Curtis et al., 2016; Kanis et al., 2000; Oden et al., 2015). The prevalence of osteoporosis has risen substantially due to the global aging of the population and changes in lifestyle habits and that is expected to continue in the future (Gullberg et al., 1997; Reginster and Burlet, 2006). The goal of

osteoporosis treatment is the prevention of fragility fractures and changes in BMD have been used as surrogate markers for osteoporosis treatment (Reid, 2020).

As an osteoporosis drug, anti-bone resorption agents have been widely used for long time. Although anti-bone resorptive agents has contributed to the prevention of fragility fracture of osteoporosis, bone anabolic agents that actively can enhance bone formation have been needed to prevent fractures in patients with severe osteoporosis with immediately (Estell and Rosen, 2021).

PTH has been reported to reduce bone mass when it acts continuously, while increasing bone mass when it is administered intermittently. PTH (1–34) has been approved in the United States as the first bone anabolic agent in 2002 and is now widely used in the world(Estell and Rosen, 2021). PTH has side effects characterized by hypercalcemia and hypercalciuria caused by the action as the Ca regulation hormone, by which the upper limit dose of PTH in osteoporosis treatment is restricted. PTH also has both bone anabolic and bone resorptive effects. The time between the major gains in bone formation and the subsequent increase in bone resorption markers can be described as the "anabolic window" (Rubin and Bilezikian, 2003). In an attempt to broaden "therapeutic window" between such bone anabolic effect and calcemic effect or "anabolic window" between bone anabolic and bone resorptive effects, abaloparatide which is a PTHrP analog peptide that selectively binds to the R^G state of the PTHR1, an active conformation accompanied with $G\alpha_s$ protein, has been developed (Compston et al., 2019). In a 18-month phase 3 clinical trial of postmenopausal osteoporosis patients, abaloparatide was significantly superior than PTH(1–34) in increasing BMD of the lumber spine (Miller et al., 2019).

Another bone anabolic agent was an anti-sclerostin antibody and recently approved in various countries as an osteoporosis drug (Mullard, 2019). Sclerostin is a Wnt-signal inhibitory protein which is expressed in mainly bone tissue. Unlike PTH, the anti-sclerostin antibody promotes bone formation without increasing bone resorption. It exhibits increasing BMD and prevention of fractures

effect based on the obvious bone formation promotion action in only 1 year (Saag et al., 2017).

Thus, bone anabolic agents have been developed in recent years, and multiple therapeutic options have begun to be provided for the patients with osteoporosis. On the other hand, both PTH and anti-sclerostin antibody are injectable agents, and considering that osteoporosis is required life-long treatment, orally available bone anabolic agents would be needed for osteoporosis treatment in the future. There are still no orally available bone anabolic agents that can be used clinically. Although an orally available small-molecule PTHR1 agonist has been reported recently (Nishimura et al., 2020; Tamura et al., 2016), its application in osteoporosis has challenges because of their relatively persistent pharmacokinetics. The further drug discovery researches that also incorporate signal biases, such as R^G state selective ligands, is required for the generation of oral therapeutics targeting PTHR1.

One of the PTH-related disease is hypoparathyroidism that presents with hypocalcemia due to insufficient secretion of endogenous PTH (Bilezikian et al., 2011; Shoback, 2008). Hypocalcemia leads to neuromuscular irritability which can manifest sensory neuron irritability with as paraesthesia in the extremities and in the peri-oral and oral area and motor neuron irritability accompanying with as muscle spasms, tetany, or life-threatening laryngospasm in some cases (Mannstadt et al., 2017). The most common cause of hypoparathyroidism is surgical destruction or injury to the parathyroid grands after the surgery of thyroid cancer and non-cancerous thyroid hypertrophy; other causes are autoimmune diseases or genetic disorders affecting secretion of endogenous PTH, function of PTH, or parathyroid gland development (Bilezikian et al., 2011). It has been reported that population prevalence of hypoparathyroidism is estimated at approximately 60,000 adults total in the United States. In the analysis of a large US health plan over a 12-month survey from 2007 to 2008, approximately 7.6% of patients undergoing neck surgery, such as thyroid cancer, were diagnosed with hypoparathyroidism, and approximately 25% of these were diagnosed with chronic

hypoparathyroidism (Powers et al., 2013).

In the conventional therapy of patients with hypoparathyroidism, high doses of oral Ca supplementation or/and activated vitamin D preparation (400-1000 IU) are given to the patients (Shoback, 2008). Although the conventional therapy with Ca supplementation or/and activated vitamin D preparation can correct the hypocalcemia, it does not restore other actions of PTH which acts as a key regulator tightly controlling Ca metabolism in the body. Correction of hypocalcemia by the therapy is accompanied by an increase of urinary excretion of Ca. It is reported that long-term treatment with the conventional therapy is associated with long-term complications, such as nephrocalcinosis and renal stones resulting in impaired renal function and reductions in the quality of life (QOL) of patients with hypoparathyroidism (Leidig-Bruckner et al., 2016; Mitchell et al., 2012; Weber et al., 1988). To establish a more natural alternative therapeutic option, PTH replacement therapy has been being investigated. Recently, a large clinical trial by using the full-length PTH, PTH(1-84), was conducted. The add-on therapy of once-daily subcutaneous injection of PTH(1–84) with conventional therapy for 24-weeks achieved the primary endpoint maintaining blood Ca above the lower limit of normal (1.87 mM) and reducing doses of Ca supplementation and active vitamin D preparations by more than 50% (Mannstadt et al., 2013), and has been approve in the United States and the European Union as the first hormone replacement therapy for hypoparathyroidism. However, PTH(1–84) did not reduce urinary Ca excretions versus Placebo group. In addition, hypercalcemia and hypocalcemia occurred more frequently in PTH(1–84) group than in placebo group due to the short pharmacokinetics.

Novel treatment options that can stably normalize blood Ca levels without causing hypercalciuria by sustained replacement of the missing hormone is therefore needed for the patients with hypoparathyroidism (Mannstadt et al., 2017; Marcucci et al., 2017).

As PTHR1 related disease, JMC has been first reported in 1934 (Jansen, 1934). It is an ultra-rare autosomal-dominant disease caused by heterozygous gain-of-function mutations in the PTHR1 (Bastepe et al., 2004; Schipani et al., 1999; Schipani et al., 1996). The patients with JMC exhibit marked defects in bone development and bone turnover that result in short stature, limb deformities, mobility impairment. Radiological analysis has shown severe metaphyseal changes, especially of long bone. The metaphyses are enlarged and expanded with a wide zone of irregular calcifications (Silverthorn et al., 1987). JMC also represents biological changes which are hypercalcemia, renal Pi wasting, and increased urinary cAMP excretion even though the blood concentrations of PTH are not low or undetectable and concentrations of PTHrP are not elevated (Kruse and Schutz, 1993; Saito et al., 2018).

Treatment options for JMC are currently very limited and only a few reports in the literature discuss treatment options for patients with JMC. The patients have multiple corrective bone surgeries through their growth and are given with drug medicines, hydrocortisone, calcitonin and bisphosphonate, aiming to ameliorate nephrocalcinosis and/or nephrolithiasis to spare renal function (Parfitt et al., 1996; Schipani et al., 1999). Although the long-term treatment with an anti-bone resorptive agent such as bisphosphonate and the subsequent addition of a thiazide diuretic showed clear clinical outcome to normalize blood Ca levels and to markedly reduce urine Ca excretion (Onuchic et al., 2012), no specific treatment to cure whole clinical features for the patients with JMC is currently available (Nampoothiri et al., 2016). The impact of the disease on patient QOL and the associated long-term health care burden emphasizes the importance to develop an effective therapeutic option for JMC.

Three peptide agonists, PTH(1–34), PTH(1–84) and abaloparatide which is a PTHrP analog, for this GPCR are used for treatment of patients with osteoporosis and hypoparathyroidism (Compston

et al., 2019; Gafni and Collins, 2019). Emerging structure analysis of related family B GPCRs provide clues as to how ligands bind to the receptor and induce activation (Ehrenmann et al., 2018; Liang et al., 2018; Zhang et al., 2017a; Zhang et al., 2018; Zhang et al., 2017b; Zhao et al., 2019). Yet substantial gaps remain in knowledges of how the peptide ligands is to be improved for treatment of each PTH-related diseases, because it is not known well how each ligand controls signaling responses in bone- and kidney-targeted cells. It is also the barrier for the substantial clinical translational research that all clinical available ligands for the PTHR1 has a general property in peptides that is short pharmacokinetics. Seeking therapeutic potential with various peptide ligands for the PTHR1 would promote a better understanding of diseases of bone and/or mineral ion metabolism and would reveal the opportunities for peptide ligands for the receptor to be used as clinical drugs. Here, the author sought to examine the proof-of-concept of an inverse agonist ligand for JMC in chapter I and report the process of the peptide modification to pursue a ligand of LA-PTH providing a potential application of the novel agonist for hypoparathyroidism in chapter II.

Chapter I

An inverse agonist ligand of the PTH receptor partially rescues skeletal defects in a mouse model of Jansen's metaphyseal chondrodysplasia.

Introduction

JMC (Jansen, 1934) is a rare disorder of autosomal-dominant disease caused by heterozygous, activating PTHR1 mutations (Schipani et al., 1995). Five different PTHR1 mutations affecting one of three different amino acid residues have been identified in patients with JMC; these mutations, H223R, T410P/R, and I458K/R, are each located at the intracellular end of transmembrane helices, namely TM-2, -6, and -7, respectively (Calvi and Schipani, 2000). Clinical hallmarks of the disease include short stature, deformed, undermineralized bones, chronic hypercalcemia and hyperphosphaturia with normal serum PTH levels, and elevated serum markers of bone turnover (Jansen, 1934; Saito et al., 2018; Schipani et al., 1996). Disease features become apparent within days or months after birth and progress with age. The overall disease profile is consistent with the critical roles that the PTHR1 plays in endochondral bone formation, and in Ca and Pi homeostasis; processes that are normally controlled by the two endogenous peptide ligands, PTH and PTHrP, respectively. Because JMC is an ultra-rare disease, with only about 30 cases identified since its first description in 1934, it has garnered little if any interest from the pharmaceutical industry in terms of therapeutic development. There is thus currently no effective treatment option available for the patients with JMC.

An inverse agonist that targets the constitutively active mutant PTH receptors of JMC could, in theory, be used to treat this disease. A number of competitive antagonist ligands for the PTHR1 developed from N-terminally truncated PTH and PTHrP analogs containing the dTrp (W)[12]

substitution, have been shown to function as inverse agonists *in vitro* and can thus suppress the basal rates of cAMP signaling in transfected COS-7 or HEK293 cells expressing a mutant PTHR1 variant of JMC . In addition to key inverse agonism substitution ($dTrp^{12}$), other substitutions were introduced that enhanced the binding affinity to the receptor resulting in that [Leu^{11},$dTrp^{12}$,Trp^{23},Tyr^{36}]-PTHrP(7–34)NH_2 was generated as the most effective inverse agonist for JMC mutants (Carter et al., 2001; Gardella et al., 1996; Saito et al., 2018). These *in vitro* findings led the author to examine whether such an inverse agonist could correct the bone growth/remodeling defects seen in JMC phenotypes. To obtain the proof-of-concept of an inverse agonist using a mouse model of JMC at first, the author thus assessed the capacity of [Leu^{11},$dTrp^{12}$,Trp^{23},Tyr^{36}]-PTHrP(7–34)NH_2 which acts as a potent inverse agonist *in vitro*, whether it would rescue the skeletal abnormalities that occur in transgenic mice expressing the PTHR1-H223R allele of JMC in osteoblasts under the control of *Collagen 1a1* promoter. Since type 1 collagen is gradually expressed from pre-osteoblasts and is most abundant in osteoblasts but not in osteocytes, the action of excessive PTHR1 signal due to the constitutively active mutation mainly induces differentiation from pre-osteoblasts to mature osteoblasts, increased bone matrix production in osteoblasts, and increased number of osteoblasts by suppression of apoptosis. This mutant transgenic mice also exhibit the induction of excessive bone resorption through the activity of the osteoblast lineage. As a result of these action, the mice exhibit a marked skeletal phenotype characterized principally by cortical bone thinning and excess cancellous bone mineral density in the marrow compartments. On the other hand, since the action of this mutation is limited to pre-osteoblasts and osteoblasts, Ca action and hypophosphatemic actions linked with PTH-like action in the kidney (promotion of Ca reabsorption, Pi excretion, and active vitamin D production) are not observed (Calvi et al., 2001).

Material and Methods

Peptides, cells and reagents. The peptides [Leu^{11},dTrp^{12},Trp^{23},Tyr^{36}]-hPTHrP(7–36)NH_2 (Carter et al., 2001) and [dTrp^{12},Nle^{8,18},Tyr^{34}]-bPTH(7–34)NH_2 (Goldman et al., 1988) and hPTH(1–34)NH_2 [PTH(1–34)] were synthesized by the Massachusetts General Hospital Biopolymer Core facility. Peptides were HPLC-purified and confirmed by mass spectroscopy. GHR-10 cells (Carter et al., 2015) are derived from HEK293 cells by stable transfection to express the luciferase-based pGlosensor-22F (GloSensor®; Promega, San Luis Obispo, CA, USA) cAMP reporter and the PTHR1-H223R mutant allele of JMC.

Functional assessment of inverse agonism in cultured cells. GHR-10 cells were seeded into white, clear-bottomed 96-well plates and used for assay 24 to 48 hours after the cell monolayers became confluent. For assay, the cells were preloaded with luciferin for 20 min at room temperature in CO_2-independent media (ThermoFisher Scientific, Waltham, MA, USA) and then treated with ligand at varying concentrations in media or media alone and luminescence was measured at 2-min intervals using a PerkinElmer Envision plate reader. For dose-response curves, the area-under-the-curve (AUC) of the time course-luminescence response at each ligand concentration was expressed as a percent of the response observed in the absence of ligand and plotted versus ligand concentration. Data from three independent experiments with duplicate wells in each were combined as means ± SD.

Mouse breeding and maintenance. Collagen1a1-PTHR1-H223R transgenic (C1HR) mice (Calvi et al., 2001) in strain FVB were maintained by mating heterozygous C1HR males to wild-type FVB females (Charles River Laboratories, Worcester, MA, USA; cat #207FVB). Genotypes were determined by PCR of genomic DNA obtained from tail tissue using

5′-GAGTCTACATGTCTAGGGTCTA-3′ and 5′-TAGTTGGCCCACGTCCTGT-3′ as forward and reverse primers, respectively. The mice were housed in facilities operated by the Center for Comparative Medicine of the Massachusetts General Hospital, and all experimental procedures were approved (protocol #: 2017N000162) by the Massachusetts General Hospital Institutional Animal Care and Use Committee and in compliance with federal, state, and local animal care rules and guidelines. C1HR mice and wild-type littermates were maintained on normal chow with a soft diet supplement (DietGel 76A plus DietGel Boost; Clear H_2O, Portland, ME, USA), which was provided due to the oversized incisors in the C1HR mice. Heterozygous C1HR mice and wild-type littermate controls were assigned randomly to treatment groups. Power calculations predicted that the number of animals used per study group would be sufficient to detect statistically significant differences in intended primary experimental outcomes (i.e., changes in bone structural and cellular parameters, blood and urine markers, and mRNA levels) (Calvi et al., 2001; Ohishi et al., 2009).

Peptide preparation and injection. A stock solution of [Leu^{11},$dTrp^{12}$,Trp^{23},Tyr^{36}]-PTHrP(7–36)NH_2 was prepared in 10 mM acetic acid at a peptide concentration of 2.0 mM. For injection, the stock solution was diluted in vehicle (150 mM NaCl, 10 mM citrate, 0.05% Tween80, pH 5.0) to a peptide concentration of 200 μM. Mice were injected twice daily (BID) subcutaneously into the interscapular area with each injection at a peptide dose of 500 nmol (1.9 mg)/kg body weight. The injection volume was 2.5 mL/kg, corresponding to 10 to 26 μL per mouse, depending on body weight, which, at age 24 days, was 12.9 ± 1.3 g (n = 17) and 6.8 ± 0.8 g (n = 19; mean ± SD) for wild-type and C1HR mice, respectively. The peptide injection dose was selected to be as high as practical given limits of peptide solubility (~7.0 mg/mL), the expected rapid rate of clearance of the peptide from the circulation (Rosen et al., 1997), a rapid rate of dissociation from the receptor (Carter et al., 2001), and the goal of achieving as close to maximum occupancy of the mutant receptor as possible. In prior studies, we

found that injection of PTH(1–34) at a dose of 50 nmol/kg into wild-type mice was sufficient to induce a frank hypercalcemic response (Maeda et al., 2013), indicating effective ligand occupancy of the PTHR1 in target tissue. The author thus predicted at least some occupancy of the mutant PTHR1-H223R would be achieved by the current inverse agonist peptide when injected at a 10-fold higher dose than used in the prior study for PTH(1–34). Control animals were injected with vehicle at the same injection volume (2.5 mL/kg). Mice were injected for 17 days at approximately 12-hour intervals beginning at 7 days of age. At 12 hours after the last injection, the mice were euthanized by exsanguination from the abdominal aorta under isoflurane-anesthesia, and tissue samples were dissected for analysis.

To double-label the bone surfaces for dynamic histomorphometric analyses, the mice were injected intraperitoneally with calcein (20 mg/kg) and then demeclocycline (40 mg/kg) at 48 and 24 hours prior to euthanasia, respectively. The two fluorochromes are incorporated at the site of active mineralization of hydroxyapatite on the bone due to their high affinity for Ca resulting in forming two separate fluorochrome bands on the bone surface with bone formation. The double-label technique is allowing bone morphometric measurements such as detecting a bone formation surface and calculating a bone formation speed by measuring a distance between two separate bands. The 24-hour labeling interval was selected based on the expected high rate of bone formation and turnover in the C1HR mice (Calvi et al., 2001), and although the interval was too short to give consistent dual bands of labels in the wild-type mice, it did yield adequate dual fluorescent labels in the C1HR mice.

Blood biochemistry. Blood was collected via the abdominal aorta under isoflurane-anesthesia prior to euthanasia by exsanguination. Plasma total Ca was determined using a Calcium LiquiColor Test kit (Stanbio Laboratory, Boerne, TX). Plasma Pi was determined using a Phosphate Colorimetric Assay Kit (BioVision, Inc, San Francisco, CA, USA). Plasma C-terminal telopeptides of type I collagen

(CTX1) was determined using the RatLaps EIA kit (Immunodiagnostic Systems Inc., Fountain Hills, AZ, USA). During a process of bone resorption, several fragments including CTX1 are released as a result of degradation of type I collagen by osteoclasts. CTX1 is thus recognized as a bone resorptive marker (Rosen et al., 2000).

Histology. Tibias were harvested, fixed with 10% formalin overnight and then washed in PBS and transferred to 70% ethanol. The fixed nondecalcified tibias were dehydrated (graded ethanol) and subsequently infiltrated and embedded in methylmethacrylate. Longitudinal sections (5 μm) were cut and stained with Goldner's Trichrome for measurements of cellular parameters, and by the method of von Kossa (Liu et al., 2016) to evaluate bone mineralization. Goldner's Trichrome is a stain able to differentiate mineralized and non-mineralized parts of the sample at same time that highlights the cellular components, due to use of ferric hematoxylin. Only "active" osteoblasts (square shape in contact with the bone) were considered following the guidelines (Dempster et al., 2013). The habitual osteoclast appearances were first grossly confirmed using tartrate-resistant acid phosphatase (TRAP) staining for specific detection of osteoclasts and then only the osteoclasts on the top of bone resorptive surface or on non-mineralized tissue were considered. Myelofibrotic cells is recognized by the characteristic bone marrow cellular shape and localization in relation to the trabecular bone. The fibrosis area was analyzed by measuring the area where the myelofibrotic cells with evident nuclear shape existed.

Dynamic bone parameters were evaluated on unstained sections by measuring the extent, the volume and the distance between double labels in relation to the rest of the tissue based on the measured area using the OsteoMeasure analyzing system (Osteometrics Inc., Decatur, GA, USA). The structural, dynamic, and cellular parameters were evaluated using standardized guidelines (Dempster et al., 2013).

Micro–computed tomography. Microcomputed tomography (μCT) analysis was performed on dissected bones using a desktop microtomographic imaging system (μCT 40; Scanco Medical AG, Brüttisellen, Switzerland). Samples were scanned with a 10-μm isotropic voxel size, 70-kV peak potential (kVp), 114-μA X-ray tube intensity, and 300-ms integration time. Intramedullary bone volume (BV) and total volume (TV) were assessed in the distal femoral metaphysis in a region beginning at the peak of the growth plate and extending proximally for 1.0 mm (100 transverse slices) as well as in a region of the proximal tibial metaphysis beginning 0.1 mm inferior to the growth plate and extending distally for 1.0 mm (100 transverse slices). The density of all pixels within the each same region (the distal femoral metaphysis and proximal tibial metaphysis) were assessed as BMD. At the femoral mid-shaft, analysis was performed on a 0.5-mm-long region (50 transverse slices) to measure medullary total area (Ma.TA) and medullary bone area (Ma.BA); the Ma.BA was normalized to the Ma.TA at each slice, and the mean value reported as the medullary bone area fraction (Ma.BA/TA).

Quantitative real-time (RT) PCR of bone cell mRNAs. Total RNA was prepared from femoral diaphyses with epiphyses and perichondrium removed and the marrow left unflushed. The bones were homogenized in TRIzol (Thermo Fisher Scientific, Waltham, MA, USA) using a Dremel Tissue Tearor homogenizer (Dremel, Racine, WI, USA), and total RNA was extracted by phase separation with chloroform followed by precipitation in isopropanol and then purified using an RNeasy Mini kit (Qiagen, Hilden, Germany). The total RNA was then reversed-transcribed using TaqMan® Reverse Transcription Reagents and the cDNA was processed using a TaqMan® quantitative RT-PCR system (TaqMan® Gene Expression Assays). For each gene, the measured mRNA level in each sample was normalized to the level of 18S rRNA in that sample and then expressed relative to the normalized level of that mRNA observed in the samples from vehicle-treated wild-type mice. The TaqMan® probes

used are shown in Table 1.

Data analysis. Data were processed using Microsoft Excel-2016 (Redmond, WA, USA) and GraphPad Prism 8.2 (La Jolla, CA, USA) software packages. Statistical analyses were performed (Prism) using a one-way ANOVA with Tukey's post hoc comparisons of means when ANOVA was significant. Values of $p < 0.05$ indicate significance.

Table 1. TaqMan® PCR probes (Thermo Fisher Scientific)

FAM-MGB™ probes			
Gene symbol	**Gene name**	**Protein symbol**	**Assay ID #**
Tnfsf11	*Tumor necrosis factor ligand superfamily, member 11*	**RANKL**	Mm00441906_m1
Tnfrsf11b	*Osteoprotegerin*	**OPG**	Mm00435454_m1
Acp5	*Acid phosphatase 5, tartrate resistant*	**TRAP-5b**	Mm00475698_m1
Sost	*Sclerostin*	**SOST**	Mm00470479_m1
Col1a1	*Collagen, type I, alpha 1*	**Col1a1**	Mm00801666_g1

VICR/TAMRA™ probe		
Gene symbol	**Description**	**Catalog #**
18S	Eukaryotic 18S rRNA Endogenous Control	4310893E

Results

Inverse agonist properties *in vitro*. The primary structure of [Leu^{11},dTrp^{12},Trp^{23},Tyr^{36}]-PTHrP(7–36)NH_2 (Carter et al., 2015; Carter et al., 2001), and its mode of action on the PTHR1-H223R mutant of JMC are depicted in Fig. 1 A. In functional studies *in vitro*, the basal cAMP signaling in HEK293 cells stably transfected to express PTHR1-H223R is higher than in the cells stably transfected to express wild-type of PTHR1 (Carter et al., 2015; Carter et al., 2001). [Leu^{11},dTrp^{12},Trp^{23},Tyr^{36}]-PTHrP(7–36)NH_2 was more effective as an inverse agonist than the PTH-based analog, [Nle^{8,18},dTrp^{12},Tyr^{34}]-bPTH(7–34)NH_2 (Goldman et al., 1988; Rosen et al., 1997), because it more effectively reduced the high basal cAMP signaling in HEK293 cells expressing PTHR1-H223R (Fig. 1 B,C). Based on these and prior cell-based studies (Carter et al., 2015; Carter et al., 2001), [Leu^{11},dTrp^{12},Trp^{23},Tyr^{36}]-PTHrP(7–36)NH_2 was selected for the studies *in vivo* described in the following sections.

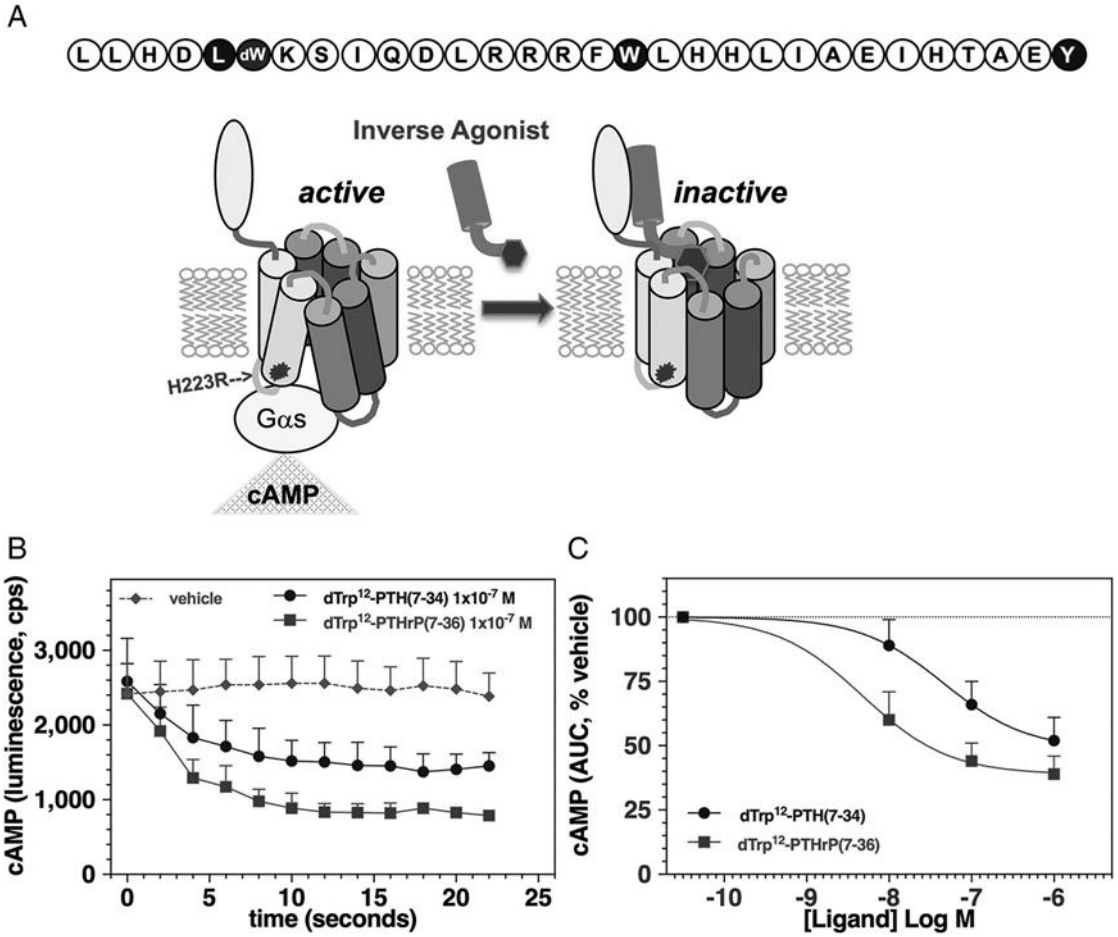

Figure 1. Properties of the inverse agonist ligand. (A) The primary structure of the inverse agonist analog used for *in vivo* studies, [Leu^{11},dTrp^{12},Trp^{23},Tyr^{36}]-PTHrP(7–36)NH_2 (Carter et al., 2001), with residues not native to human PTHrP shown in black circles, and a model of inverse agonism. The H223R mutation of JMC is located at the base of TM helix 2 and induces an active-state receptor conformation that mediates ligand-independent $G\alpha_s$ coupling and cAMP signaling; binding of the inverse agonist reverts the receptor to an inactive conformation and decreases basal signaling. (B) Inverse agonist responses in HEK293 cells stably expressing PTHR1-H223R and the GloSensor cAMP reporter (GHR-10 cells); the cells were treated with [Leu^{11},dTrp^{12},Trp^{23},Tyr^{36}]-PTHrP(7–36)NH_2 (dTrp^{12}-PTHrP (7–36)) or the PTH-based antagonist/inverse agonist, [dTrp^{12},Nle^{8,18},Tyr^{34}]-bPTH(7–34)NH_2 (Goldman et al., 1988) (dTrp^{12}-PTH(7–34)), each at 100 nM, or with vehicle, and cAMP-dependent GloSensor luminescence was recorded at 2-min intervals for 22 min. (C) Dose-response curves generated from the area-under-the-curve of time-course data obtained as in B at varying concentrations of ligand. Data are means ± SD of three experiments, each in duplicate.

Properties of Col1-PTHR-H223R mice and peptide dose selection. Col1-H223R transgenic mice (referred to as C1HR mice herein) express the PTHR1-H223R variant under the control of the collagen1a1 promoter, which is active predominantly in osteoblasts (Calvi et al., 2001). Compared to wild-type mice, C1HR mice exhibit a pronounced accumulation of trabecular bone in the marrow compartments of the long bones, a thinning of the bone cortices, an accumulation of fibrotic stromal cells in the marrow spaces between bone trabeculae, and high rates of bone turnover (Calvi et al., 2001; Ohishi et al., 2009; Ohishi et al., 2012). In a pilot study, the author found that once-daily injection of [Leu^{11},$dTrp^{12}$,Trp^{23},Tyr^{36}]-PTHrP(7–36)NH_2, henceforth referred to as inverse agonist, into the C1HR mice for 2 weeks at a daily dose of 500 nmol/kg did not result in any noticeable change in the bone phenotype, as assessed histologically at the proximal tibias. For the current experiment, the author sought to increase ligand exposure and thus injected the mice BID with the inverse agonist at a dose of 500 nmol/kg/injection. The injections were started on postnatal day 7 and continued every 12 hours for 17 days. As controls, C1HR littermate mice were injected with vehicle, and wild-type littermates were injected with either vehicle or inverse agonist. The C1HR mice were small, with body weights that were about 60% less than that of their wild-type littermates, as reported (Calvi et al., 2001). For either the wild-type or C1HR mice, no change in mean body weight occurred with inverse agonist treatment, as compared to with vehicle treatment (Fig. 2), and the overall health appearance of the mice did not change over the 17-day treatment period. Twelve hours after the last injection, the mice were euthanized and bones as well as blood and urine samples were collected for analysis.

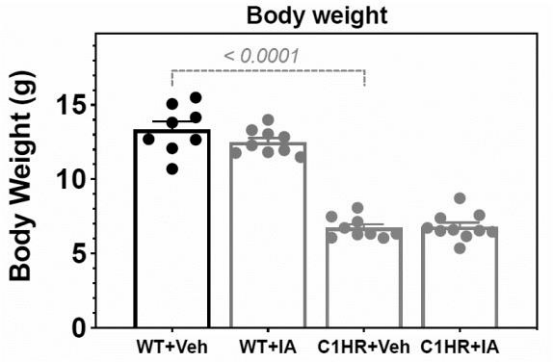

Figure 2. Body weights. Body weights at the study end-point of wild-type (WT) or Col1-PTHR1-H223R (C1HR) mice injected twice-daily with either vehicle (veh) or inverse agonist (IA) for 17 days. Data are means ± SD; *p* value derived by ANOVA with Tukey's ad hoc comparison.

Inverse agonist treatment reduces bone mass and increases bone length in C1HR mice. μCT was used to assess the effects of inverse agonist treatment on bone mineral density and bone structure in the C1HR mice. μCT scans of the femurs and tibias isolated from the vehicle-treated C1HR mice revealed the expected marked increases in trabecular bone in the metaphyseal regions of the distal femur and proximal tibia, as well as in the medullary region of the femur mid-shaft, as compared to the corresponding regions of the bones isolated from vehicle-treated wild-type mice (Figs. 3 A,B, 4 and 5). Quantification of bone volume fraction (BV/TV, %) and bone mineral density (mg hydroxyapatite/cm^3) in the metaphyseal regions of the distal femurs and proximal tibias, and of cross-sectional bone area at the femoral mid-shaft confirmed this increase in bone in the vehicle-treated C1HR mice relative to the vehicle-treated wild-type mice (Fig. 3 C). Significantly less bone was measured in these compartments of the femurs and tibias obtained from C1HR mice treated with inverse agonist, as compared to the bones from vehicle-treated C1HR mice (Figs. 3, 4 and 5). No change in these structural parameters was observed in the bones obtained from wild-type mice treated with inverse agonist, as compared to those obtained from wild-type mice treated with vehicle.

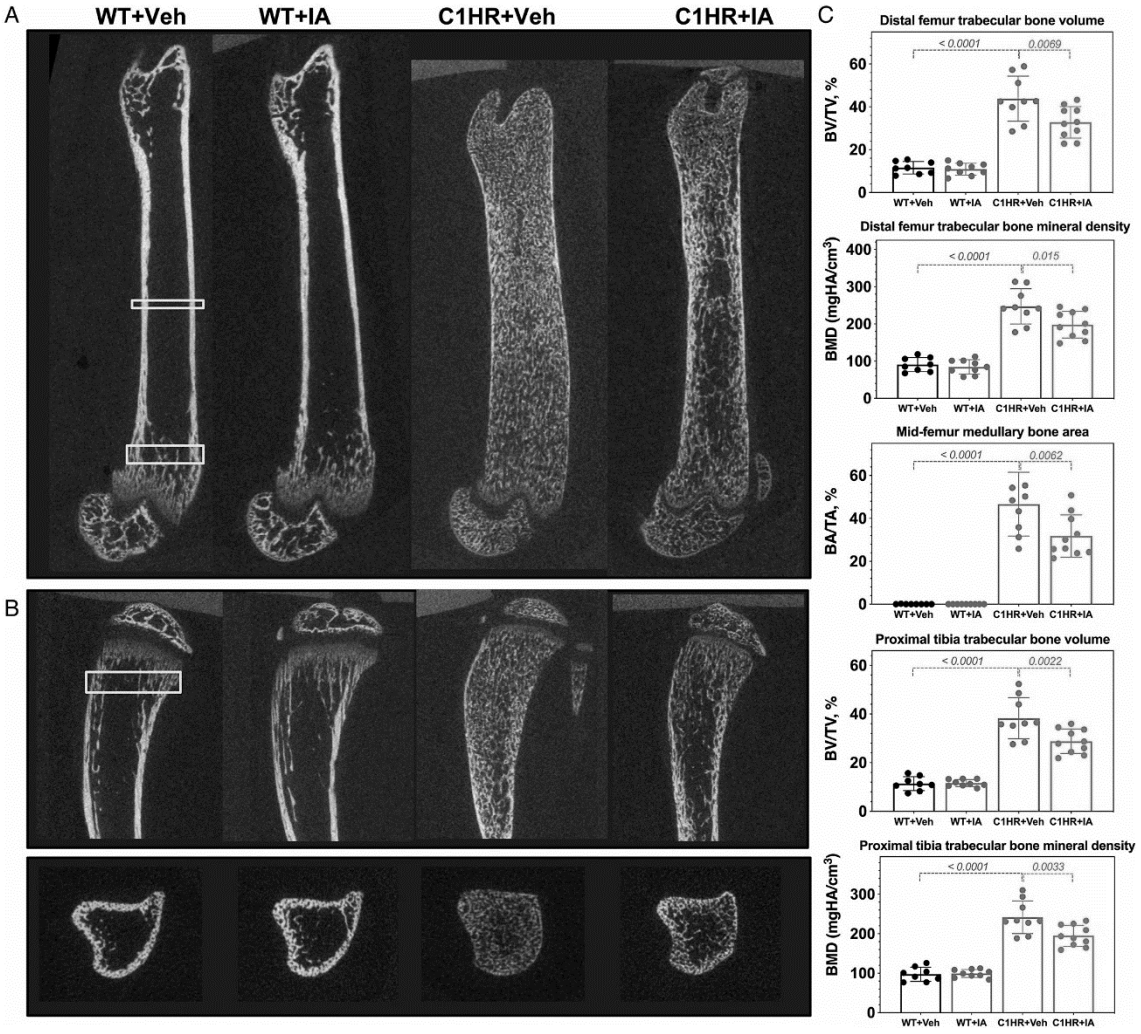

Figure 3. Micro-CT analysis of the effects of inverse agonist treatment on bone density in WT and C1HR mice. Femurs and tibias isolated from WT and C1HR mice after 17 days of treatment with inverse agonist, IA, or Veh were analyzed by μCt. (A) Representative sagittal views of the whole femur. (B) Representative sagittal views and corresponding transverse views of the proximal tibia. (C) Quantification of trabecular BV/TV (%) and BMD (mg hydroxyapatite/cm^3) at the distal femur and proximal tibia, and of cross-sectional medullary BA/TA (%) at the femur mid-shaft. Measurements were made between the cortices in the regions of interest shown by the boxes in the vehicle-treated WT images in A and B. Data are means ± SD; *p* values (Tukey's multiple comparison test after ANOVA) are shown for paired groups marked by brackets (n = 8–10 per group). μCT = micro–computed tomography; C1HR = Col1-PTHR1-H223R; WT = wild-type; Veh = vehicle; IA = [Leu^{11},dTrp^{12},Trp^{23},Tyr^{36}]-PTHrP(7–36)NH$_2$; BV/TV = bone volume relative to tissue volume; BMD = bone mineral density; BA/TA = bone area relative to total area.

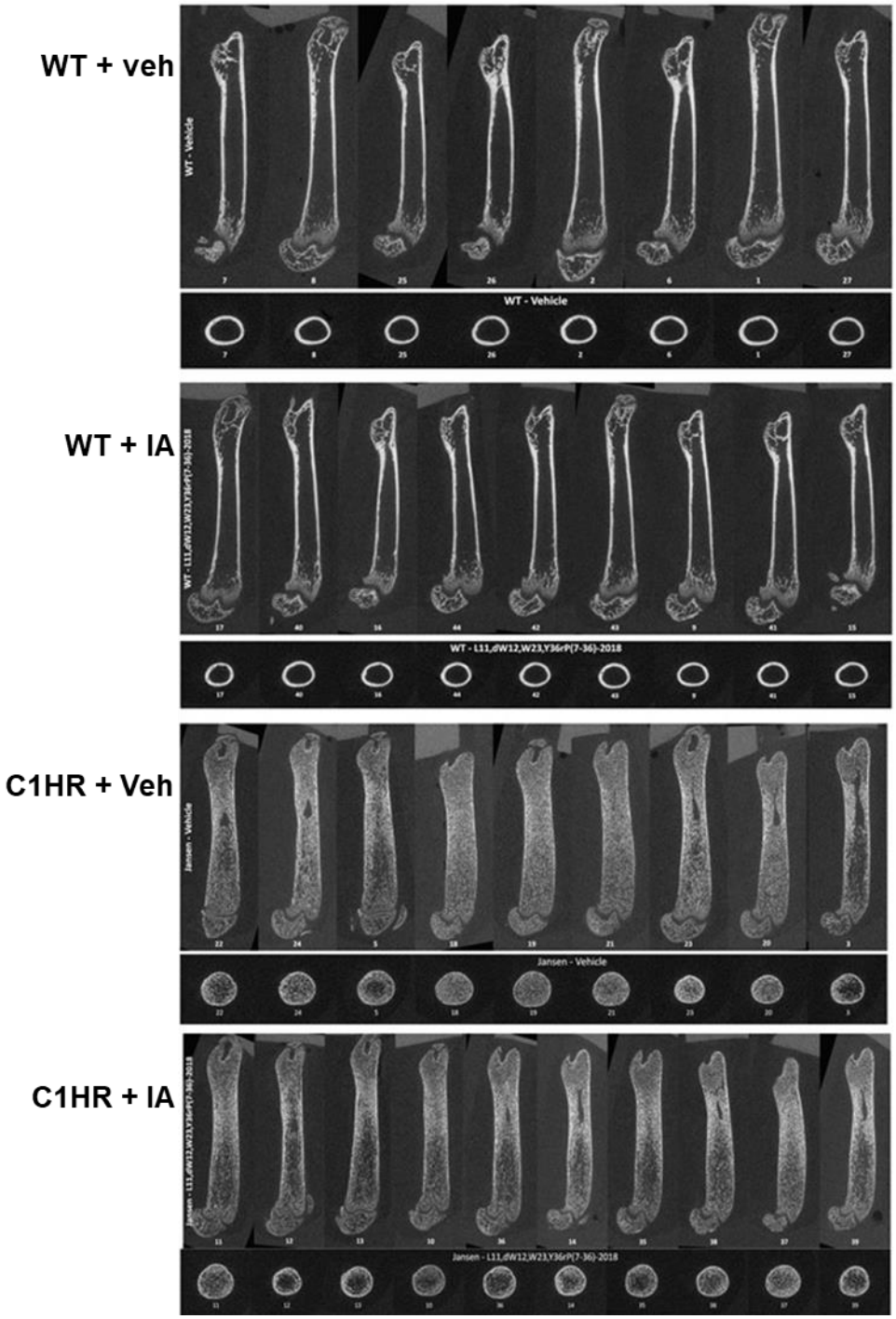

Figure 4. Micro-CT images of femur. Sagittal views of the total femur and corresponding transverse views of the mid-shaft of femurs obtained from wild-type (WT) or Col1-PTHR1-H223R (C1HR) mice injected twice-daily with vehicle (veh) or inverse agonist (IA) for 17 days.

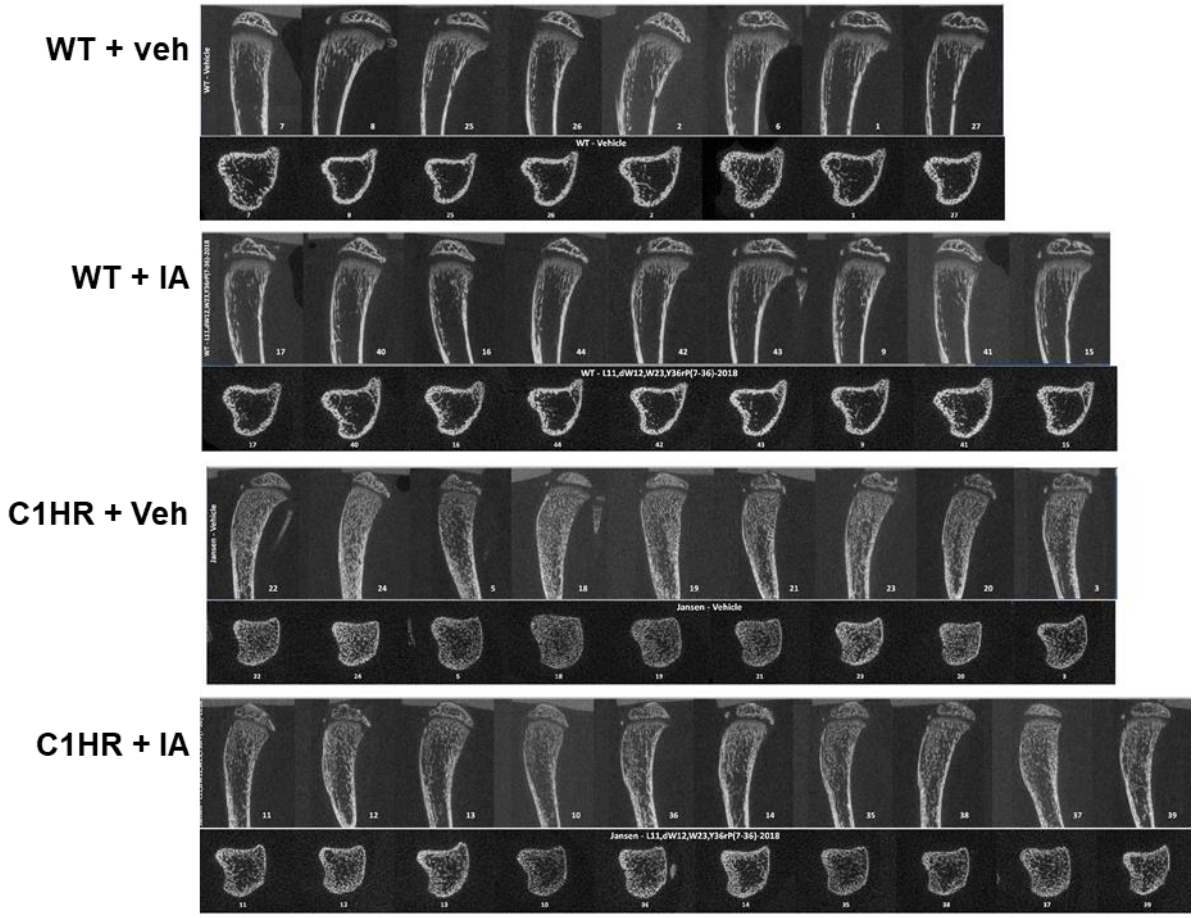

Figure 5. Micro-CT images of tibia. Sagittal and corresponding transverse views of the proximal regions of tibiae obtained from wild-type (WT) or Col1-PTHR1-H223R (C1HR) mice injected twice-daily with vehicle (Veh) or inverse agonist (IA) for 17 days: transverse views show a region approximately 1 mm below the growth plates.

Inverse agonist treatment reduces osteoblast number, bone marrow fibrosis, and bone formation rates in C1HR mice. The author further explored the effects of the inverse agonist on bone properties by examining histological sections of the proximal tibias obtained from the mice. Consistent with the μCT imaging, staining of the tibia sections with von Kossa dye revealed the expected increase in mineralized trabecular bone in the tibias of the vehicle-treated C1HR mice, as compared to those of the vehicle-treated wild-type mice, and this trabecular bone mass was reduced in the C1HR mice by inverse agonist treatment (Fig. 6 A). Higher magnification views of sections stained with the Goldner's Trichrome reagent revealed the expected accumulation of fibrotic, stromal-like cells in the intertrabecular spaces in the tibias from the vehicle-treated C1HR mice, whereas these spaces in bones from wild-type mice were populated by smaller hematopoietic-type cells (Calvi et al., 2001; Kuznetsov et al., 2004; Ohishi et al., 2009; Ohishi et al., 2012) (Fig. 6 B). Treatment with the inverse agonist reduced the abundance of these fibrotic cells in the tibiae of the C1HR mice, as compared to the amounts of these cells seen in the tibias from the C1HR mice injected with vehicle, and there was concomitantly an apparent increase in the abundance of smaller hematopoietic-type cells (Fig. 6 B). Quantitative histomorphometric analyses confirmed these observations, as inverse agonist treatment, relative to vehicle treatment in the C1HR mice significantly reduced the measured bone mass, the number of bone trabeculae, as well as the amount of marrow cell fibrosis (Fig. 6 C, Table 2). The effect on bone trabeculae was also supported by the significant improvement in reduced space between trabecular bones in C1HR mice, although inverse agonist did not affect trabecular bone thickness (Fig. 7 A). Inverse agonist treatment in C1HR mice also reduced the number of osteoblasts per unit length of bone perimeter, whereas it increased the number of osteoclasts; the latter effect could be explained by a reduction in the total bone area in the C1HR mice with a corresponding smaller change in the total number of osteoclasts in the measured area (Fig. 6 C, Table 2).

The differences given in the previous paragraph in bone structural parameters observed in the C1HR

mice treated with or without inverse agonist likely reflect, at least in part, effects on rates of bone formation. To assess rates of bone mineralization and formation, the mice were sequentially injected with the fluorescent bone-labeling dyes, calcein and demeclocycline, at two days and one day, respectively, before the last injection (day 17). The 24-hour interval between dye injections was selected based on the higher bone formation rate predicted for the C1HR mice from previous studies (Calvi et al., 2001; Ohishi et al., 2009). This interval was too short to provide consistent double labels in the bones of wild-type mice, which precluded reliable rate measurements in the bones of these animals. In the bones of the C1HR mice, adequate double labels were obtained, and the distances measured between the two labels clearly indicated that inverse agonist treatment reduced the rates of bone mineral apposition (MAR) and bone formation (BFR) in C1HR mice (Figs. 6 C, 7, and Table 2). Quantitative histomorphometric analyses performed on the sections of proximal tibiae also revealed that osteocytes in vehicle-treated C1HR mice significantly increased comparing in vehicle-treated wild-type mice but inverse agonist did not affect the number of osteocytes (Fig. 7A).

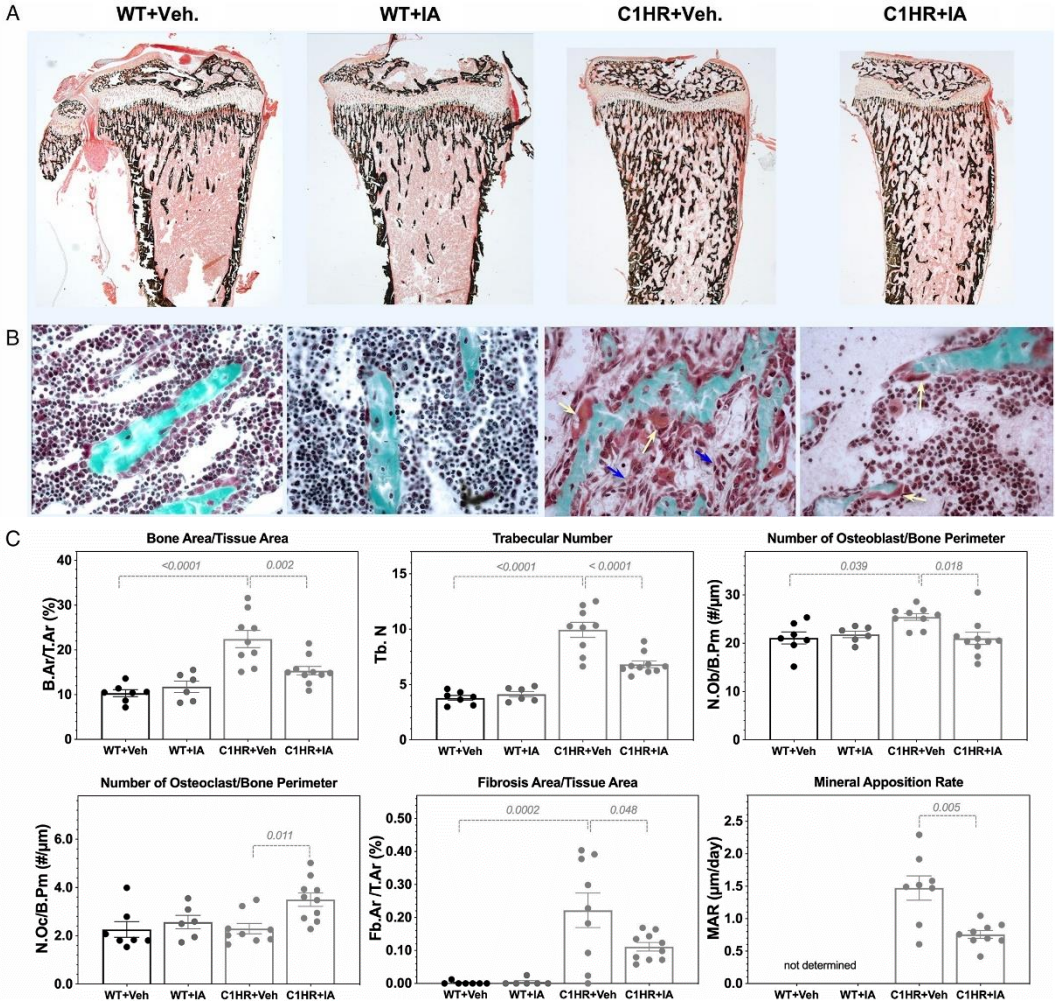

Figure 6. Histological analysis of the effects of inverse agonist treatment on bone in WT and C1HR mice. Tibias isolated from WT and C1HR mice after 17 days of treatment with IA or Veh were analyzed histologically in the proximal region. (A) Representative sagittal views of sections stained with von Kossa dye to show mineralized bone tissue (magnification ×40). (B) Higher magnification (×400) views of sections stained with Goldner's trichrome dye to show bone trabeculae (green) and surrounding cells and tissue. Blue arrows in the C1HR + Veh image point to areas of stromal cell fibrosis; yellow arrows point to osteoclasts. (C) Quantification of histomorphometric parameters in a region just below the center of the growth plate in the proximal tibia. Mineral apposition rate was not determined in bones of WT mice due to inadequate separation of double labels. Data are means ± SD; *p* values (Tukey's multiple comparison test after ANOVA) are shown for paired groups marked by brackets (n = 8–10 per group). WT = wild-type; C1HR = Col1-PTHR1-H223R; IA = inverse agonist; Veh = vehicle.

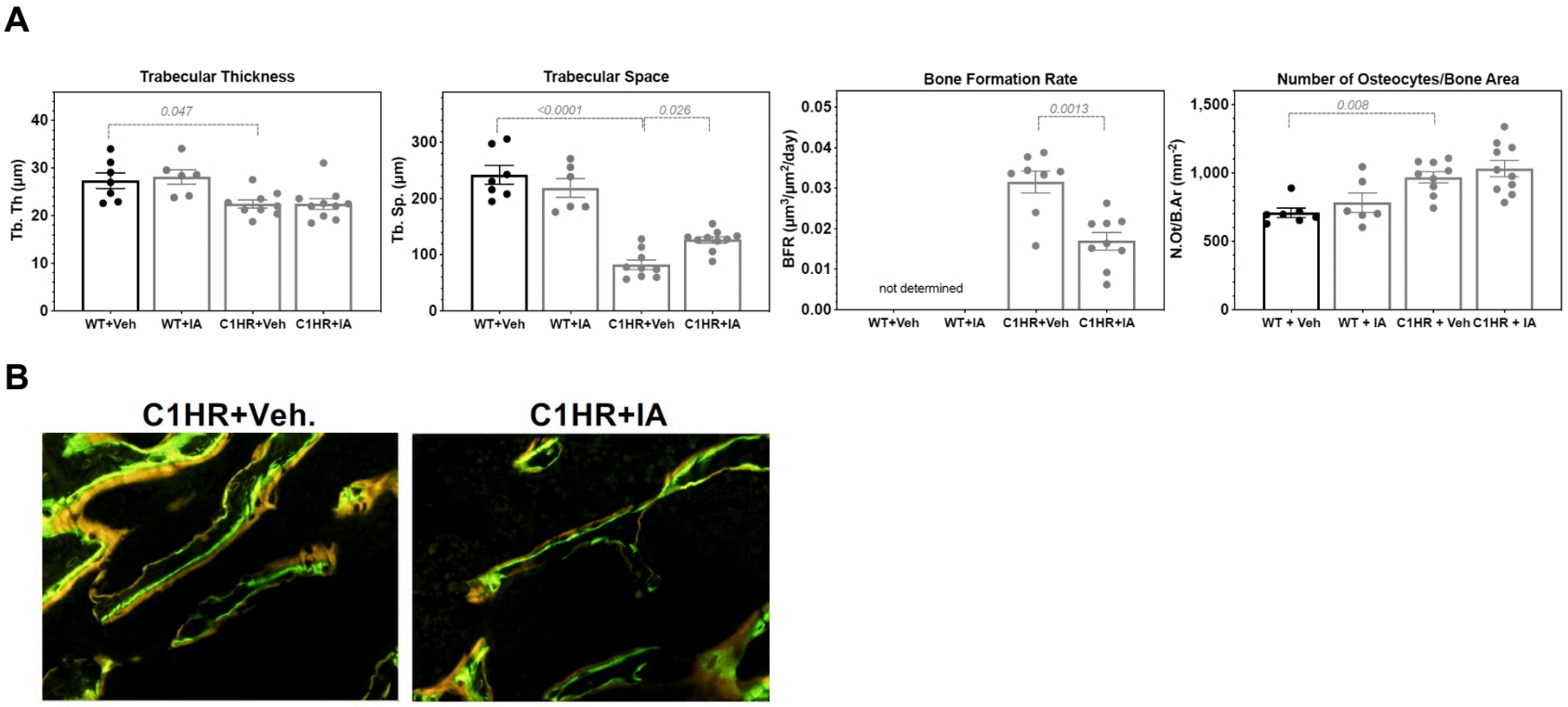

Figure 7. Histomorphometry of tibiae. Tibiae from wild-type (WT) or Col1-PTHR1-H223R (C1HR) mice after 17 days of twice-daily injection with either vehicle (Veh) or inverse agonist (IA) were analyzed histomorphometrically in a region just below the proximal growth plate. (A) Quantification of histomorphometric parameters. Data are means ± SD; *p* values (Tukey's multiple comparison test after ANOVA) are shown for paired groups marked by brackets. Bone formation rate was not determined in bones of WT mice due to inadequate separation of calcein and demeclocycline fluorescent labels. (B) Fluorescent microscopy images of bone trabeculae in tibia from C1HR mice showing incorporated calcein (green) and demeclocycline (orange) labels administered two days and one day before sacrifice, respectively (400X).

Table 2. Histomorphometry of tibiae from mice injected with vehicle or inverse agonist.

	WT					Col1-H223R				
	Vehicle	n	Inverse Agonist	P vs. WT-Veh	n	Vehicle	n	P vs. WT-veh.	Inverse Agonist	n	P vs. C1HR-Veh
B.Ar/T.Ar (%)	10.3 ± 0.8	7	11.8 ± 3.1	0.91	6	22.4 ± 5.8	9	<0.0001	15.3 ± 3.0	10	0.00
N.Ob/T.Ar (mm^{-2})	158 ± 8	7	179 ± 21	0.96	6	511 ± 129	9	<0.0001	290 ± 61	10	<0.0001
N.Oc/T.Ar (mm^{-2})	17.0 ± 2.0	7	20.8 ± 4.0	0.90	6	44.9 ± 11.9	9	<0.0001	47.7 ± 11.6	10	0.93
N.Ob/B.Pm (mm^{-1})	21.1 ± 1.2	7	21.8 ± 1.7	0.97	6	25.4 ± 2.1	9	0.039	21.0 ± 4.0	10	0.018
N.Oc/B.Pm (mm^{-1})	2.26 ± 0.32	7	2.57 ± 0.68	0.89	6	2.30 ± 0.64	9	>0.99	3.50 ± 0.87	10	0.011
Ob.Pm/B.Pm (%)	15.5 ± 1.2	7	15.3 ± 1.3	>0.99	6	18.0 ± 3.5	9	0.263	14.2 ± 1.8	10	0.020
Oc.Pm/B.Pm (%)	3.50 ± 0.40	7	3.92 ± 0.97	0.95	6	4.30 ± 1.37	9	0.67	6.91 ± 1.77	10	0.0019
N.Ot/B.Ar (mm^{-2})	708 ± 32	7	783 ± 169	0.80	6	968 ± 123	9	0.0085	1031 ± 184	10	0.79
Fb.Ar./T.Ar/ (%)	0.0017 ± 0.0017	7	0.0041 ± 0.0101	>0.99	6	0.22 ± 0.16	9	0.0002	0.11 ± 0.04	10	0.048
MAR (um/day)	N.D.		N.D.			1.47 ± 0.53	8		0.76 ± 0.18	9	0.0050
BFR/BS (um^3/um^2/day)	N.D.		N.D.			0.031 ± 0.008	8		0.017 ± 0.006	9	0.0013

Proximal tibiae were analyzed in a ~1.0x1.0 mm area located ~1.0 mm below the center of the growth plate. Data are means ±SD; P values were determined by Tukey's multiple comparison test after ANOVA. N.D., not determined -- inadequate separation of demeclocycline and calcein labels in bones of WT mice precluded assessment of mineral apposition and bone formation rates.

B.Ar/T.Ar(%) Bone area/tissue area

N.Ob/T.Ar (mm^{-2}) number of osteoblasts/tissue area

N.Oc/T.Ar (mm^{-2}) number of osteoclasts/tissue area

N.Ob/B.Pm (mm^{-1}) number of osteoblast/bone perimeter

N.Oc/B.Pm (mm^{-1}) number of osteoclast/bone perimeter

Ob.Pm/B.PM (%) osteoblast perimeter/bone perimeter

Oc.Pm/B.PM (%) osteoclast perimeter/bone perimeter

N.Ot/B.Ar (mm^{-2}) number of osteocytes/bone area

Fb.Ar./T.Ar. (%) fibrosis area/tissue area

MAR (μm/day) mineral apposition rate

BFR/BS ($\mu m^3/\mu m^2$/day)Bone formation rate

Inverse agonist treatment reduces markers of bone turnover in C1HR mice. Serum levels of CTX1 were significantly elevated in the vehicle-treated C1HR mice, as compared to the levels in the vehicle-treated wild-type mice, and these levels in C1HR mice were reduced by inverse agonist treatment (Fig. 8 A). Serum concentrations of total Ca were not different between the four groups, whereas serum Pi was unchanged between groups of wild-type mice and the vehicle-treated C1HR mice but was significantly reduced in C1HR mice treated with the inverse agonist, as compared to C1HR mice treated with vehicle (Fig. 8 B, C). Urine levels of both Ca and Pi were significantly elevated in vehicle-treated C1HR mice, and were reduced in the C1HR mice by inverse agonist treatment, although the effect was significant only for urine Ca (Fig. 8 D, E). Unlike the case of PTH acting systemically, C1HR mice does not affect the PTHR1 signal in the kidney. In the mutant mice, Ca and Pi released from the bone into the blood due to the excessive bone resorption might have been therefore excreted directly into urine. The elevations in urinary Ca and Pi, and plasma CTX1 observed in the vehicle-treated C1HR mice, as compared to the levels in wild-type mice, were consistent with an increase in the rate of osteoclast-mediated bone resorption, as induced indirectly by the constitutive signaling activity of the mutant PTHR1-H223R in bone osteoblasts, whereas the reductions in these markers with inverse agonist treatment were consistent with a suppression of PTHR1-H223R signaling activity in the osteoblasts of the transgenic mice and an indirect suppression of osteoclast-mediated bone turnover.

The levels of mRNAs encoding several osteoblast-produced proteins that are regulated by PTHR1 signaling, including collagen-1a1, RANKL, which stimulates osteoclast differentiation and activity, and osteoprotegerin (OPG), which inhibits RANKL by acting as a decoy receptor (Udagawa et al., 2000), as well as the osteoclastic gene product, TRAP5b, were elevated in femurs isolated from vehicle-treated C1HR mice, as compared to femurs isolated from vehicle-treated wild-type mice (Fig. 9). Inverse agonist treatment had only a minor if any effect on the levels of these mRNAs in C1HR

mice, although collagen-1a1 mRNA levels were reduced significantly (p value = 0.048).

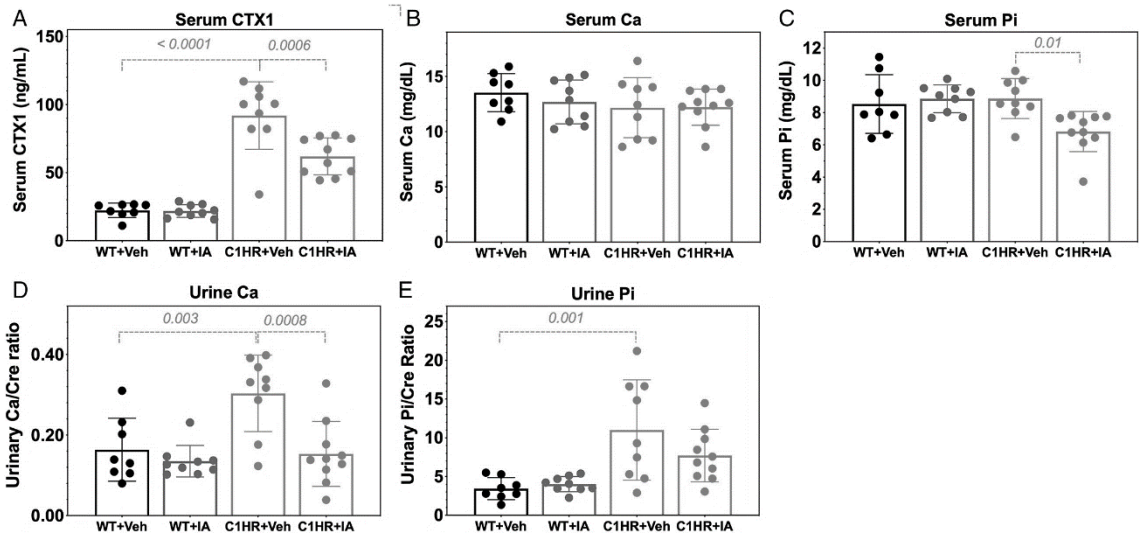

Figure 8. Effects of inverse agonist treatment on markers of bone and mineral metabolism in blood and urine. Blood and urine samples collected from WT and C1HR mice after 17 days of treatment with IA or Veh were analyzed for CTX1 (A), total Ca (B, D), and Pi (urine values are normalized to creatinine) (C, E). Data are means ± SD; p values (Tukey's multiple comparison test after ANOVA) are shown for paired groups marked by brackets (n = 8–10 per group). WT = wild-type; C1HR = Col1-PTHR1-H223R; IA = inverse agonist; Veh = vehicle; Pi = inorganic phosphate.

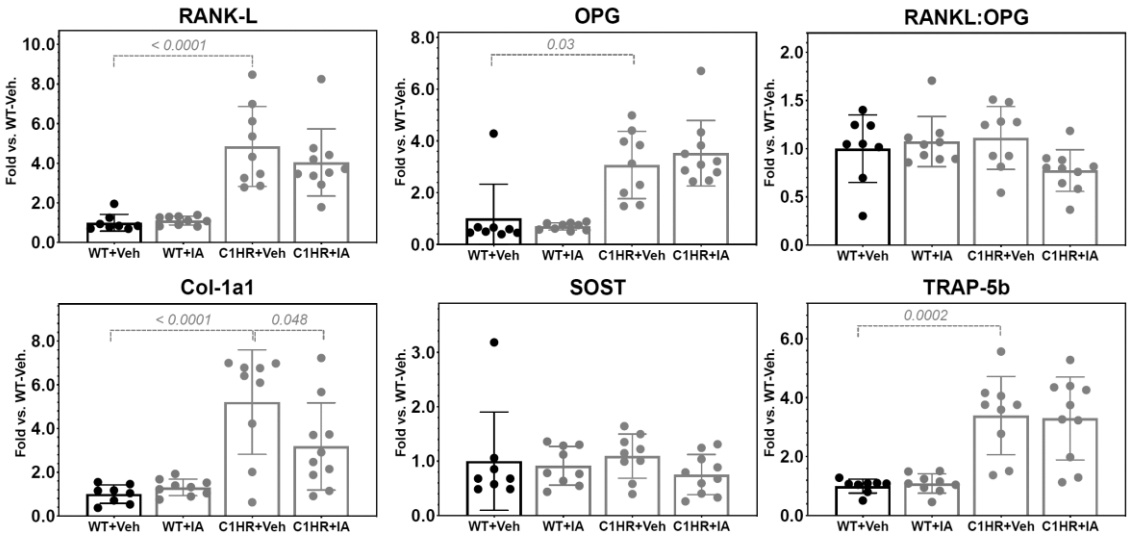

Figure 9. Effect of inverse agonist treatment on mRNA levels in femurs of WT or C1HR mice. Total RNA isolated from femurs obtained from wild-type (WT) or Col1-PTHR1-H223R (C1HR) mice after 17 days of twice-daily injection with either vehicle (Veh) or inverse agonist (IA) was analyzed by real-time (RT) PCR for mRNAs corresponding to the indicated genes. RT-PCR values for each gene were normalized to the value for 18sRNA and then by the corresponding 18S-normalized value obtained in WT-vehicle controls. Data are means±SD; *p* values (Tukey's multiple comparison test after ANOVA) are shown for paired groups marked by brackets.

Table 3. Effect of inverse agonist treatment on bone length.

	WT					Col1-H223R				
	Vehicle	Inverse Agonist		*P vs.WT-Veh*		Vehicle	*P vs.WT-Veh*	Inverse Agonist	*P* vs. C1HR- Veh	
		n			n			n		n
Femur length (mm)	**10.7 ± 0.4**	8	**10.6 + 0.4**	*0.95*	9	**9.0 ± 0.4**	*<0.0001*	9	**9.4 ± 0.4**	*0.080*	10
Tibia length (mm)	**13.4 ± 0.6**	6	**13.4 ± 0.3**	*0.99*	9	**11.6 ± 0.5**	*<0.0001*	8	**12.1 ± 0.5**	*0.195*	10

Bone length determined by micro CT. Data are means ± SD; *p* values determined by Tukey's multiple comparison test after ANOVA.

Discussion

Because JMC is an ultra-rare disease, with only about 30 cases identified since its first description in 1934 (Jansen, 1934; Saito et al., 2018), it has garnered little if any interest from the pharmaceutical industry in terms of therapeutic development. There is thus no effective drug therapy available for the disease, despite a clear medical need (Nampoothiri et al., 2016) and precise knowledge of the molecular target (Gardella et al., 1996; Schipani et al., 1996; Schipani et al., 1997). Those considerations provided the key impetus for the current study, which is the first time that an inverse agonist ligand for a constitutively active mutant PTHR1 has been tested *in vivo*. The overall results provide proof-of-concept support for the hypothesis that such an inverse agonist ligand can be effective at suppressing the constitutive activity of a JMC PTHR1 variant *in vivo*. The author thus found that administration of [Leu^{11},$dTrp^{12}$,Trp^{23},Tyr^{36}]-PTHrP(7–36)NH_2 to C1HR mice expressing the PTHR1-H223R mutant allele in osteoblasts can prevent and/or correct at least some of the skeletal and mineral ion abnormalities that otherwise occur in these JMC model mice.

The author selected the [Leu^{11},$dTrp^{12}$,Trp^{23},Tyr^{36}]-PTHrP(7–36)NH_2 analog for use in this study because of its proven effectiveness in suppressing the basal cAMP signaling activity of the PTHR1-H223R mutant in transfected cells (Carter et al., 2015; Carter et al., 2001). The C1HR transgenic mice were used as a model of JMC because they express the PTHR1-H223R mutant allele, which is the most common JMC disease variant (Saito et al., 2018), and they exhibit a robust, well-characterized phenotype in skeletal tissue, which is the main site affected in patients. After only 17 days of treatment the inverse agonist produced significant reductions in the excess trabecular bone mass that otherwise accumulates in the long bones of the C1HR mice. It also quantitatively reduced the rate of new bone formation, the levels of bone resorption markers in the blood or urine, and the abundance of fibrotic stromal cells that otherwise populate the marrow compartments of the long

bones of the C1HR mice (Kuznetsov et al., 2004; Ohishi et al., 2012).

A surprising finding was that although inverse agonist treatment in the C1HR mice led to a significant reduction in serum levels of CTX1, it increased the number and/or size of osteoclasts lining the bone perimeters (Fig. 8 A, Table 2). Although the underlying mechanisms are not clear, it is possible that the bone-resorbing activity of the osteoclasts did not increase proportionally with an increase in the size and/or number of these cells. An increase in osteoclast size and/or number with a concomitant decrease in serum CTX1 was observed previously by Ko and colleagues (Ko et al., 2017) in young wild-type mice in response to 8 weeks of alendronate treatment. Although these findings appear similar to ours, the upstream mechanisms likely differ, because the effect involved treatment with a bisphosphonate, whereas our current study involves effects on PTHR1 signaling.

The author detected no significant change in any bone parameter in wild-type mice treated with the inverse agonist. The absence of a skeletal effect in the wild-type mice suggests that the inverse agonist acts with at least some degree of selectivity on the PTHR1-H223R variant, relative to on the wild-type PTHR1, and thus can have efficacy toward that variant without causing major alterations to the normal physiology regulated by the wild-type PTHR1 and its two endogenous ligands, PTH and PTHrP, acting in the principal target tissues of bone and kidney. Although a formal toxicological analysis was not performed, there was no sign of systemic toxicity associated with ligand treatment in either the wild-type or C1HR mice. In support of this, inverse agonist treatment in either strain of mice resulted in no change in body weight, which provides at least an initial assessment of systemic drug toxicity (Parasuraman, 2011) (Fig. 2), nor a change in serum Ca (Fig. 8 B).

Bone phenotypes in this osteoblast-specific mouse model of JMC well reflected the PTH actions on osteoblasts, such as increased numbers of mature osteoblasts (N.Ob/B.Pm) and increased MAR and BFR linked to upregulated bone matrix production and osteoblast activity (Figs. 6 C, 7 A and table 2). Inverse agonist improved these bone phenotypes significantly but did not affect the

increased number of osteocyte in the C1HR mice (Fig. 7 C), in which the increase osteocyte might be derived from osteoblasts induced by the constitutively active mutant PTHR1. These results also support that inverse agonist acted specifically on the PTHR1-H223R expressing only on osteoblasts, not on osteocytes.

The lengths of the tibias and femurs in the C1HR mice were ~15% shorter than those in wild-type mice, consistent with prior studies (Calvi and Schipani, 2000; Ohishi et al., 2009) , and the mean lengths of the bones in the C1HR mice tended to increase modestly (3% to 5%) with inverse agonist treatment, although the effects were not significant (Table 3). Potential effects on bone length are of interest because impaired limb development and reduced overall height are prominent clinical features of JMC (Nampoothiri et al., 2016). An inverse agonist could conceivably induce changes in bone length in C1HR mice via actions in the growth plates, because expression of the PTHR1-H223R transgene is detected at low levels in growth plate chondrocytes of the C1HR mice(Calvi et al., 2001), and PTHR1 signaling is well known to play a major role in growth plate chondrocyte differentiation and hence bone growth (Chagin and Kronenberg, 2014; Khan et al., 2018; Lanske et al., 1998; Schipani et al., 1996). The author administered the inverse agonist starting at 7 days of age, and so the analog was present in the mice during a period of active bone growth. Elucidating how processes of growth plate maturation and bone growth might be altered by constitutive PTHR1 signaling and potentially modulated with an inverse agonist ligand are important research objectives, given the impact that such altered signaling has on skeletal development in children with JMC (Nampoothiri et al., 2016; Saito et al., 2018).

Prominent laboratory abnormalities reported for patients with JMC including hypercalcemia and hypophosphatemia (Saito et al., 2018) are also inconsistent with the phenotype of C1HR mice. These abnormalities could lead to renal frailer resulting in lower the long-term prognosis. Further investigation to use other model mice such as H223R-PTHR1 knock-in mice would be needed to

evaluate the effect of inverse agonist on the kidney.

The recent high-resolution structures of the PTHR1 in partially active (Ehrenmann et al., 2018) and active-state (Zhao et al., 2019) conformations, together with the structures obtained for several other family B GPCRs (de Graaf et al., 2017; Glukhova et al., 2018; Yin et al., 2017) help shed light on the mechanisms by which the PTHR1 and these peptide hormone receptors as a class function. Particularly noteworthy is the finding that all known JMC mutations map to three residue positions in the PTHR1: His223, Thr410, and Ile458, which are each located at the cytosolic base of a TMD helix and at a position that strongly suggests a critical role in receptor activation. His223 in TM2 and Thr410 in TM6 are thus seen to be directly involved in a network of polar residues that acts as a switch to control the outward movements of the TMD helices that occur during activation and which lead to the formation of a cavity on the cytosolic face of the receptor that is used for G protein coupling (de Graaf et al., 2017; Glukhova et al., 2018; Hjorth et al., 1998; Yin et al., 2017). Ile458 in TM7 is adjacent to Tyr459, which also participates in the same polar network. A fourth key residue in this polar network of the PTHR1 is Glu302 in TM3, which so far has not been associated with JMC. Overall, the disease phenotype of JMC patients confirms the functional significance of this polar network. Although this polar network is highly conserved in family B GPCRs, it is not reported that another disorder is caused by an activating mutation in any of these other GPCRs, even though mutations introduced at these sites in several of them have been shown to result in constitutive activity when tested in transfected cells(Hjorth et al., 1998; Yin et al., 2017). Whether the apparent absence of a disease association for these other receptors is due to poor expression of the constitutively active mutant allele in the respective target tissue, or by some other overriding factor is unknown.

The current structural data predict that the PTHR1 mutations of JMC shift the receptor to an active-state conformation by perturbing key molecular interactions that occur within the polar network at the base of the TMD bundle. The mechanism by which the binding of the inverse agonist ligand to

the receptor's extracellularly exposed orthosteric pocket promotes the inactive receptor conformation is less clear. The dTrp^{12} modification of the ligand, which replaces the L-glycine that is conserved at this position in native PTH and PTHrP agonist ligands, is likely to play a key role, because it is required for the inverse agonist effect (Gardella et al., 1996). Several small-molecule antagonist ligands have been identified for the PTHR1, but none so far has been reported to function as an inverse agonist (Carter et al., 2015; Carter et al., 2007; McDonald et al., 2007).

The rarity of JMC is likely to be at least partly explained by a limited number of sites in the PTHR1 that can result in functional constitutive activity when mutated; ie, those impacting the conserved polar residue network comprised of His223, Glu302, Thr410, and Tyr458. In contrast to the activating mutations of JMC, heterozygous loss-of-function mutations have been identified at a number of dispersed sites in the PTHR1 in patients with defects in tooth eruption (Roth et al., 2014). In the very rare homozygous state, such loss-of-function PTHR1 mutations lead to the perinatal lethal condition of Blomstrand's chondrodysplasia (Zhang et al., 1998), which is characterized by a hypermineralized skeleton, in contrast to the low bone mineral density seen in patients with JMC (Nampoothiri et al., 2016).

Summary in chapter I

JMC is a rare disease of bone and mineral ion physiology that is caused by activating mutations in PTHR1. Ligand-independent signaling by the mutant receptors in cells of bone and kidney results in abnormal skeletal growth, excessive bone turnover, and chronic hypercalcemia and hyperphosphaturia. Clinical features further include short stature, limb deformities, nephrocalcinosis, and progressive losses in kidney function. There is no effective treatment option available for JMC. In previous cell-based assays, the author's group found certain N-terminally truncated PTH and PTHrP antagonist peptides function as inverse agonists and thus can reduce the high rates of basal cAMP signaling exhibited by the mutant PTHR1s of JMC *in vitro*. Here the author explored whether one such inverse agonist ligand, [Leu^{11},dTrp^{12},Trp^{23},Tyr^{36}]-PTHrP(7–36)NH_2, can be effective *in vivo* and thus ameliorate the skeletal abnormalities that occur in transgenic mice expressing the PTHR1-H223R allele of JMC in osteoblastic cells via the collagen-1α1 promoter (C1HR mice). The author observed that after 2 weeks of twice-daily injection and relative to vehicle controls, the inverse agonist ligand improved at least some of the skeletal and mineral ion defects caused by transgenic expression in osteoblasts of a constitutively active PTHR1-H223R allele of JMC. This study is the first demonstration that an inverse agonist for the PTHR1 can be effective *in vivo*, and thus provides proof-of-concept support for the notion that such a ligand could potentially be developed as a therapy for JMC. Although full phenotypic rescue was not achieved in the current, short-term studies, this was not an essential goal, given that the transgenic mice utilized here, as well as other available JMC transgenic mice (Bellido et al., 2005; O'Brien et al., 2008), are not precise models of the disease, because the mutant allele in the mice is expressed in a restricted tissue or cell type, eg, bone osteoblasts, whereas in patients it is expressed in all endogenous PTHR1 target sites, including bone, kidneys, and the growth-plates. The current findings nevertheless show that inverse agonist efficacy *in vivo* is possible

for the mutant PTH receptors of JMC, and they also suggest that further studies aimed at improving the receptor-binding properties of such ligands as well as their pharmacokinetic properties should be important goals of future research.

Chapter II

Optimization of PTH/PTHrP hybrid peptides to derive a long-acting PTH analog (LA-PTH).

Introduction

Hypoparathyroidism is an endocrine disorder in which the parathyroid grands cannot produce enough PTH and presents with hypocalcemia hyperphosphatemia. It causes tetanic symptoms, including systemic muscle cramps, shivering, paresthesias of the extremities, and seizures, resulting in bronchospasm, laryngospasm, and heart rate abnormalities. The disorder is mainly caused by the removal or damage of the parathyroid glands when the thyroid gland is removed for treatments of thyroid cancer. Other inherited disorders also lead to the development of hypoparathyroidism. In some cases, it is also caused by autoimmune diseases (Bilezikian et al., 2011; Gafni and Collins, 2019; Mannstadt et al., 2017; Shoback, 2008).

Conventional therapy of hypoparathyroidism, high doses of oral Ca and active vitamin D analogs, can increase the risk of hypercalciuria (Mitchell et al., 2012; Underbjerg et al., 2013). Human PTH(1–84) has recently been approved by the US Food and Drug Administration and the European Medicines Agency as a treatment option for hypoparathyroidism. It would theoretically maintain serum Ca while reducing Ca and requirements of vitamin D analogs by replacing the missing hormone. However, due to its short half-life, daily injection of human PTH(1–84) is insufficient to maintain serum Ca at a steady-state level without excessive urinary Ca excretion in a double-blind, placebo-controlled randomized phase 3 study (Mannstadt et al., 2013). There exists therefore an unmet medical need for hypoparathyroidism; that is, prolonged PTH replacement therapy without causing hypercalciuria could be a cure treatment option for patients with the disease.

It was previously reported that LA-PTH which is a M-PTH(1–14)/PTH(15–36) hybrid analog, [Ala^{1,3,12,18,19,22},Gln^{10},Arg^{11},Trp^{14},Lys^{26}]-PTH(1–14)/PTHrP(15–36), was previously reported that produces sustained calcemic responses in thyroparathyroidectomized (TPTX) rats and in normal monkeys (Shimizu et al., 2016a). Not reported are the extensive structure–activity relationship studies that led to the development of this analog, as well as the evidence that LA-PTH is the most desirable ligand analog for the intended purpose. In this work, the author characterized the series of PTH/PTHrP hybrid molecules that formed the basis for LA-PTH development. The design used the carboxyl terminal portion of PTHrP based on the evidence that it bound with higher affinity to the ECD of the PTH receptor, as compared with the PTH C-terminal segment, and the author further included the optimized N-terminal portion of PTH modified with the activity-enhancing "M" substitutions (Ala^{1,3,12},Gln^{10},Arg^{11},Trp^{14}) that were identified in previous work on the PTH(1–14) scaffold (Shimizu et al., 2001a; Shimizu et al., 2000b; Shimizu et al., 2001b). Seven different hybrid molecules with various boundaries between the N-terminal M-PTH and C-terminal PTHrP segments ranging from positions 11/12 to positions 30/31 were synthesized and evaluated the binding affinity for PTHR1 *in vitro*, assessing both the G protein-coupled and uncoupled receptor conformations, R^G and R^0, respectively. Previous studies revealed that relative affinity for the R^0 conformation correlates with duration of cAMP signaling (Okazaki et al., 2008). Most importantly, the analogs were evaluated *in vivo* and thus assessed their capacities to stimulate a calcemic response in normal rats after a single intravenous injection. These evaluations identified the most potent PTH/PTHrP hybrid analog as M-PTH(1–14)/PTHrP(15–36) (Shimizu et al., 2016a). However, in the initial assessment of this analog, it has a relatively low solubility in aqueous solutions at neutral pH. With further investigation, the author identified several amino acid substitutions in the C-terminal PTHrP region that led to improved solubility while retaining high R^0 binding affinity, as well as prolonged *in vivo* calcemic actions. It was this work that led to the choice of [Ala^{1,3,12,18,19,22},Gln^{10},Arg^{11},Trp^{14},Lys^{26}]-PTH(1–14)/PTHrP(15–

36) as an optimized analog, LA-PTH. Here the author presents key findings that led to the selection of LA-PTH as an optimum ligand in the series and provides further data that compare the Ca-mobilizing actions of this type of hybrid PTH/PTHrP analog with those of a vitamin D analog in TPTX rats.

Material and Methods

Peptides. All peptides used were based on the human PTH or PTHrP amino acid peptide sequence, except for the PTH(1–34) analog used for radiolabeling, which was based on the rat PTH sequence. Specific analogs assessed for function were PTH(1–34), LA-PTH ([Ala^{1,3,12},Gln^{10},Arg^{11},Trp^{14}]PTH(1–14)/[Ala^{18,22},Lys^{26}]PTHrP(15–36)COOH), and M-PTH(1–15) ([Ala^{1,12},Aib^{3},Nle^{8},Gln^{10},Har^{11},Trp^{14},Tyr^{15}]-PTH(1–15)NH_2)—in which Aib is α-aminoisobutyric acid, Har is homoarginine, and Nle is norleucine. The radioligands used were ^{125}I-PTH(1–34), (^{125}I-[Nle^{8,21},Tyr^{34}]-rat PTH(1–34)NH_2), and ^{125}I-M-PTH(1–15). They were prepared by chloramine-T-based radioiodination, followed by reversed-phase HPLC purification. Peptides were prepared by conventional chemical synthesis. Peptide identity was established by mass spectrometry; purity was confirmed to be greater than 95% by reverse-phase HPLC.

Cell culture and transfection. GP-2.3 cells, an HEK-293 cell- (ATCC CRL-1573) derived cell line that stably expresses the luciferase-based pGloSensor-22F (GloSensor) cAMP reporter plasmid (Promega Corp., San Luis Obispo, CA, USA) along with the human PTHR1, were cultured in DMEM (Thermo Fisher Scientific, Waltham, MA, USA) supplemented with FBS (10%). Cells were seeded into white 96-well plates for GloSensor cAMP assays, and used for assay 2 to 3 days after the monolayer became confluent (Ferrandon et al., 2009). UGS-56 cells were derived from the UMR106 rat osteoblastic cell line by stably transfecting the cells to express the GloSensor-cAMP reporter. B64 cells are a derivative of the porcine kidney cell line, LLC-PK1 that stably expresses the human PTHR1. COS-7 cells (ATCC CRL-1661) were seeded into 10-cm dishes and transiently transfected to express the human PTHR1 with or without a high-affinity, negative-dominant $G\alpha_s$ subunit; 2 days after transfection, the cells were harvested for membrane preparations (Dean et al., 2006). All transfections

were performed using the FuGENE HD reagent (Promega Corp.).

cAMP signaling assays. Changes in cAMP levels were assessed in intact GP-2.3 or UGS-56 cells via the (GloSensor) cAMP reporter. The intact cells in white 96-well plates were preloaded with luciferin in CO_2-independent culture media (Thermo Fisher Scientific) for 20 min at room temperature, then treated with a test ligand diluted in the same media and placed into a Envision plate reader (PerkinElmer, Waltham, MA, USA) for an additional 30 min, during which time cAMP-dependent luminescence was measured at 2-min intervals (ligand-on phase). Ligand dose–response curves were generated by plotting ligand concentrations versus the AUC of the time versus luminescence plot obtained at each ligand dose and expressing that AUC as a percent of the maximum AUC observed in the same experiment for PTH(1–34). For washout responses, the cells were treated as above, and after the ligand-on phase, the plate was removed from the plate reader, the cells were rinsed with media, then fresh media containing only luciferin was added and luminescence was measured for an additional 90 min (washout phase). EC_{50} values were determined using the 4-parameter sigmoidal dose–response equation in Prism 8.0 (GraphPad Software, Inc., La Jolla, CA, USA).

Competition binding assays. Ligand binding to the human PTHR1 in R^0 and R^G conformations were assessed by competition methods using membranes prepared from COS-7 cells and either ^{125}I-PTH(1–34) (R^0) or 125I-M-PTH(1–15) (R^G) as tracer radioligand and GTPγS (10 μM) included in the R^0 assays (Dean et al., 2006). Binding reactions were performed in 96-well vacuum filtration plates and were incubated at room temperature for 90 min; the plates were then processed by vacuum filtration; after washing, the filters were removed and counted for gamma irradiation. Nonspecific binding was determined in reactions containing an excess (0.5 μM) of unlabeled PTH(1–34). Curves were fit to the data using a 4-parameter sigmoidal dose–response equation.

Peptide solubility assay. Peptides were initially dissolved in 10 mM acetic acid to obtain a stock solution of peptide at 1.0 to 2.0 mM. For assay, a stock solution was diluted in aqueous vehicle (pH 5.0) or assay buffer (pH 7.4) to concentrations of 10 – 30 μM, at which all peptides exhibited good solubility. For certain peptides, including, the M-PTH/PTHrP hybrid and PTHrP(1–36), precipitation or turbidity was observed in aqueous neutral pH buffer at a higher peptide concentration (>100 μM), which led the author to perform further optimization of the C-terminal PTHrP portion of the peptide scaffold. To assess solubility, a volume of each stock peptide solution that contained 75-μg peptide mass was placed, in duplicate, into a 1.5-mL microcentrifuge tube and lyophilized to dryness. For each peptide, one of the duplicate lyophilized samples was reconstituted in 50 μL of 10-mM acetic acid to a final concentration of 1.5 mg/mL; the other duplicate sample was reconstituted in 50 μL of PBS, pH 7.4. The solutions were then incubated for 24 hours at room temperature, then centrifuged at 16,000 × g for 2 min at room temperature. A 10-μL aliquot of the upper supernatant phase of each sample was removed in duplicate and assayed for protein concentration using the BCA protein assay (Pierce, Rockford, IL, USA). The protein concentration (mg/mL) of each sample was then derived from a standard curve generated with bovine serum albumin. The relative solubility in PBS was calculated as: 100 × (protein concentration of PBS supernatant/protein concentration of acetic acid supernatant).

***In vivo* pharmacology and pharmacokinetics studies.** All animal studies were approved by the Institutional Animal Care and Use Committee of Chugai Pharmaceutical, and were conducted in accordance with the approved protocols (protocol #: 07-317) and the Guidelines for the Care and Use of Laboratory Animals at Chugai. Chugai Pharmaceutical is fully accredited by the Association for Assessment and Accreditation of Laboratory Animal Care (AAALAC) International.

Calcemic actions in normal rats. Peptides were diluted in phosphate–citrate-buffered saline vehicle (prepared by adding 23 mmol/L citric acid/100 mmol/L NaCl added to 25 mmol/L sodium-phosphate/ 100 mmol/L NaCl until the pH of 5.0 was attained) containing 0.05% Tween-80 (Tokyo Chemical Industry Co., Ltd., Tokyo, Japan). Six-week-old normal rats were randomly assigned to test groups, and M-PTH/PTHrP hybrid analogs were administrated by a single *i.v.* administration. Blood was collected in a glass capillary from tail vein at 2-min intervals; blood ionized Ca^{2+} (iCa^{2+}) was measured by Ca analyzer (GE Healthcare, Piscataway, NJ, USA).

Pharmacological studies in TPTX rats. Surgical TPTX was performed on 6-week old rats (Charles River Laboratories Japan, Inc, Kanagawa, Japan). All rats received atropine (0.05 mg/mL/kg) for suppression of mucus production and an analgesic (flunixin 2.5 mg/mL/kg) by *s.c*. injection prior to the operation. The cervical skin region was incised under isoflurane anesthesia after the disinfectant using povidone-iodine and then the paratracheal muscles was separated to expose the trachea. The right and left thyroid glands accompanied with the parathyroid glands on the trachea surface was gently removed, and after adequate hemostasis, the surgical site was closed, and was disinfected with 5% chlorhexidine solution. The postoperative rats were maintained properly on a warm incubator (37 °C) for body temperature recovery until awakening, and received an analgesic (flunixin 2.5 mg/mL/kg) by *s.c.* injection once daily for 2 days after surgery. Pellet food (CE-2; CLEA Japan, Inc., Tokyo, Japan) containing 1.10% Ca and 1.09% Pi moisturized with tap water was supplied inside each cage for easy access. postsurgical rats exhibiting serum Ca (sCa) levels less than 8.0 mg/dL were selected for subsequent peptide injection studies. TPTX rats were injected *i.v.* or *s.c*. with vehicle or vehicle containing a PTH peptide, or orally treated once daily with vehicle (medium-chain triglyceride; Chugai Pharma Manufacturing, Tokyo, Japan) or vehicle containing alfacalcidol (Chugai

Pharma Manufacturing) for 11 days. Blood samples were obtained from the tail or jugular vein immediately before and at times after injection. Urine samples at 0 to 8 hours or 8 to 24 hours, were collected in metabolic cages. sCa and urinary Ca (uCa), serum Pi (sPi) and urinary Pi (uPi), and creatinine (uCre) were measured with an automatic analyzer (7180; Hitachi, Ltd, Chiyoda, Tokyo, Japan). Urinary deoxypyridinoline (uDpD) which is a crosslink of type 1 collagen released during bone resorption was measured using a Metra DPD EIA kit (DS Pharma Biomedical, Osaka, Japan), and the data were normalized to the uCre concentrations. Serum FGF23 was measured using FGF23 ELISA assay (Immunodiagnostik AG, Bensheim, Germany). Serum $1,25(OH)_2D_3$ levels were determined by an ELISA (Immunodiagnostic System Ltd, Bolden, UK).

For pharmacokinetic studies, plasma samples were prepared in the presence of protease inhibitors (aprotinin, leupeptin, EDTA). Plasma levels of PTH(1–34) were assessed by ELISA assay (Human PTH(1–34) Specific ELISA Kit; Immutopics Inc, San Clemente, CA, USA), and plasma levels of M-PTH/PTHrP were assessed by ELISA assay (PTH-RP 1–34 Human Enzyme Immunoassay Kit; Peninsula Laboratories International, San Carlos CA, USA) using M-PTH/PTHrP peptides as standard solutions.

Monkeys. Male cynomolgus monkeys at age 3 to 4 years were purchased from Hamri Co. Ltd (Tokyo, Japan). Cynomolgus monkeys were randomly assigned and injected *s.c.* with either vehicle, M-PTH/PTHrP, or LA-PTH. Blood samples were collected from the saphenous vein and assessed for sCa or sPi levels.

Statistical analysis. Data are represented as the mean ± SEM and statistical significance was determined using JMP Ver.11 (SAS Institute Japan, Tokyo, Japan). A Dunnet test was performed to

assess the significant differences in the PTH(1–34), M-PTH/PTHrP, or LA-PTH groups compared with the vehicle groups. A Student's t test was used to assess the significance between two data sets (TPTX-vehicle versus sham). Values of $p < 0.05$ indicate significance.

Results

Binding and cAMP signaling properties of PTH/PTHrP hybrid peptides *in vitro* and calcemic actions in normal rats. The primary structures of the M-PTH/PTHrP hybrid peptides evaluated in this study are shown in Figure 10, and their PTHR1-binding properties, assessed in membranes prepared from COS-7 cells transfected to express the human PTHR1, as well as their cAMP signaling properties, assessed in GP-2.3 cells (HEK293 cells stably transfected to express the hPTHR1 and GloSensor cAMP reporter), are reported in Tables 4 and 5. Affinities at the R^G PTHR1 conformation were similar for all analogs tested, whereas each hybrid peptide bound to the R^0 conformation with an affinity several-fold higher than that of PTH(1–34), and only slight differences in affinity were detected between any of the hybrid analogs (Table 4 and 5). All M-PTH/PTHrP hybrid analogs exhibited more prolonged cAMP signaling responses on human PTHR1, as compared with PTH(1–34) and PTHrP(1–36) (Fig. 11).

Having established adequate receptor-binding properties *in vitro*, the author next tested the calcemic actions of the M-PTH/PTHrP hybrid analogs in normal rats. The peptides were administered by a single *i.v.* injection at a dose of 5.0 nmol/kg of body weight for each analog (Fig. 12 A–C), as well as at multiple doses (Fig. 13 A–C). M-PTH(1–11)/PTHrP(12–36) and M-PTH(1–14)/PTHrP(15–36) at 5 nmol/kg significantly increased blood iCa^{2+} levels at 1 hour, and further increased blood iCa^{2+} levels up to 6 hours after administration (Fig. 12 A). M-PTH(1–18)/PTHrP(19–36) increased blood iCa^{2+} at 1 hour, and sustained levels for up to 6 hours. M-PTH(1–17)/PTHrP(18–36), M-PTH(1–22)/PTHrP(23–36), M-PTH(1–26)/PTHrP(27–36), and M-PTH(1–30)/PTHrP(31–36) increased blood iCa^{2+} levels more transiently, with peak responses occurring at 1 to 2 hours, and then blood iCa^{2+} levels returning to basal levels gradually. As M-PTH(1–14)/PTHrP(15–36) exerted the most robust and prolonged calcemic action at the 5 mmol/kg dose, this analog was selected, hereafter referred to as

M-PTH/PTHrP, for further testing.

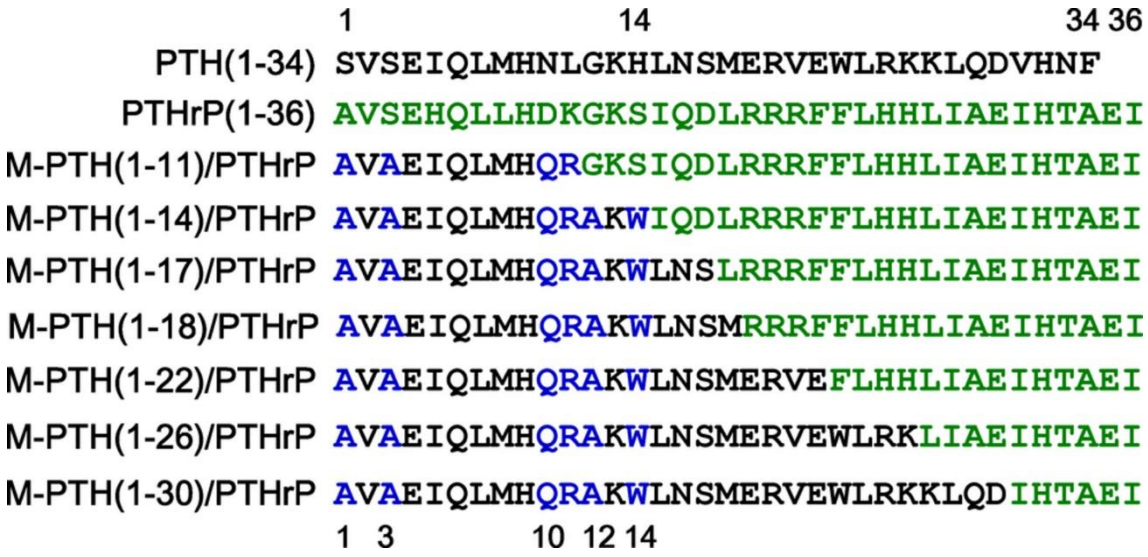

Figure 10. Primary structure of PTH, PTHrP, and M-PTH/PTHrP hybrid analogs. Amino acid sequences of human PTH(1–34), human PTHrP(1–36), and PTH/PTHrP hybrid analogs. PTH and PTHrP residues are colored black and green, respectively, and the N-terminal "M" modifications at positions 1, 3, 10, 11, 12, and 14 in PTH are colored blue. M-PTH(1–14)/PTHrP(15–36) analog is also referred to as M-PTH/PTHrP in the text.

Table 4. Binding to the RG and R^0 conformations of human PTHR1.

	R^0				R^G			
			p versus				*p* versus	
	IC_{50} (nM)	*n*	PTH(1–34)	PTHrP(1–36)	IC_{50} (nM)	*n*	PTH(1–34)	PTHrP(1–36)
PTH(1–34)	**10.4 ± 3.7**	**8**	**1.00**	**0.67**	**0.16 ± 0.08**	**8**	**1.00**	**0.30**
PTHrP(1–36)	**8.20 ± 3.41**	**3**	**0.67**	**1.00**	**0.07 ± 0.01**	**3**	**0.30**	**0.30**
M-PTH(1–11)/PTHrP(12–36)	**2.14 ± 0.47**	**3**	**0.06**	**0.22**	**0.55**	**2**		
M-PTH(1–14)/PTHrP(15–36)	**2.69 ± 0.99**	**3**	**0.08**	**0.24**	**0.67 ± 0.05**	**3**	**0.0006**	**0.0064**
M-PTH(1–17)/PTHrP(18–36)	**1.91 ± 0.39**	**4**	**0.06**	**0.20**	**0.23 ± 0.02**	**4**	**0.42**	**0.0000**
M-PTH(1–18)/PTHrP(19–36)	**1.66 ± 0.22**	**4**	**0.05**	**0.19**	**0.13 ± 0.02**	**4**	**0.72**	**0.02**
M-PTH(1–22)/PTHrP(23–36)	**7.80 ± 2.55**	**3**	**0.58**	**0.93**	**0.67 ± 0.02**	**3**	**0.0004**	**0.0001**
M-PTH(1–26)/PTHrP(27–36)	**1.73 ± 0.75**	**5**	**0.05**	**0.19**	**0.13 ± 0.04**	**5**	**0.73**	**0.21**
M-PTH(1–30)/PTHrP(31–36)	**2.98 ± 0.48**	**4**	**0.09**	**0.26**	**0.21 ± 0.03**	**4**	**0.60**	**0.013**

Equilibrium competition binding reactions were performed either in the presence (R^0) or absence (R^G) of GTPγS, and R^G reactions used membranes from cells transfected with a high-affinity $G\alpha_s$-dominant-negative mutant in addition to the PTHR1. Data are means ± SEM of the number of experiments indicated by n; *p* = Student's t test versus PTH(1–34) or PTHrP(1–36). IC_{50} values are peptide concentrations (nM) that resulted in 50% inhibition of binding of ^{125}I-labeled PTH(1–34) radioligand (R^0) or ^{125}I-labeled M-PTH(1–15) radioligand (R^G) to the hPTHR1 expressed in membranes of transiently transfected COS-7 cells.

Table 5. cAMP responses of human PTHR1 in GP-2.3 cells.

		p versus			*p* versus	
	EC_{50} (nM)	**PTH(1–34)**	**PTHrP(1–36)**	**E_{max} (%)**	**PTH(1–34)**	**PTHrP(1–36)**
PTH(1–34)	**1.4 ± 0.6**	**1.00**	**0.55**	**100 ± 0**	**1.00**	**0.81**
PTHrP(1–36)	**1.82 ± 0.45**	**0.55**	**1.00**	**99 ± 3**	**0.81**	**1.00**
M-PTH(1–11)/PTHrP(12–36)	**4.46 ± 1.27**	**0.088**	**0.13**	**103 ± 3**	**0.46**	**0.46**
M-PTH(1–14)/PTHrP(15–36)	**5.18 ± 1.07**	**0.029**	**0.044**	**105 ± 4**	**0.37**	**0.36**
M-PTH(1–17)/PTHrP(18–36)	**6.78 ± 1.98**	**0.067**	**0.084**	**105 ± 5**	**0.36**	**0.34**
M-PTH(1–18)/PTHrP(19–36)	**6.01 ± 1.59**	**0.055**	**0.073**	**107 ± 5**	**0.28**	**0.26**
M-PTH(1–22)/PTHrP(23–36)	**2.58 ± 0.26**	**0.12**	**0.20**	**104 ± 4**	**0.39**	**0.37**
M-PTH(1–26)/PTHrP(27–36)	**1.79 ± 0.41**	**0.56**	**0.97**	**106 ± 5**	**0.38**	**0.35**
M-PTH(1–30)/PTHrP(31–36)	**1.52 ± 0.14**	**0.81**	**0.56**	**106 ± 4**	**0.21**	**0.21**

EC_{50} values are peptide concentrations that stimulated 50% of the maximum response (E_{max}) for that peptide. Data were derived from the area-under-the-curves (AUC) of time-course luminescence responses measured at multiple doses and calculated as a % of the maximum AUC response attained in each assay with PTH(1–34), the average of which was $104 \pm 19 \times 10^5$ counts per second (cps) • min, and the corresponding basal value (not subtracted) was $0.52 \pm 0.13 \times 10^{-8}$ cps • min. Data are means ± SEM of four experiments; *p* values determined by Student's t-test compare responses to PTH(1–34) and PTHrP(1–36). cAMP responses were measured in GP-2.3 cells (HEK293 cells stably transfected to express the hPTHR1 and GloSensor cAMP reporter).

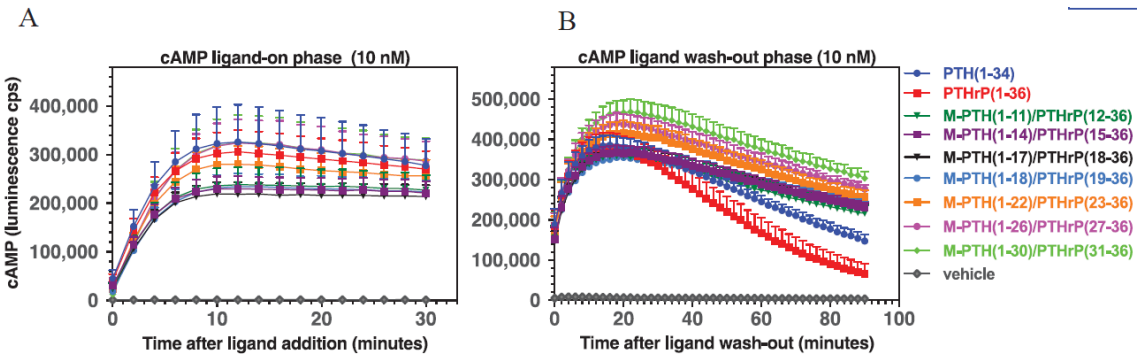

Figure 11. PTH ligand-induced cAMP-signaling responses in GP-2.3 cells. Time course of the cAMP-dependent luminescence response measured at 2-minute intervals in the presence of each ligand at 10 nM (Ligand on-phase) and B) Time course of the cAMP-dependent luminescence response measured at 2-minute intervals after washout of unbound ligand (Ligand wash-out phase). GP-2.3 cells preloaded with luciferin were treated with a concentration of PTH ligand at a concentration of 10 nM for 30 min, and cAMP-dependent luminescence was measured at two-minute intervals (ligand-on phase). The cells were then removed from the plate reader, rinsed twice with media to remove unbound ligand, and then fresh media containing luciferin, but lacking ligand was added and luminescence was assessed for additional 90 min (Ligand wash-out phase). Data are means (± SEM) of four experiments, each performed in triplicate.

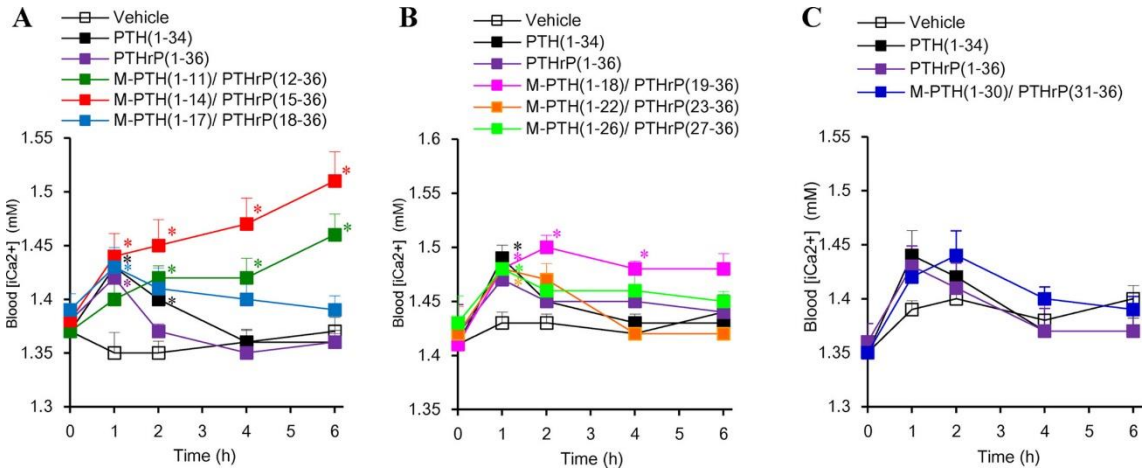

Figure 12. Calcemic actions of M-PTH/PTHrP hybrid analogs in normal rats. M-PTH/PTHrP hybrid analogs, PTH(1–34) and PTHrP(1–36) at 5.0 nmol/kg were *i.v.* administered, and blood ionized Ca (iCa^{2+}), collected from the tail vein, was measured at the indicated time points. (A) M-PTH(1–11)/PTHrP(12–36) to M-PTH(1–17)/PTHrP(18–36) hybrid analogs in experiment 1. (B) M-PTH(1–18)/PTHrP(19–36) to M-PTH(1–26)/PTHrP(27–36) in experiment 2. (C) M-PTH(1–30)/PTHrP(31–36) in experiment 3. Data are means ± SEM; n = 6. *$p < 0.05$ versus vehicle.

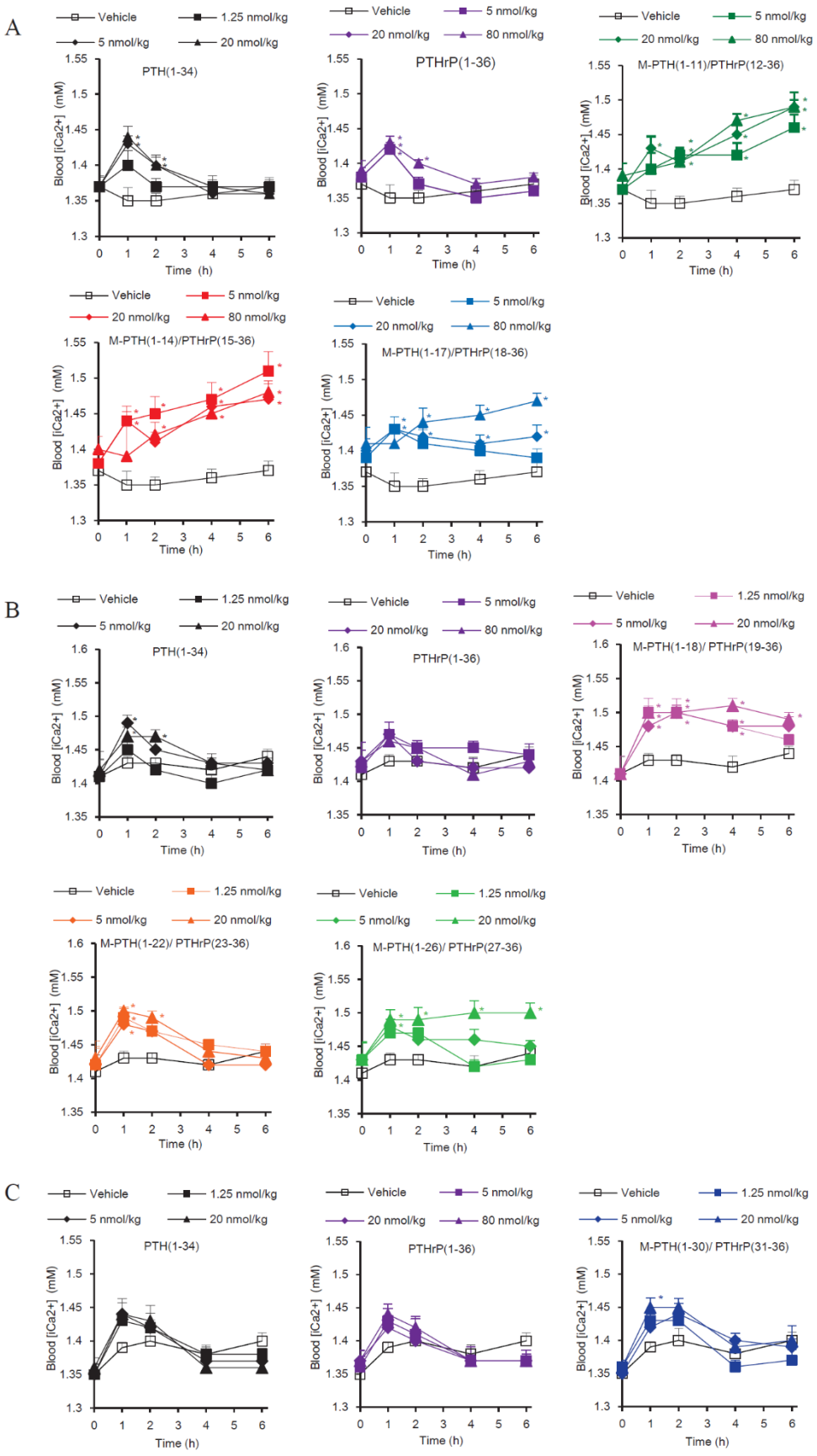
A
Vehicle
1.25 nmol/kg
5 nmol/kg
20 nmol/kg
PTH(1-34)
Blood [iCa2+] (mM)
Time (h)
Vehicle
5 nmol/kg
20 nmol/kg
80 nmol/kg
PTHrP(1-36)
Blood [iCa2+] (mM)
Time (h)
Vehicle
5 nmol/kg
20 nmol/kg
80 nmol/kg
M-PTH(1-11)/PTHrP(12-36)
Blood [iCa2+] (mM)
Time (h)
Vehicle
5 nmol/kg
20 nmol/kg
80 nmol/kg
M-PTH(1-14)/PTHrP(15-36)
Blood [iCa2+] (mM)
Time (h)
Vehicle
5 nmol/kg
20 nmol/kg
80 nmol/kg
M-PTH(1-17)/PTHrP(18-36)
Blood [iCa2+] (mM)
Time (h)
B
Vehicle
1.25 nmol/kg
5 nmol/kg
20 nmol/kg
PTH(1-34)
Blood [iCa2+] (mM)
Time (h)
Vehicle
5 nmol/kg
20 nmol/kg
80 nmol/kg
PTHrP(1-36)
Blood [iCa2+] (mM)
Time (h)
Vehicle
1.25 nmol/kg
5 nmol/kg
20 nmol/kg
M-PTH(1-18)/ PTHrP(19-36)
Blood [iCa2+] (mM)
Time (h)
Vehicle
1.25 nmol/kg
5 nmol/kg
20 nmol/kg
M-PTH(1-22)/ PTHrP(23-36)
Blood [iCa2+] (mM)
Time (h)
Vehicle
1.25 nmol/kg
5 nmol/kg
20 nmol/kg
M-PTH(1-26)/ PTHrP(27-36)
Blood [iCa2+] (mM)
Time (h)
C
Vehicle
1.25 nmol/kg
5 nmol/kg
20 nmol/kg
PTH(1-34)
Blood [iCa2+] (mM)
Time (h)
Vehicle
5 nmol/kg
20 nmol/kg
80 nmol/kg
PTHrP(1-36)
Blood [iCa2+] (mM)
Time (h)
Vehicle
1.25 nmol/kg
5 nmol/kg
20 nmol/kg
M-PTH(1-30)/ PTHrP(31-36)
Blood [iCa2+] (mM)
Time (h)

Figure 13. *In vivo* calcemic actions of M-PTH/PTHrP hybrid analogs in normal rats. The indicated M-PTH/PTHrP hybrid analogs along with PTH(1–34) and PTHrP(1–36) controls, were administered at the indicated doses by *i.v.* injection, and at the indicated time points blood was collected from the tail vein and measured for iCa^{2+}. Panels A–C represent three separate experiments. Data are means ± SEM; n = 6 or 4 (80 nmol/kg of M-PTH(1–11)/PTHrP(12–36), M-PTH(1–14)/PTHrP(12–36), M-PTH(1–17)/PTHrP(18–36) and 1.25 nmol/kg of M-PTH(1–30)/PTHrP(31–36)). $*p < 0.05$ versus Vehicle.

In vivo **calcemic actions of M-PTH/PTHrP in thyroparathyroidectomized rats by a single administration.** The author then evaluated the capacity of M-PTH/PTHrP to modulate blood iCa^{2+} levels in TPTX rats by a single *i.v*. administration and in comparison with PTH(1–34) (Fig. 14 A). Normal blood iCa^{2+} levels are around 1.3 mM (data not shown here), but these TPTX rats exhibit moderate hypocalcemia in the basal state as shown in Fig. 14, as nor and thus represent a model of surgical hypoparathyroidism. Injection of M-PTH/PTHrP at each of two doses resulted in a significant increase in blood iCa^{2+} levels. Whereas the higher dose of 5.0 nmol/kg resulted in frank hypercalcemia (iCa^{2+} >1.6 mM) by 24-hour post-injection, the lower dose of 1.25 nmol/kg restored blood iCa^{2+} levels to nearly the normal level (approximately 1.2 mM) by 6 hours, and the restorative effect persisted for up to 24 hours. At the even higher dose of 20 nmol/kg, PTH(1–34) produced a much smaller and more transient increase in blood iCa^{2+}.

The author then compared the pharmacokinetic properties of M-PTH/PTHrP and PTH(1–34) by *i.v*. injecting the peptides at equivalent doses (10 nmol/kg) into normal rats and measuring the blood concentrations of the peptides at times after injection by ELISA immunoassay (Fig. 14 B). Initial experiments established the M-PTH/PTHrP analog cross-reacted adequately with an ELISA assay targeted to PTHrP. Upon *i.v*. injection, each peptide disappeared rapidly from the circulation, such that the plasma concentrations declined to the lowest detection level by the 60-min time point. This rapid decline in serum ligand concentrations, coupled with a prolonged pharmacodynamic profile of M-PTH/PTHrP observed in intact and TPTX rats, is consistent with the rapid clearance rate and prolonged calcemic responses observed for LA-PTH and similar M-PTH analogs in previous studies (Okazaki et al., 2008; Shimizu et al., 2016a).

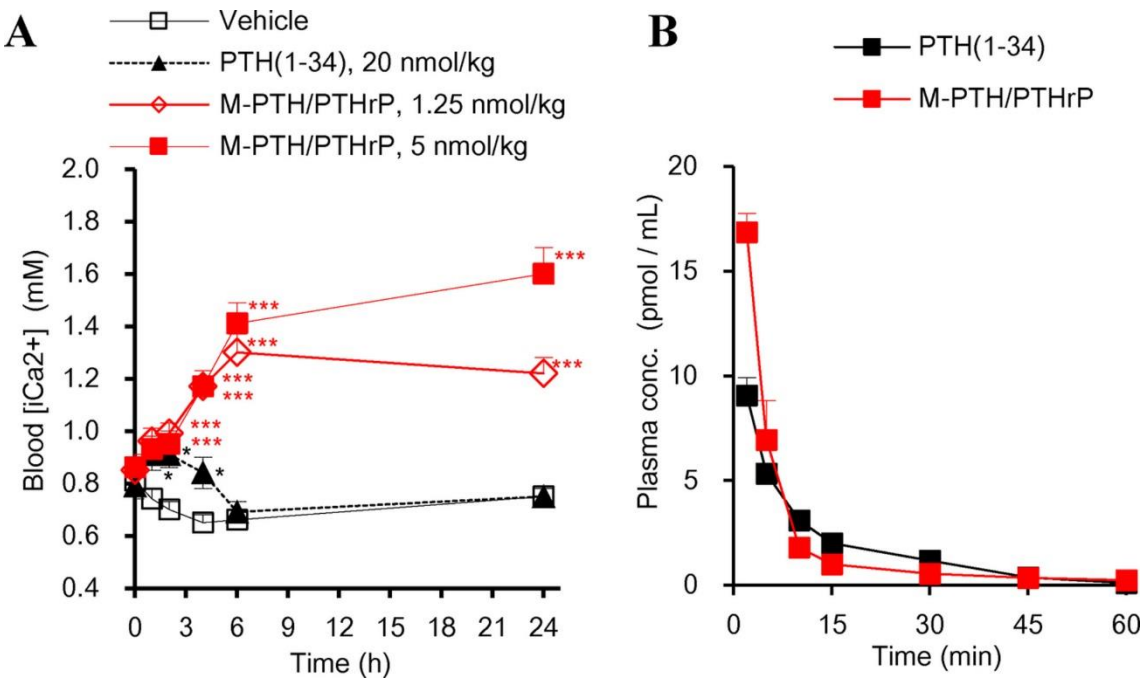

Figure 14. Pharmacodynamic and pharmacokinetic profiles of M-PTH/PTHrP and PTH(1–34) in rats. (A) Effects of M-PTH/PTHrP and PTH(1–34) on blood ionized Ca (iCa^{2+}) in TPTX rats by *i.v.* injection. M-PTH/PTHrP and PTH(1–34) were injected intravenously in TPTX rats at the indicated doses, and blood samples were collected from the tail vein measured for ionized Ca; data are means ± SEM; n = 5 or 3 [PTH(1–34)]. $*p < 0.05$, $**p < 0.01$, $***p < 0.005$ M-PTH/PTHrP or PTH(1–34) versus TPTX-vehicle. Blood iCa^{2+} in TPTX rats injected with M-PTH/PTHrP at 1.25 and 5.0 nmol/kg at 1 hour were statistically higher than those in vehicle-injected TPTX rats ($*p < 0.05$). (B) Pharmacokinetics of M-PTH/PTHrP and PTH(1–34). M-PTH/PTHrP and PTH(1–34) each at a dose of 10 nmol/kg were *i.v.* administered, and blood samples were collected from the jugular vein in the presence of proteinase inhibitors (Aprotinin, Leupeptin, and EDTA) and the plasma samples were assessed for peptide concentration using a hPTHrP(1–34)-targeted EIA for M-PTH/PTHrP and an hPTH(1–34)-targeted ELISA for PTH(1–34). Data are means ± SEM; n = 4 (M-PTH/PTHrP) or 3 [PTH(1–34)].

Effects of repeated daily administrations of M-PTH/PTHrP in thyroparathyroidectomized rats.

Next, the author studied the effects of M-PTH/PTHrP on total sCa in comparison with the vitamin D analog, alfacalcidol (1α-hydroxycholecalciferol), over a course of 12 days in TPTX rats. TPTX control showed lower in sCa than sham control and no significant changed in uCa, serum $1,25(OH)_2D_3$, and urinary bone resorption marker, uDpD. M-PTH/PTHrP dose-dependently increased sCa levels, as measured at 8 and 24 hours after the last administration on day 12 (Fig. 15 A, B). At a dose of 4.0 nmol/kg, M-PTH/PTHrP resulted in sCa levels that were comparable to those in the sham-operated control group, whereas uCa levels, measured at the intervals of 0 to 8 hours and 8 to 24 hours, remained low (Fig. 15 C, D). At the 8.0 nmol/kg dose of M-PTH/PTHrP, frank hypercalcemia was observed at 8 hours after administration, and uCa at 0 to 8 hours, and uDpD at 0 to 24 hours increased significantly after the last administration (Figs. 15 C,D, and 16 B). Daily administration of alfacalcidol also dose-dependently increased sCa levels, and the higher dose of 0.2 μg/kg increased sCa to levels comparable to those of the sham group; however, this dose of alfacalcidol was accompanied by high uCa excretion levels at both 0- to 8- and 8- to 24-hour time intervals. No significant change in serum $1,25(OH)_2D_3$ was observed among all groups (Fig. 16 A).

Compared with the sham control animals, the TPTX rats exhibited elevated urine levels of sPi, and daily injection with M-PTH/PTHrP dose dependently decreased these levels, with the 4.0 nmol/kg dose achieving a sPi level that was comparable to that of the sham control at 8 and 24 hours (Fig. 17 A,B). This lowering of sPi was accompanied by a significant increase in uPi excretion over the 0- to 8-hour interval but not over the 8- to 24-hour period (Fig. 17 C, D). Alfacalcidol also normalized sPi levels, especially at the 0.2 μg/kg dose, with a significant increase of uPi excretions between 8- to 24-hour period, although it did not change between 0- to 8-hour period. Serum levels of FGF23 in TPTX control dramatically decreased comparing in sham control consistent with previous report (Saito et al., 2005). As it has been reported that FGF23 is induced by both PTH and sCa levels (David et al., 2013;

Rhee et al., 2011), the reduction of serum FGF levels therefore would be occurred by conditions with absent of PTH or hypocalcemia. M-PTH/PTHrP at 4.0 and 8.0 nmol/kg and alfacalcidol at 0.2 μg/kg significantly increased the levels of serum FGF23 (Fig. 16 C). Consistent with a previous report regarding strong induction of FGF23 by $1,25(OH)_2D_3$, (Saito et al., 2005) alfacalcidol especially at the dose of 0.2 μg/kg promoted higher serum FGF23 levels more than 10-fold than TPTX control.

Despite of the effect in decrease of sPi, both alfacalcidol and M-PTH/PTHrP did not increase uPi in the 0- to 8-hour or 8- to 24-hour period, respectively. The reason for the inconsistency between sPi and uPi is unclear but Pi load such as intestinal Pi absorption could have been in low levels through the experimental day. It was possibly that multiple blood and urine samplings over time might have made TPTX rats lower food intake. PTH acts directly on the proximal tubule to increase uPi excretion in early, while alfacalcidol promotes slower uPi excretion via induction of FGF23. That could be the reason for the time differences between PTH and alfaclcidol in the effect on uPi.

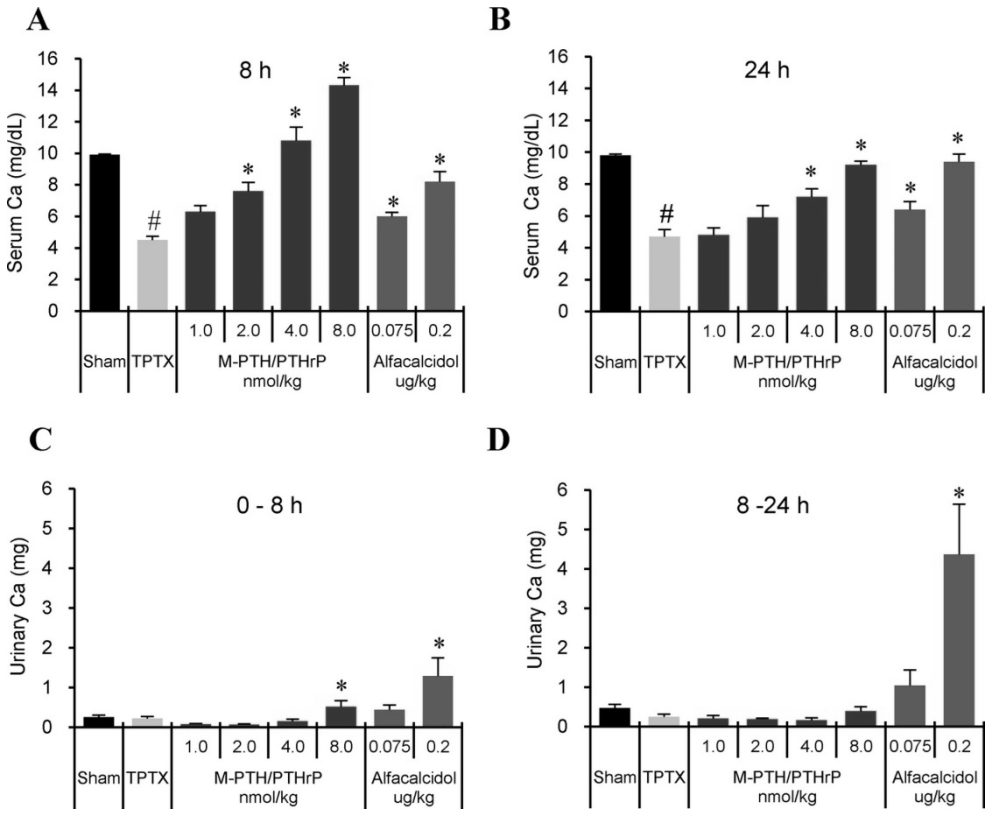

Figure 15. Effects of 11-day treatment (12-day study) with M-PTH/PTHrP or alfacalcidol on serum Ca (sCa) in thyroparathyroidectomized (TPTX) rats. TPTX rats were treated for 11 days with daily *s.c.* injection of either vehicle or M-PTH/PTHrP, or with daily oral alfacalcidol at the indicated doses, and sham-surgery control rats were *s.c.* injected daily with vehicle. The levels of Ca in serum and urine were assessed. Blood samples were collected from the jugular vein at 8 hours (A) and at 24 hours (B) after the last treatment administration, and assessed for total sCa. Total urine was collected in metabolic cages over the time intervals of 0 to 8 hours (C), and 8 to 24 hours (D) and assessed for total urinary Ca. Data are means ± SEM; n = 6 or 5 (2.0 and 4.0 nmol/kg of M-PTH/PTHrP); *$p < 0.05$ M-PTH/PTHrP versus TPTX-vehicle; #$p < 0.05$ TPTX vehicle versus sham.

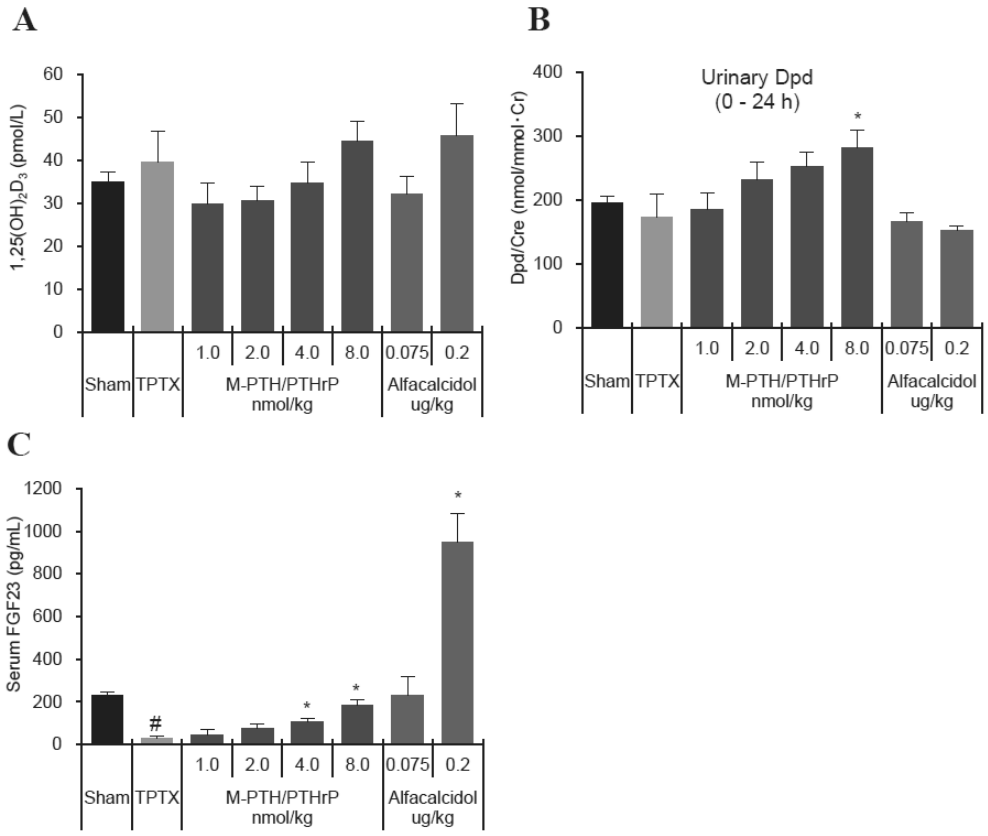

Figure 16. Effects of 11 days treatment (12 days study) of M-PTH/PTHrP on serum $1,25(OH)_2D_3$, urinary deoxypyridinoline (Dpd) and serum FGF23 in TPTX rats. Serum and urine samples obtained from the TPTX and sham control rats of the two-week daily-administration experiment shown in Figure 15 were analyzed by ELISA for the indicated markers. A) serum $1,25(OH)_2D_3$. B) urinary deoxypyridinoline (DpD)/Cre. C) serum FGF23. Data are means ± SEM; n = 6 or 5 (2.0 and 4.0 nmol/kg of M-PTH/PTHrP); *$p < 0.05$ M-PTH/PTHrP versus TPTX-vehicle, #$p < 0.05$ TPTX-vehicle versus sham.

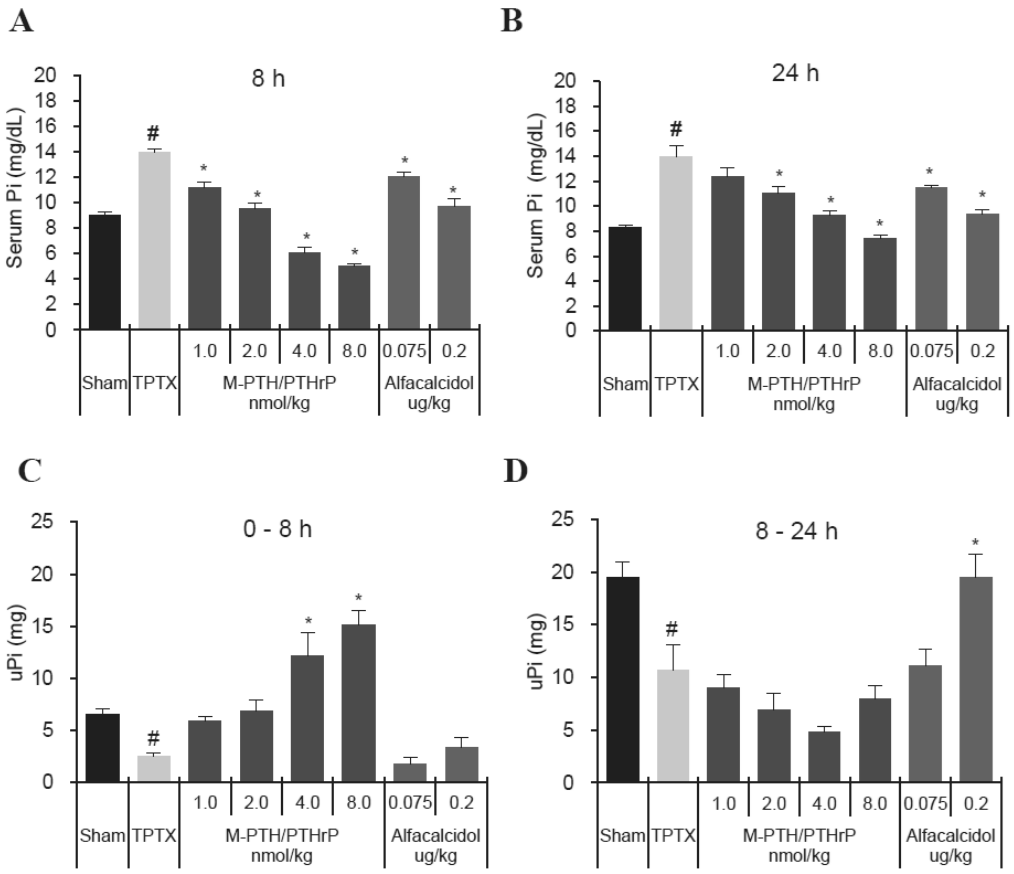

Figure 17. Effects of 11 days treatment (12 days study) of M-PTH/PTHrP on serum and urine inorganic phosphorus in TPTX rats. Serum and urine samples obtained from the TPTX and sham control rats of the two-week daily-administration experiment shown in Figure 15 were analyzed for total inorganic phosphate (Pi). Data are means ± SEM; n = 6 or 5 (2.0 and 4.0 nmol/kg of M-PTH/PTHrP); *$p < 0.05$ M-PTH/PTHrP versus TPTX-vehicle, #$p < 0.05$ TPTX-vehicle versus sham.

Optimizing solubility of the M-PTH/PTHrP scaffold to derive LA-PTH. In the course of this work, the author found that several of the hybrid analogs containing the C-terminal portion of PTHrP, including M-PTH/PTHrP, as well as PTHrP(1–36) itself, were poorly soluble at high concentrations (> approximately 0.3 mg/mL) in aqueous buffers at neutral pH. This led the author to investigate amino acid substitutions in the C-terminal PTHrP sequence that could improve peptide solubility yet preserve functional activity. The author first assessed for functional effects utilizing the PTHrP(1–28) scaffold peptide, as critical residues of receptor binding are known to be located in the 15–28 domain. An initial alanine scan through the (15–28) segment of PTHrP(1–28) revealed that positions 18, 22, 25, and 26 were tolerant of alanine replacement, for both PTHR1 binding and stimulating cAMP formation (Fig. 18 A,B). A subsequent "Type" substitution analysis, by which the author introduced at each of those four sites, a representative amino acid of each of the main side chain biochemical groups (eg, aromatic, hydrophobic, charged, polar), revealed that each of the four sites, particularly, 18, 22, and 26, were broadly tolerant of substitution (Fig. 18 C,D). The author then explored various combinations of residues at 18, 22, and 26 and identified Ala18, Ala22, and Lys26 as a combination that when introduced into the full-length scaffold peptide, M-PTH(1–14)/PTHrP(15–36), preserved or even enhanced PTHR1-binding affinity (Fig. 18 C) and cAMP-stimulating activity, (Fig. 19, Table 6) and improved peptide solubility, (Fig. 18 E) and thus resulted in the analog LA-PTH.

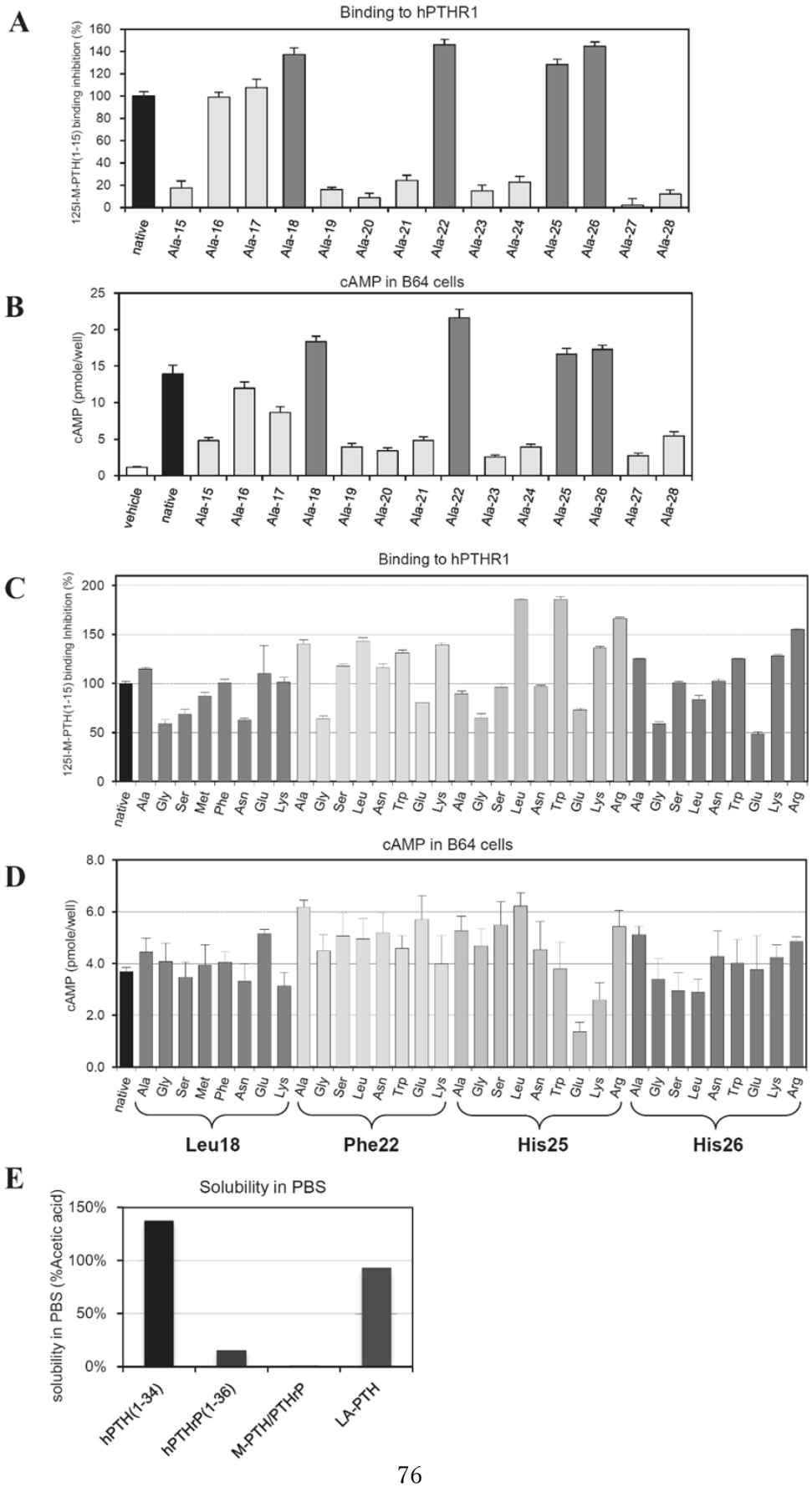
A
Binding to hPTHR1
125I-M-PTH(1-15) binding inhibition (%)
native
Ala-15
Ala-16
Ala-17
Ala-18
Ala-19
Ala-20
Ala-21
Ala-22
Ala-23
Ala-24
Ala-25
Ala-26
Ala-27
Ala-28
B
cAMP in B64 cells
cAMP (pmole/well)
vehicle
native
C
Binding to hPTHR1
125I-M-PTH(1-15) binding Inhibition (%)
D
cAMP in B64 cells
cAMP (pmole/well)
Leu18
Phe22
His25
His26
E
Solubility in PBS
solubility in PBS (%Acetic acid)
hPTH(1-34)
hPTHrP(1-36)
M-PTH/PTHrP
LA-PTH

Figure 18. Substitution analysis of the 15–25 region of PTHrP(1–28) and optimization of M-PTH(1–14)/PTHrP(15–36) solubility. (A) Alanine-scan analysis of the (15–28) region of PTHrP(1–28) for effects on binding to the R^G conformation of the hPTHR1. Native PTHrP(1–28) and analogs thereof containing the indicated single alanine substitutions were assessed at a concentration of 1 nM for the capacity to inhibit binding of ^{125}I-M-PTH(1–15) tracer radioligand to membranes prepared from COS-7 cells transiently transfected to express the hPTHR1 and a high affinity GγS negative-dominant mutant. Data are expressed as a percent of the inhibition of specific binding observed with native PTHrP(1–28), which was 39 ± 2 percent of the complete inhibition observed with 3 μM unlabeled M-PTH(1–15). (B) The same peptides were assessed at a concentration of 3 nM for the capacity to stimulate cAMP formation in HKRK-B64 cells (LLC-PK1 cells stably expressing the hPTHR1, cAMP measured by RIA). The basal cAMP levels were 1.2 ± 0.1 pmol/well. Data in A and B are means (±SEM) of three experiments, each performed in triplicate or quadruplicate. (C) Type-substitution analysis, in which amino acids with varying side chain structures (e.g., small, bulky, charged, aromatic) are introduced, was performed on residue positions 18, 22, 25 and 26 of PTHrP(1–28), which were identified as tolerant to Ala substitution in the experiments of panels A and B, and the analogs were assessed at a concentration of 1.0 nM for the capacity to inhibit binding of ^{125}I-M-PTH(1–15) to the hPTHR1 (R^G) in COS-7 cell membranes. Data are means (±SEM) of triplicate determinations expressed as a percent of the inhibition of binding observed with native PTHrP(1–28), which was, 41 ± 1 percent of the maximum binding inhibition (NSB, subtracted) observed with unlabeled M-PTH(1–15). (D) The same analogs as in C were assessed at a 3.0 nM concentration for the capacity to stimulate cAMP formation in HKRK-B64 cells. Data are means (± SEM) of three experiments, each performed in duplicate. Basal cAMP levels were 0.3 ± 0.1 pmol/well. (E) Peptide solubility in PBS was assessed by incubating each indicated peptide at a concentration of 1.5 mg/ml in either PBS at pH 7.4 or in 10 mM acetic acid for 24 h, and then, after centrifugation (15,000 × g/ 20 mins.) determining the peptide concentrations of the upper phases and expressing each peptide concentration in the PBS supernatants as a percent of the concentration of the same peptide in the acetic acid supernatant. Data are means (± SEM) of duplicate determinations of a single experiment representative of three others.

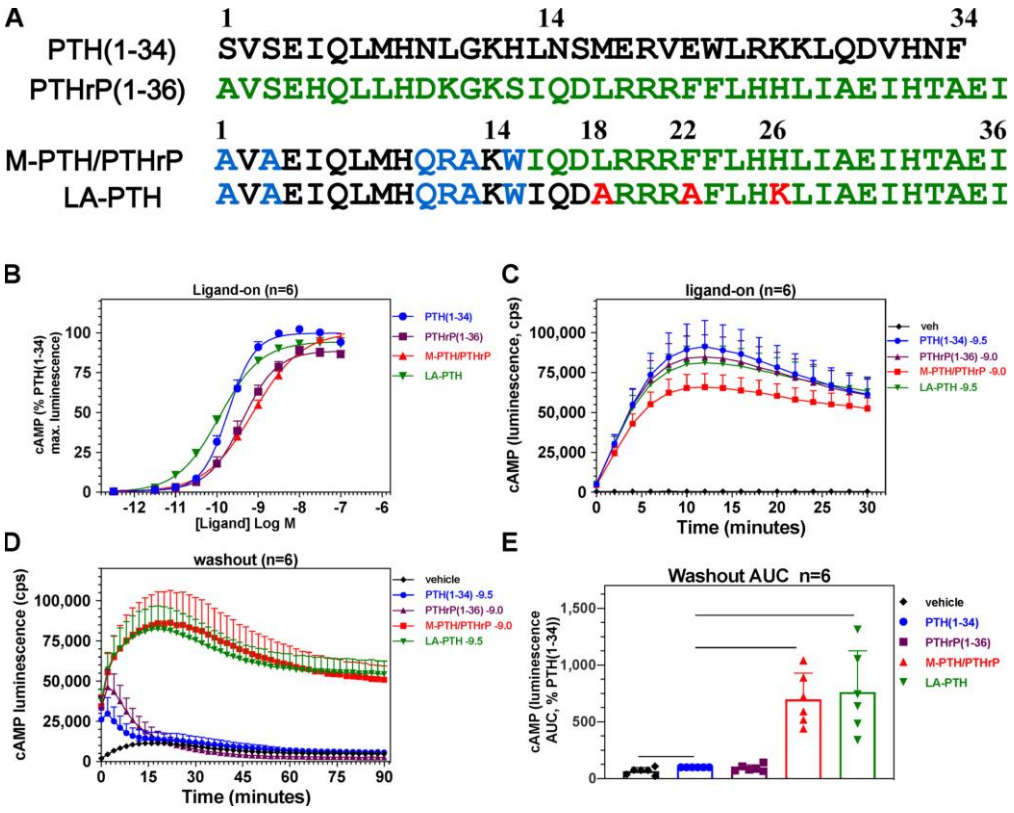

Figure 19. Sequence and functional comparison of M-PTH/PTHrP and LA-PTH in a rat osteoblast-derived cell line. (A) Sequence of PTH(1–34), PTHrP(1–36) and hybrid analogs, M-PTH/PTHrP, and LA-PTH. (B) Dose–response for stimulation of cAMP signaling in a UMR106-derived rat osteoblastic cell line (UGS-56 cells). (C) Time course of the cAMP-dependent luminescence response measured at 2-min intervals in the presence of a near-EC_{50} concentration of each ligand: PTH (1–34) (0.3 nM), PTHrP (1–36) (1.0 nM), M-PTH/PTHrP (1 nM), and LA-PTH (0.3 nM). (D) Time course of the cAMP-dependent luminescence response measured in the same cells as in (C), but after washout of unbound ligand. (E) Area-under-the-curve (AUC) values of the washout responses shown in (D). Data are means (± SEM) of six experiments, each performed in triplicate. Dose–response EC_{50} and washout-AUC values are reported in Table 6.

Table 6. cAMP Responses in UMR106/GloSensor cells.

Ligands	EC_{50} (nM)		E_{max} (%)		Washout AUC (%)	
		p		*p*		*p*
PTH(1–34)	**0.20 ± 0.03**	**1.000**	**100 ± 0.4**	**1.000**	**100 ± 0**	**1.000**
PTHrP(1–36)	**0.46 ± 0.11**	**0.062**	**88.4 ± 2.8**	**0.007**	**92 ± 11**	**0.530**
M-PTH/PTHrP	**0.72 ± 0.13**	**0.012**	**96.2 ± 2.4**	**0.143**	**700 ± 85**	**< 0.0001**
LA-PTH	**0.12 ± 0.01**	**0.020**	**94.7 ± 2.9**	**0.105**	**763 ± 135**	**0.001**

Responses at each ligand concentration were calculated as the area-under-the-curve (AUC) values obtained from the time-course plots of cAMP-dependent luminescence versus time measured over 30 min, and then expressed as a percent of the maximum AUC response observed for PTH(1–34) in each assay, the average of which was $3.13 \pm 0.66 \times 10^6$ counts per second (cps) • min; the corresponding minimum value (not subtracted) was $3.58 \pm 2.16 \times 10^8$ cps • min. Washout values report the AUC of the cAMP-dependent luminescence versus time measured for each ligand at a near EC_{50}-concentration over 90 min and expressed as a percent of the response observed for PTH(1–34) (0.3 nM) in each assay, the average of which was $0.96 \pm 0.87 \times 10^6$ cps • min; and the corresponding value in vehicle-treated cells (not subtracted) was $0.48 \pm 0.1 \times 10^6$ cps • min. Data are means ± SEM of six experiments, with duplicate wells in each; *p* = Student's t test versus PTH(1–34). cAMP responses were measured in rat osteoblastic UMR-106/GloSensor (UGS-56) cells. EC_{50} values are peptide concentrations (nM) that stimulated 50% of the maximum response (E_{max}) observed for that peptide.

Efficacy of M-PTH/PTHrP and LA-PTH in thyroparathyroidectomized rats and normal monkeys. The author then compared the capacity of LA-PTH to modulate sCa and sPi levels in comparison with M-PTH/PTHrP by a single *i.v.* administration in TPTX rats (Fig. 20 A, B). LA-PTH and M-PTH/PTHrP caused comparable increases in total sCa levels over the sham control group that peaked at 10 hours post-injection and persisted at near the sham-control levels by 48 hours, until returning to near baseline levels by the 72-hour time point. In parallel, the sPi levels were reduced and persisted near the normal sham-control levels for at least 72 hours after the dose administration. The efficacy and the duration of the responses induced by LA-PTH in these TPTX rats were thus comparable to those induced by the M-PTH/PTHrP parent hybrid peptide.

The effects of LA-PTH and M-PTH/PTHrP on total sCa and sPi levels in normal monkeys were further compared. Upon a single *s.c.* injection, both LA-PTH and M-PTH/PTHrP significantly increased sCa levels by 24 hours after administration, and each analog similarly maintained sCa at higher levels for up to 48 hours (Fig. 21 A, B). The hypophosphatemic effects of LA-PTH in monkeys were also comparable to those of M-PTH/PTHrP as each analog decreased sPi levels for up to 72 hours after injection. These results confirmed that LA-PTH retains the strong calcemic and hypophosphatemic effects of the parent hybrid peptide, M-PTH/PTHrP, in TPTX rats as well as in normal monkeys.

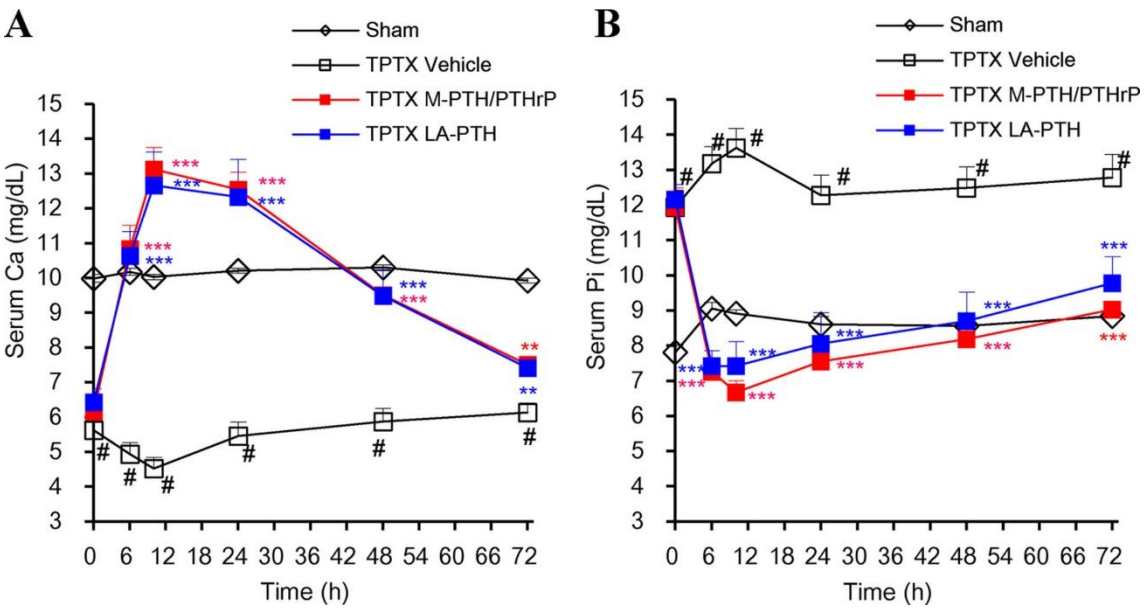

Figure 20. Effects of M-PTH/PTHrP and LA-PTH on serum Ca (sCa) and serum Pi (sPi) in thyroparathyroidectomized (TPTX) rats. TPTX rats were *i.v.* injected with vehicle, LA-PTH, or M-PTH/PTHrP. Each peptide was at a dose of 1.25 nmol/kg, and sham control rats were injected with vehicle. Blood samples were collected from the jugular vein and assessed for total Ca (A) and Pi (B). Data are means ± SEM; n = 6; *$p < 0.05$, **$p < 0.01$, ***$p < 0.005$ LA-PTH and M-PTH/PTHrP versus vehicle.

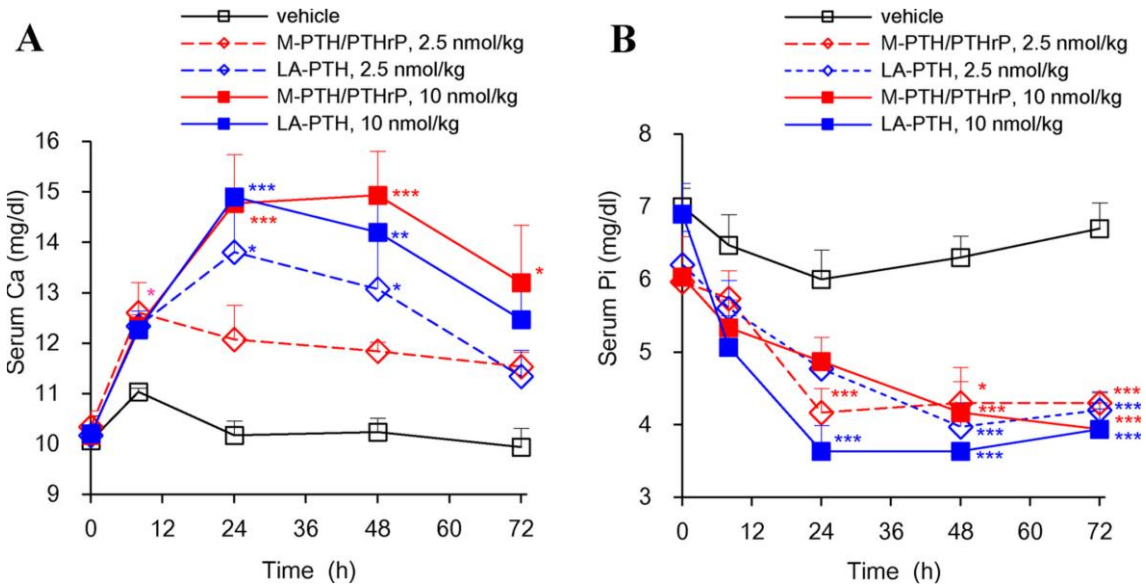

Figure 21. Effects of M-PTH/PTHrP and LA-PTH on total serum Ca (sCa) and serum Pi (sPi) in normal monkeys. Cynomolgus monkeys were *s.c.* injected with either vehicle, LA-PTH, or M-PTH/PTHrP. Each peptide was at a dose of 2.5 or 10 nmol/kg, and blood samples were collected from the saphenous vein and assessed for total sCa (A) and sPi (B). Data are means ± SEM; n = 3; *$p < 0.05$, **$p < 0.01$, ***$p < 0.005$, LA-PTH and M-PTH/PTHrP versus vehicle.

Discussion

In this study, the author systematically explored a series of hybrid molecules composed of PTH and PTHrP. The rationale in combining the M-PTH amino terminal region with the carboxyl terminal region of PTHrP to achieve enhanced binding and signaling activity on the PTHR1 was based on the evidence that the PTHrP(15–36) fragment binds with approximately twofold higher affinity to the amino-terminal ECD portion of the receptor than does the PTH(15–34) fragment (Pioszak et al., 2009), and that N-terminal PTH fragments with the "M" modifications, such as M-PTH(1–14) and M-PTH(1–11), exhibit enhanced binding and signaling interactions with the transmembrane domain region of the PTHR1, as shown by previous structure–activity relationship studies (Shimizu et al., 2001a; Shimizu et al., 2000b; Shimizu et al., 2001b). The hybrid analog that proved most active *in vivo* in Ca-elevating potency was M-PTH(1–14)/PTHrP(15–36). Furthermore, repeated administrations of M-PTH/PTHrP at an optimal dose (4.0 nmol/kg) normalized sCa levels without increasing uCa, whereas alfacalcidol increased sCa levels, but was associated with hypercalciuria. These results support the concept that the M-PTH/PTHrP class of ligands could have beneficial pharmacological effects over alfacalcidol in the treatment of hypoparathyroidism, as suggested by a similar comparative study about the effects of a PTHR1 small molecule agonist and alfacalcidol on sCa and uCa has been reported previously (Tamura et al., 2016).

The low solubility observed for M-PTH/PTHrP and related analogs containing the C-terminal PTHrP(15–36) sequence when prepared at high concentrations in aqueous neutral buffer led the author to explore amino acid substitutions that would improve solubility yet preserve activity on the PTHR1. Using PTHrP(1–28) as a scaffold peptide for substitution analysis, the author thus identified three changes: Leu18➔Ala, Phe22➔Ala, and His26➔Lys, which when combined into the MPTH(1–14)/PTHrP(15–36) peptide had the desired effect. The resulting analog,

[Ala^{1,3,12,18,22},Gln^{10},Arg^{11},Trp^{14},Lys^{26}]-PTH(1–14)/PTHrP(15–36), termed LA-PTH, was thus found to be equally potent to the M-PTH/PTHrP parent hybrid peptide *in vitro* and *in vivo* (Figs. 19–21), and is shown in a previous report to satisfactorily normalize sCa levels in TPTX rats without increases in uCa or causing adverse changes in bone structural parameters, including cortical porosity, when administered daily for 4 weeks at an optimal dose (Shimizu et al., 2016a). The capacity of LA-PTH and PTH analogs of this class to form highly stable complexes with the PTHR1, which underlies their prolonged pharmacodynamic actions, is highlighted by the recently reported high-resolution cryo-electron microscopy structure of LA-PTH bound to the PTHR1 and a partner heterotrimeric G protein (Zhao et al., 2019), as well as the X-ray crystallographic structure of a PTH(1–34) analog containing N-terminal modifications similar to those of LA-PTH bound to a thermo-stabilized PTHR1 in a G protein-uncoupled state (Ehrenmann et al., 2018). As in each case, the process of structure determination was likely facilitated by the stability provided the ligand analog. It will now be interesting to see, perhaps using computational modeling approaches, how other PTH and PTHrP analogs bind to the PTHR1, and how the binding modes at the PTHR1 may vary, depending on ligand structure. This would extend to the orally available small molecule PTHR1 agonist, PCO371 (Nishimura et al., 2020), which has been shown to restore sCa and lower sPi levels in TPTX rats (Tamura et al., 2016), and is currently being evaluated in an early-stage clinical trial for hypoparathyroidism.

Summary in chapter II

Prolonged signaling at the PTHR1 correlates with the capacity of a ligand to bind to a G protein-independent receptor conformation (R^0). As LA-PTH ligand holds interest as potential treatments for hypoparathyroidism, we explored the structural basis in the ligand for stable R^0 binding and prolonged cAMP signaling. A series of PTH/PTHrP hybrid analogs were synthesized and tested for actions *in vitro* and *in vivo*. Of the series, [Ala^{1,3,12},Gln^{10},Arg^{11},Trp^{14}]-PTH(1–14)/PTHrP(15–36) (M-PTH/PTHrP) bound with high affinity to R^0, induced prolonged cAMP responses in UMR106 rat osteoblast-derived cells, and induced the most prolonged increases in sCa in normal rats. Daily *s.c.* injection of M-PTH/PTHrP into TPTX rats, a model of hypoparathyroidims, normalized sCa without raising uCa. In contrast, oral alfacalcidol, a widely used treatment for hypoparathyroidism, normalized sCa, but induced frank hypercalciuria. M-PTH/PTHrP exhibited low solubility in aqueous solutions of neutral pH; however, replacement of Leu18, Phe22, and His26 with the less hydrophobic residues, Ala, Ala, and Lys, at those respective positions markedly improved solubility while maintaining bioactivity. Indeed, we recently showed that the resultant analog [Ala^{18,22},Lys^{26}]-M-PTH/PTHrP or LA-PTH, effectively normalizes sCa in TPTX rats and mediates prolonged actions in monkeys. These studies provide useful information for optimizing PTH and PTHrP ligand analogs for therapeutic development and also support further testing of LA-PTH for the patients with hypoparathyroidism.

Conclusion

JMC is a rare disease caused by heterozygous gain-of-function mutations in the PTHR1. Patients with JMC exhibit marked defects in bone development and bone turnover that result in short stature, limb deformities, mobility impairment, and chronic imbalance of blood/ urine Ca and Pi handling systems. There is no treatment option for JMC that directly targets the underlying molecular defect. In these studies, the author demonstrated that an inverse agonist ligand, [Leu^{11},dTrp^{12},Trp^{23},Tyr^{36}]-hPTHrP(7–36)NH_2, for the PTHR1 could ameliorate at least some of the bone and mineral ion defects that occur in this osteoblast-specific mouse model of JMC. These overall findings provide a proof-of-concept supporting for the notion that inverse agonist ligands targeted to the mutant PTHR1 variants of JMC can have efficacy *in vivo*. Further studies of such PTHR1 ligand analogs could help open paths toward the first treatment option for this debilitating skeletal disorder.

Hypoparathyroidism is an endocrine disorder in which the parathyroid glands cannot produce enough parathyroid hormone. Conventional therapy of hypoparathyroidism, Ca supplementation or/and activated vitamin D preparation, can increase of urinary excretion of Ca resulting in impaired renal function and reductions in the QOL of patients with hypoparathyroidism. PTH(1–84) has recently been approved as a treatment option for hypoparathyroidism. It would be expected to maintain serum Ca while requirements of Ca supplementation or/and activated vitamin D preparation by replacing the missing hormone. However, due to its short half-life, multiple injections are necessary to maintain serum Ca at a steady level. Novel treatment options that can stably normalize blood Ca levels without causing hypercalciuria by PTH action is needed for the patients with hypoparathyroidism. In these studies, the author identified the most potent PTH/PTHrP hybrid analog as M-PTH(1–14)/PTHrP(15–36) based on the concept that more potent ligands for R^0 state could have more prolonged calcemic action. M-PTH(1–14)/PTHrP(15–36) exhibits to control serum Ca and

serum Pi without excess urinary Ca excretion, and illustrates its superiority to treatment with active vitamin D analog. Moreover, the author modified the initial analog to improved solubility while retaining high R^0 binding affinity and finally identified LA-PTH as the best clinical candidate. LA-PTH could be a useful drug for hypoparathyroidism that can stably normalize blood Ca levels without causing hypercalciuria.

Currently, only three peptide agonists for the PTHR1, PTH(1–34), PTH(1–84) and abaloparatide, are clinically available for the treatment option of patients with osteoporosis and hypoparathyroidism. Considering the wide range of biological roles of PTHR1, to endow each ligand with suitable property for each disease biology could provide therapeutic options for diseases related to PTHR1 signaling widely. In these studies, the author showed potential applications of an inverse agonist for JMC and of LA-PTH for hypoparathyroidism, thus expanding a potential of the PTHR1 as an important drug target.

Peptide drugs, on the other hand, commonly have limitations in pharmacokinetics that have been recognized even with previous challenges of antagonist peptides for hyperparathyroidism as well as an inverse agonist for JMC. The process of modification of peptide ligands to generate long-acting PTH/PTHrP analog provides here one of the options to overcome the limitations by using the concept of a new prolonged cAMP signaling. Since it has been reported that the concept is shared with other GPCRs, the insights could be widely applied not only to PTHR1-related diseases but also widely to other GPCR related diseases.

In addition, considering current companion-animal health care, some of bone metabolic-related diseases such as CKD and ectopic hyperthyroidism in dogs and cats and bone fractures in racehorses and rabbits are still accompanied with difficulties to treat in some situations. Scientific insights obtained in a series of these studies would be useful to focus on the potential applications of ligands for the PTHR1 to above diseases in companion-animals health care.

Acknowledgments

The author would like to express the deep gratitude to the patients and their families for their providing invaluable information to help the author's in-depth understanding of the diseases at the beginning of this study.

The author sincerely appreciates Dr. Ken-ichi Otsuguro, Professor of Laboratory of Pharmacology, Faculty of Veterinary Medicine, Hokkaido University, Dr. Mitsuyoshi Takiguchi, Professor of Laboratory of Veterinary Internal Medicine, Faculty of Veterinary Medicine, Hokkaido University, and Dr. Yuko Okamatsu, Associate Professor of Laboratory of Biochemistry, Faculty of Veterinary Medicine, Hokkaido University, for their guidance and critical review on this thesis. The author would also like to thank Dr. Hiroaki Kariwa, Professor of Laboratory of Public Health, Faculty of Veterinary Medicine, Hokkaido University, for his giving the author this opportunity and careful guidance and warm encouragement to develop this study.

The author would like to thank Dr. Thomas J. Gardella, Associate Professor of Medicine, Endocrine Unit, Massachusetts General Hospital and Harvard Medical School, Dr. John T. Potts, Jackson Distinguished Professor of Clinical Medicine, Massachusetts General Hospital and Harvard Medical School, Dr. Harald W. Jüeppner, Professor of Pediatrics, Endocrine Unit, Massachusetts General Hospital and Harvard Medical School, Dr. Henry M. Kronenberg, Professor of Medicine, Endocrine Unit, Massachusetts General Hospital and Harvard Medical School, Dr. Marie B. Demay, Professor of Medicine, Endocrine Unit, Massachusetts General Hospital and Harvard Medical School, Dr. Michael Mannstadt, Associate Professor of Medicine, Endocrine Unit, Massachusetts General Hospital and Harvard Medical School, and Dr. Masaru Shimizu, Research Division, Chugai Pharmaceutical Co., Ltd. for their helpful discussion, comments, guidance, and sincere and continuous support throughout the series of PTH research. The author is grateful to all those for

supports and guidance in the Endocrine Unit at Massachusetts General Hospital, Fuji-Gotemba Research Laboratories of Chugai Pharmaceutical Co., Ltd. and Chugai Research Institute for Medical Science, Inc.

Finally, the author would like to thank author's family for their encouragement, understanding and providing many supports to author's challenge thorough this study.

本論文の掲載元は以下の URL を参照してください。

1. Noda, H., Guo, J., Khatri, A., Dean, T., Reyes, M., Armanini, M., Brooks, D.J., Martins, J.S., Schipani, E., Bouxsein, M.L., Demay, M.B., Potts, J.T., Jr., Juppner, H., Gardella, T.J., 2020a. An Inverse Agonist Ligand of the PTH Receptor Partially Rescues Skeletal Defects in a Mouse Model of Jansen's Metaphyseal Chondrodysplasia. J Bone Miner Res 35, 540-549. https://asbmr.onlinelibrary.wiley.com/doi/full/10.1002/jbmr.3913

2. Noda, H., Okazaki, M., Joyashiki, E., Tamura, T., Kawabe, Y., Khatri, A., Jueppner, H., Potts, J.T., Jr., Gardella, T.J., Shimizu, M., 2020b. Optimization of PTH/PTHrP Hybrid Peptides to Derive a Long-Acting PTH Analog (LA-PTH). JBMR Plus 4, e10367. https://asbmr.onlinelibrary.wiley.com/doi/10.1002/jbm4.10367

References

Abou-Samra, A.B., Juppner, H., Force, T., Freeman, M.W., Kong, X.F., Schipani, E., Urena, P., Richards, J., Bonventre, J.V., Potts, J.T., Jr., et al., 1992. Expression cloning of a common receptor for parathyroid hormone and parathyroid hormone-related peptide from rat osteoblast-like cells: a single receptor stimulates intracellular accumulation of both cAMP and inositol trisphosphates and increases intracellular free calcium. Proc Natl Acad Sci U S A 89, 2732-2736.

Alexander, S.P., Benson, H.E., Faccenda, E., Pawson, A.J., Sharman, J.L., Spedding, M., Peters, J.A., Harmar, A.J., Collaborators, C., 2013. The Concise Guide to PHARMACOLOGY 2013/14: G protein-coupled receptors. Br J Pharmacol 170, 1459-1581.

Amizuka, N., Karaplis, A.C., Henderson, J.E., Warshawsky, H., Lipman, M.L., Matsuki, Y., Ejiri, S., Tanaka, M., Izumi, N., Ozawa, H., Goltzman, D., 1996. Haploinsufficiency of parathyroid hormone-related peptide (PTHrP) results in abnormal postnatal bone development. Dev Biol 175, 166-176.

Aubin, J.E., 2001. Regulation of osteoblast formation and function. Rev Endocr Metab Disord 2, 81-94.

Baron, R., Hesse, E., 2012. Update on bone anabolics in osteoporosis treatment: rationale, current status, and perspectives. J Clin Endocrinol Metab 97, 311-325.

Bastepe, M., Raas-Rothschild, A., Silver, J., Weissman, I., Wientroub, S., Juppner, H., Gillis, D., 2004. A form of Jansen's metaphyseal chondrodysplasia with limited metabolic and skeletal abnormalities is caused by a novel activating parathyroid hormone (PTH)/PTH-related peptide receptor mutation. J Clin Endocrinol Metab 89, 3595-3600.

Bellido, T., Ali, A.A., Gubrij, I., Plotkin, L.I., Fu, Q., O'Brien, C.A., Manolagas, S.C., Jilka, R.L., 2005. Chronic elevation of parathyroid hormone in mice reduces expression of sclerostin by osteocytes: a novel mechanism for hormonal control of osteoblastogenesis. Endocrinology 146, 4577-4583.

Ben-Dov, I.Z., Galitzer, H., Lavi-Moshayoff, V., Goetz, R., Kuro-o, M., Mohammadi, M., Sirkis, R., Naveh-Many, T., Silver, J., 2007. The parathyroid is a target organ for FGF23 in rats. J Clin Invest 117, 4003-4008.

Bergwitz, C., Gardella, T.J., Flannery, M.R., Potts, J.T., Jr., Kronenberg, H.M., Goldring, S.R., Juppner, H., 1996. Full activation of chimeric receptors by hybrids between parathyroid hormone and calcitonin. Evidence for a common pattern of ligand-receptor interaction. J Biol Chem 271, 26469-26472.

Biber, J., Hernando, N., Forster, I., Murer, H., 2009. Regulation of phosphate transport in proximal tubules. Pflugers Arch 458, 39-52.

Bilezikian, J.P., Khan, A., Potts, J.T., Jr., Brandi, M.L., Clarke, B.L., Shoback, D., Juppner, H., D'Amour, P., Fox, J., Rejnmark, L., Mosekilde, L., Rubin, M.R., Dempster, D., Gafni, R., Collins, M.T., Sliney, J., Sanders, J., 2011. Hypoparathyroidism in the adult: epidemiology, diagnosis, pathophysiology, target-organ involvement, treatment, and challenges for future research. J Bone Miner Res 26, 2317-2337.

Bond, R.A., Leff, P., Johnson, T.D., Milano, C.A., Rockman, H.A., McMinn, T.R., Apparsundaram, S., Hyek, M.F., Kenakin, T.P., Allen, L.F., et al., 1995. Physiological effects of inverse agonists in transgenic mice with myocardial overexpression of the beta 2-adrenoceptor. Nature 374, 272-276.

Boyce, B.F., Rosenberg, E., de Papp, A.E., Duong, L.T., 2012. The osteoclast, bone remodelling and treatment of metabolic bone disease. Eur J Clin Invest 42, 1332-1341.

Braestrup, C., Schmiechen, R., Neef, G., Nielsen, M., Petersen, E.N., 1982. Interaction of convulsive ligands with benzodiazepine receptors. Science 216, 1241-1243.

Brewer, H.B., Jr., Ronan, R., 1970. Bovine parathyroid hormone: amino acid sequence. Proc Natl Acad Sci U S A 67, 1862-1869.

Brown, E.M., Watson, E.J., Leombruno, R., Underwood, R.H., 1983. Extracellular calcium is not necessary for acute, low calcium- or dopamine-stimulated PTH secretion in dispersed bovine parathyroid cells. Metabolism 32, 1038-1044.

Calebiro, D., Nikolaev, V.O., Gagliani, M.C., de Filippis, T., Dees, C., Tacchetti, C., Persani, L., Lohse, M.J., 2009. Persistent cAMP-signals triggered by internalized G-protein-coupled receptors. PLoS Biol 7, e1000172.

Calvi, L.M., Schipani, E., 2000. The PTH/PTHrP receptor in Jansen's metaphyseal chondrodysplasia. J Endocrinol Invest 23, 545-554.

Calvi, L.M., Sims, N.A., Hunzelman, J.L., Knight, M.C., Giovannetti, A., Saxton, J.M., Kronenberg, H.M., Baron, R., Schipani, E., 2001. Activated parathyroid hormone/parathyroid hormone-related protein receptor in osteoblastic cells differentially affects cortical and trabecular bone. J Clin Invest 107, 277-286.

Carter, P.H., Dean, T., Bhayana, B., Khatri, A., Rajur, R., Gardella, T.J., 2015. Actions of the small molecule ligands SW106 and AH-3960 on the type-1 parathyroid hormone receptor. Mol Endocrinol

29, 307-321.

Carter, P.H., Liu, R.Q., Foster, W.R., Tamasi, J.A., Tebben, A.J., Favata, M., Staal, A., Cvijic, M.E., French, M.H., Dell, V., Apanovitch, D., Lei, M., Zhao, Q., Cunningham, M., Decicco, C.P., Trzaskos, J.M., Feyen, J.H., 2007. Discovery of a small molecule antagonist of the parathyroid hormone receptor by using an N-terminal parathyroid hormone peptide probe. Proc Natl Acad Sci U S A 104, 6846-6851.

Carter, P.H., Petroni, B.D., Gensure, R.C., Schipani, E., Potts, J.T., Jr., Gardella, T.J., 2001. Selective and nonselective inverse agonists for constitutively active type-1 parathyroid hormone receptors: evidence for altered receptor conformations. Endocrinology 142, 1534-1545.

Caulfield, M.P., McKee, R.L., Goldman, M.E., Duong, L.T., Fisher, J.E., Gay, C.T., DeHaven, P.A., Levy, J.J., Roubini, E., Nutt, R.F., et al., 1990. The bovine renal parathyroid hormone (PTH) receptor has equal affinity for two different amino acid sequences: the receptor binding domains of PTH and PTH-related protein are located within the 14-34 region. Endocrinology 127, 83-87.

Chagin, A.S., Kronenberg, H.M., 2014. Role of G-proteins in the differentiation of epiphyseal chondrocytes. J Mol Endocrinol 53, R39-45.

Chorev, M., Goldman, M.E., McKee, R.L., Roubini, E., Levy, J.J., Gay, C.T., Reagan, J.E., Fisher, J.E., Caporale, L.H., Golub, E.E., et al., 1990. Modifications of position 12 in parathyroid hormone and parathyroid hormone related protein: toward the design of highly potent antagonists. Biochemistry 29, 1580-1586.

Collip, J.B., 1925. Extraction of a parathyroid hormone which will prevent or control parathyroid tetany and which regulates the level of blood calcium. J Biol Chem, 395–438.

Compston, J.E., McClung, M.R., Leslie, W.D., 2019. Osteoporosis. Lancet 393, 364-376.

Cordomi, A., Ismail, S., Matsoukas, M.T., Escrieut, C., Gherardi, M.J., Pardo, L., Fourmy, D., 2015. Functional elements of the gastric inhibitory polypeptide receptor: Comparison between secretin- and rhodopsin-like G protein-coupled receptors. Biochem Pharmacol 96, 237-246.

Curtis, E.M., van der Velde, R., Moon, R.J., van den Bergh, J.P., Geusens, P., de Vries, F., van Staa, T.P., Cooper, C., Harvey, N.C., 2016. Epidemiology of fractures in the United Kingdom 1988-2012: Variation with age, sex, geography, ethnicity and socioeconomic status. Bone 87, 19-26.

David, V., Dai, B., Martin, A., Huang, J., Han, X., Quarles, L.D., 2013. Calcium regulates FGF-23 expression in bone. Endocrinology 154, 4469-4482.

de Graaf, C., Song, G., Cao, C., Zhao, Q., Wang, M.W., Wu, B., Stevens, R.C., 2017. Extending the Structural View of Class B GPCRs. Trends Biochem Sci 42, 946-960.

de Groot, T., Lee, K., Langeslag, M., Xi, Q., Jalink, K., Bindels, R.J., Hoenderop, J.G., 2009. Parathyroid hormone activates TRPV5 via PKA-dependent phosphorylation. J Am Soc Nephrol 20, 1693-1704.

De Lean, A., Stadel, J.M., Lefkowitz, R.J., 1980. A ternary complex model explains the agonist-specific binding properties of the adenylate cyclase-coupled beta-adrenergic receptor. J Biol Chem 255, 7108-7117.

Dean, T., Linglart, A., Mahon, M.J., Bastepe, M., Juppner, H., Potts, J.T., Jr., Gardella, T.J., 2006. Mechanisms of ligand binding to the parathyroid hormone (PTH)/PTH-related protein receptor: selectivity of a modified PTH(1-15) radioligand for GalphaS-coupled receptor conformations. Mol Endocrinol 20, 931-943.

Dean, T., Vilardaga, J.P., Potts, J.T., Jr., Gardella, T.J., 2008. Altered selectivity of parathyroid hormone (PTH) and PTH-related protein (PTHrP) for distinct conformations of the PTH/PTHrP receptor. Mol Endocrinol 22, 156-166.

Dempster, D.W., Compston, J.E., Drezner, M.K., Glorieux, F.H., Kanis, J.A., Malluche, H., Meunier, P.J., Ott, S.M., Recker, R.R., Parfitt, A.M., 2013. Standardized nomenclature, symbols, and units for bone histomorphometry: a 2012 update of the report of the ASBMR Histomorphometry Nomenclature Committee. J Bone Miner Res 28, 2-17.

Divieti, P., Inomata, N., Chapin, K., Singh, R., Juppner, H., Bringhurst, F.R., 2001. Receptors for the carboxyl-terminal region of pth(1-84) are highly expressed in osteocytic cells. Endocrinology 142, 916-925.

Dresner-Pollak, R., Yang, Q.M., Behar, V., Nakamoto, C., Chorev, M., Rosenblatt, M., 1996. Evaluation in vivo of a potent parathyroid hormone antagonist: [Nle8,18,D-Trp12,Tyr34]bPTH(7-34)NH2. J Bone Miner Res 11, 1061-1065.

Ehrenmann, J., Schoppe, J., Klenk, C., Rappas, M., Kummer, L., Dore, A.S., Pluckthun, A., 2018. High-resolution crystal structure of parathyroid hormone 1 receptor in complex with a peptide agonist. Nat Struct Mol Biol 25, 1086-1092.

Estell, E.G., Rosen, C.J., 2021. Emerging insights into the comparative effectiveness of anabolic therapies for osteoporosis. Nat Rev Endocrinol 17, 31-46.

Feinstein, T.N., Wehbi, V.L., Ardura, J.A., Wheeler, D.S., Ferrandon, S., Gardella, T.J., Vilardaga, J.P., 2011. Retromer terminates the generation of cAMP by internalized PTH receptors. Nat Chem Biol 7, 278-284.

Feinstein, T.N., Yui, N., Webber, M.J., Wehbi, V.L., Stevenson, H.P., King, J.D., Jr., Hallows, K.R., Brown, D., Bouley, R., Vilardaga, J.P., 2013. Noncanonical control of vasopressin receptor type 2 signaling by retromer and arrestin. J Biol Chem 288, 27849-27860.

Ferrandon, S., Feinstein, T.N., Castro, M., Wang, B., Bouley, R., Potts, J.T., Gardella, T.J., Vilardaga, J.P., 2009. Sustained cyclic AMP production by parathyroid hormone receptor endocytosis. Nat Chem Biol 5, 734-742.

Franceschi, R.T., Ge, C., Xiao, G., Roca, H., Jiang, D., 2007. Transcriptional regulation of osteoblasts. Ann N Y Acad Sci 1116, 196-207.

Fraser, W.D., 2009. Hyperparathyroidism. Lancet 374, 145-158.

Gafni, R.I., Collins, M.T., 2019. Hypoparathyroidism. N Engl J Med 380, 1738-1747.

Gardella, T.J., Luck, M.D., Jensen, G.S., Schipani, E., Potts, J.T., Jr., Juppner, H., 1996. Inverse agonism of amino-terminally truncated parathyroid hormone (PTH) and PTH-related peptide (PTHrP) analogs revealed with constitutively active mutant PTH/PTHrP receptors. Endocrinology 137, 3936-3941.

Gensure, R.C., Ponugoti, B., Gunes, Y., Papasani, M.R., Lanske, B., Bastepe, M., Rubin, D.A., Juppner, H., 2004. Identification and characterization of two parathyroid hormone-like molecules in zebrafish. Endocrinology 145, 1634-1639.

Gesty-Palmer, D., Chen, M., Reiter, E., Ahn, S., Nelson, C.D., Wang, S., Eckhardt, A.E., Cowan, C.L., Spurney, R.F., Luttrell, L.M., Lefkowitz, R.J., 2006. Distinct beta-arrestin- and G protein-dependent pathways for parathyroid hormone receptor-stimulated ERK1/2 activation. J Biol Chem 281, 10856-10864.

Glukhova, A., Draper-Joyce, C.J., Sunahara, R.K., Christopoulos, A., Wootten, D., Sexton, P.M., 2018. Rules of Engagement: GPCRs and G Proteins. ACS Pharmacol Transl Sci 1, 73-83.

Goldman, M.E., McKee, R.L., Caulfield, M.P., Reagan, J.E., Levy, J.J., Gay, C.T., DeHaven, P.A., Rosenblatt, M., Chorev, M., 1988. A new highly potent parathyroid hormone antagonist: [D-Trp12,Tyr34]bPTH-(7-34)NH2. Endocrinology 123, 2597-2599.

Goltzman, D., Peytremann, A., Callahan, E., Tregear, G.W., Potts, J.T., Jr., 1975. Analysis of the requirements for parathyroid hormone action in renal membranes with the use of inhibiting analogues. J Biol Chem 250, 3199-3203.

Guerreiro, P.M., Renfro, J.L., Power, D.M., Canario, A.V., 2007. The parathyroid hormone family of peptides: structure, tissue distribution, regulation, and potential functional roles in calcium and phosphate balance in fish. Am J Physiol Regul Integr Comp Physiol 292, R679-696.

Gullberg, B., Johnell, O., Kanis, J.A., 1997. World-wide projections for hip fracture. Osteoporos Int 7, 407-413.

Gutierrez, O.M., Januzzi, J.L., Isakova, T., Laliberte, K., Smith, K., Collerone, G., Sarwar, A., Hoffmann, U., Coglianese, E., Christenson, R., Wang, T.J., deFilippi, C., Wolf, M., 2009. Fibroblast growth factor 23 and left ventricular hypertrophy in chronic kidney disease. Circulation 119, 2545-2552.

Hattersley, G., Dean, T., Corbin, B.A., Bahar, H., Gardella, T.J., 2016. Binding Selectivity of Abaloparatide for PTH-Type-1-Receptor Conformations and Effects on Downstream Signaling. Endocrinology 157, 141-149.

Hjorth, S.A., Orskov, C., Schwartz, T.W., 1998. Constitutive activity of glucagon receptor mutants. Mol Endocrinol 12, 78-86.

Horiuchi, N., Holick, M.F., Potts, J.T., Jr., Rosenblatt, M., 1983. A parathyroid hormone inhibitor in vivo: design and biological evaluation of a hormone analog. Science 220, 1053-1055.

Horwitz, M.J., Tedesco, M.B., Sereika, S.M., Hollis, B.W., Garcia-Ocana, A., Stewart, A.F., 2003. Direct comparison of sustained infusion of human parathyroid hormone-related protein-(1-36) [hPTHrP-(1-36)] versus hPTH-(1-34) on serum calcium, plasma 1,25-dihydroxyvitamin D concentrations, and fractional calcium excretion in healthy human volunteers. J Clin Endocrinol Metab 88, 1603-1609.

Huang, Z., Chen, Y., Pratt, S., Chen, T.H., Bambino, T., Nissenson, R.A., Shoback, D.M., 1996. The N-terminal region of the third intracellular loop of the parathyroid hormone (PTH)/PTH-related peptide receptor is critical for coupling to cAMP and inositol phosphate/Ca2+ signal transduction pathways. J Biol Chem 271, 33382-33389.

Iida-Klein, A., Guo, J., Takemura, M., Drake, M.T., Potts, J.T., Jr., Abou-Samra, A., Bringhurst, F.R., Segre, G.V., 1997. Mutations in the second cytoplasmic loop of the rat parathyroid hormone

(PTH)/PTH-related protein receptor result in selective loss of PTH-stimulated phospholipase C activity. J Biol Chem 272, 6882-6889.

Isakova, T., Wahl, P., Vargas, G.S., Gutierrez, O.M., Scialla, J., Xie, H., Appleby, D., Nessel, L., Bellovich, K., Chen, J., Hamm, L., Gadegbeku, C., Horwitz, E., Townsend, R.R., Anderson, C.A., Lash, J.P., Hsu, C.Y., Leonard, M.B., Wolf, M., 2011. Fibroblast growth factor 23 is elevated before parathyroid hormone and phosphate in chronic kidney disease. Kidney Int 79, 1370-1378.

Ishizuya, T., Yokose, S., Hori, M., Noda, T., Suda, T., Yoshiki, S., Yamaguchi, A., 1997. Parathyroid hormone exerts disparate effects on osteoblast differentiation depending on exposure time in rat osteoblastic cells. J Clin Invest 99, 2961-2970.

Jansen, M., 1934. Über atypische Chondrodystrophie (Achondroplasie) und über eine noch nicht beschriebene angeborene Wachstumsstörung des Knochensystems: Metaphysäre Dysostosis. Zeitschr Orthop Chir. 61, 253-286.

Jilka, R.L., 2007. Molecular and cellular mechanisms of the anabolic effect of intermittent PTH. Bone 40, 1434-1446.

Juppner, H., 2011. Phosphate and FGF-23. Kidney Int Suppl, S24-27.

Juppner, H., Abou-Samra, A.B., Freeman, M., Kong, X.F., Schipani, E., Richards, J., Kolakowski, L.F., Jr., Hock, J., Potts, J.T., Jr., Kronenberg, H.M., et al., 1991. A G protein-linked receptor for parathyroid hormone and parathyroid hormone-related peptide. Science 254, 1024-1026.

Kanis, J.A., Johnell, O., Oden, A., Sembo, I., Redlund-Johnell, I., Dawson, A., De Laet, C., Jonsson, B., 2000. Long-term risk of osteoporotic fracture in Malmo. Osteoporos Int 11, 669-674.

Karaplis, A.C., Luz, A., Glowacki, J., Bronson, R.T., Tybulewicz, V.L., Kronenberg, H.M., Mulligan, R.C., 1994. Lethal skeletal dysplasia from targeted disruption of the parathyroid hormone-related peptide gene. Genes Dev 8, 277-289.

Keller, H., Kneissel, M., 2005. SOST is a target gene for PTH in bone. Bone 37, 148-158.

Khan, S.K., Yadav, P.S., Elliott, G., Hu, D.Z., Xu, R., Yang, Y., 2018. Induced Gnas(R201H) expression from the endogenous Gnas locus causes fibrous dysplasia by up-regulating Wnt/beta-catenin signaling. Proc Natl Acad Sci U S A 115, E418-E427.

Khosla, S., Westendorf, J.J., Oursler, M.J., 2008. Building bone to reverse osteoporosis and repair fractures. J Clin Invest 118, 421-428.

Ko, F.C., Karim, L., Brooks, D.J., Bouxsein, M.L., Demay, M.B., 2017. Bisphosphonate Withdrawal: Effects on Bone Formation and Bone Resorption in Maturing Male Mice. J Bone Miner Res 32, 814-820.

Komori, T., 2006. Regulation of osteoblast differentiation by transcription factors. J Cell Biochem 99, 1233-1239.

Kramer, I., Loots, G.G., Studer, A., Keller, H., Kneissel, M., 2010. Parathyroid hormone (PTH)-induced bone gain is blunted in SOST overexpressing and deficient mice. J Bone Miner Res 25, 178-189.

Krishnan, V., Bryant, H.U., Macdougald, O.A., 2006. Regulation of bone mass by Wnt signaling. J Clin Invest 116, 1202-1209.

Kronenberg, H.M., 2006. PTHrP and skeletal development. Ann N Y Acad Sci 1068, 1-13.

Kruse, K., Schutz, C., 1993. Calcium metabolism in the Jansen type of metaphyseal dysplasia. Eur J Pediatr 152, 912-915.

Kulkarni, N.H., Halladay, D.L., Miles, R.R., Gilbert, L.M., Frolik, C.A., Galvin, R.J., Martin, T.J., Gillespie, M.T., Onyia, J.E., 2005. Effects of parathyroid hormone on Wnt signaling pathway in bone. J Cell Biochem 95, 1178-1190.

Kuznetsov, S.A., Riminucci, M., Ziran, N., Tsutsui, T.W., Corsi, A., Calvi, L., Kronenberg, H.M., Schipani, E., Robey, P.G., Bianco, P., 2004. The interplay of osteogenesis and hematopoiesis: expression of a constitutively active PTH/PTHrP receptor in osteogenic cells perturbs the establishment of hematopoiesis in bone and of skeletal stem cells in the bone marrow. J Cell Biol 167, 1113-1122.

Lanske, B., Divieti, P., Kovacs, C.S., Pirro, A., Landis, W.J., Krane, S.M., Bringhurst, F.R., Kronenberg, H.M., 1998. The parathyroid hormone (PTH)/PTH-related peptide receptor mediates actions of both ligands in murine bone. Endocrinology 139, 5194-5204.

Lanske, B., Karaplis, A.C., Lee, K., Luz, A., Vortkamp, A., Pirro, A., Karperien, M., Defize, L.H., Ho, C., Mulligan, R.C., Abou-Samra, A.B., Juppner, H., Segre, G.V., Kronenberg, H.M., 1996. PTH/PTHrP receptor in early development and Indian hedgehog-regulated bone growth. Science 273, 663-666.

Lee, C., Gardella, T.J., Abou-Samra, A.B., Nussbaum, S.R., Segre, G.V., Potts, J.T., Jr., Kronenberg, H.M., Juppner, H., 1994. Role of the extracellular regions of the parathyroid hormone (PTH)/PTH-

related peptide receptor in hormone binding. Endocrinology 135, 1488-1495.

Leidig-Bruckner, G., Bruckner, T., Raue, F., Frank-Raue, K., 2016. Long-Term Follow-Up and Treatment of Postoperative Permanent Hypoparathyroidism in Patients with Medullary Thyroid Carcinoma: Differences in Complete and Partial Disease. Horm Metab Res 48, 806-813.

Liang, Y.L., Khoshouei, M., Glukhova, A., Furness, S.G.B., Zhao, P., Clydesdale, L., Koole, C., Truong, T.T., Thal, D.M., Lei, S., Radjainia, M., Danev, R., Baumeister, W., Wang, M.W., Miller, L.J., Christopoulos, A., Sexton, P.M., Wootten, D., 2018. Phase-plate cryo-EM structure of a biased agonist-bound human GLP-1 receptor-Gs complex. Nature 555, 121-125.

Liu, E.S., Martins, J.S., Raimann, A., Chae, B.T., Brooks, D.J., Jorgetti, V., Bouxsein, M.L., Demay, M.B., 2016. 1,25-Dihydroxyvitamin D Alone Improves Skeletal Growth, Microarchitecture, and Strength in a Murine Model of XLH, Despite Enhanced FGF23 Expression. J Bone Miner Res 31, 929-939.

Luck, M.D., Carter, P.H., Gardella, T.J., 1999. The (1-14) fragment of parathyroid hormone (PTH) activates intact and amino-terminally truncated PTH-1 receptors. Mol Endocrinol 13, 670-680.

Luttrell, L.M., Lefkowitz, R.J., 2002. The role of beta-arrestins in the termination and transduction of G-protein-coupled receptor signals. J Cell Sci 115, 455-465.

Maeda, A., Okazaki, M., Baron, D.M., Dean, T., Khatri, A., Mahon, M., Segawa, H., Abou-Samra, A.B., Juppner, H., Bloch, K.D., Potts, J.T., Jr., Gardella, T.J., 2013. Critical role of parathyroid hormone (PTH) receptor-1 phosphorylation in regulating acute responses to PTH. Proc Natl Acad Sci U S A 110, 5864-5869.

Malecz, N., Bambino, T., Bencsik, M., Nissenson, R.A., 1998. Identification of phosphorylation sites in the G protein-coupled receptor for parathyroid hormone. Receptor phosphorylation is not required for agonist-induced internalization. Mol Endocrinol 12, 1846-1856.

Mannstadt, M., Bilezikian, J.P., Thakker, R.V., Hannan, F.M., Clarke, B.L., Rejnmark, L., Mitchell, D.M., Vokes, T.J., Winer, K.K., Shoback, D.M., 2017. Hypoparathyroidism. Nat Rev Dis Primers 3, 17080.

Mannstadt, M., Clarke, B.L., Vokes, T., Brandi, M.L., Ranganath, L., Fraser, W.D., Lakatos, P., Bajnok, L., Garceau, R., Mosekilde, L., Lagast, H., Shoback, D., Bilezikian, J.P., 2013. Efficacy and safety of recombinant human parathyroid hormone (1-84) in hypoparathyroidism (REPLACE): a double-blind, placebo-controlled, randomised, phase 3 study. Lancet Diabetes Endocrinol 1, 275-283.

Marcucci, G., Della Pepa, G., Brandi, M.L., 2017. Drug safety evaluation of parathyroid hormone for hypocalcemia in patients with hypoparathyroidism. Expert Opin Drug Saf 16, 617-625.

Martin, T.J., Sims, N.A., Ng, K.W., 2008. Regulatory pathways revealing new approaches to the development of anabolic drugs for osteoporosis. Osteoporos Int 19, 1125-1138.

McCauley, L.K., Martin, T.J., 2012. Twenty-five years of PTHrP progress: from cancer hormone to multifunctional cytokine. J Bone Miner Res 27, 1231-1239.

McDonald, I.M., Austin, C., Buck, I.M., Dunstone, D.J., Gaffen, J., Griffin, E., Harper, E.A., Hull, R.A., Kalindjian, S.B., Linney, I.D., Low, C.M., Patel, D., Pether, M.J., Raynor, M., Roberts, S.P., Shaxted, M.E., Spencer, J., Steel, K.I., Sykes, D.A., Wright, P.T., Xun, W., 2007. Discovery and characterization of novel, potent, non-peptide parathyroid hormone-1 receptor antagonists. J Med Chem 50, 4789-4792.

Miao, D., He, B., Karaplis, A.C., Goltzman, D., 2002. Parathyroid hormone is essential for normal fetal bone formation. J Clin Invest 109, 1173-1182.

Miao, D., He, B., Lanske, B., Bai, X.Y., Tong, X.K., Hendy, G.N., Goltzman, D., Karaplis, A.C., 2004. Skeletal abnormalities in Pth-null mice are influenced by dietary calcium. Endocrinology 145, 2046-2053.

Miller, P.D., Hattersley, G., Lau, E., Fitzpatrick, L.A., Harris, A.G., Williams, G.C., Hu, M.Y., Riis, B.J., Russo, L., Christiansen, C., 2019. Bone mineral density response rates are greater in patients treated with abaloparatide compared with those treated with placebo or teriparatide: Results from the ACTIVE phase 3 trial. Bone 120, 137-140.

Mitchell, D.M., Regan, S., Cooley, M.R., Lauter, K.B., Vrla, M.C., Becker, C.B., Burnett-Bowie, S.A., Mannstadt, M., 2012. Long-term follow-up of patients with hypoparathyroidism. J Clin Endocrinol Metab 97, 4507-4514.

Miyamoto, K., Segawa, H., Ito, M., Kuwahata, M., 2004. Physiological regulation of renal sodium-dependent phosphate cotransporters. Jpn J Physiol 54, 93-102.

Mullard, A., 2019. FDA approves first-in-class osteoporosis drug. Nat Rev Drug Discov 18, 411.

Nagai, S., Okazaki, M., Segawa, H., Bergwitz, C., Dean, T., Potts, J.T., Jr., Mahon, M.J., Gardella, T.J., Juppner, H., 2011. Acute down-regulation of sodium-dependent phosphate transporter NPT2a involves predominantly the cAMP/PKA pathway as revealed by signaling-selective parathyroid hormone analogs. J Biol Chem 286, 1618-1626.

Nampoothiri, S., Fernandez-Rebollo, E., Yesodharan, D., Gardella, T.J., Rush, E.T., Langman, C.B., Juppner, H., 2016. Jansen Metaphyseal Chondrodysplasia due to Heterozygous H223R-PTH1R Mutations With or Without Overt Hypercalcemia. J Clin Endocrinol Metab 101, 4283-4289.

Nasrallah, M.M., El-Shehaby, A.R., Salem, M.M., Osman, N.A., El Sheikh, E., Sharaf El Din, U.A., 2010. Fibroblast growth factor-23 (FGF-23) is independently correlated to aortic calcification in haemodialysis patients. Nephrol Dial Transplant 25, 2679-2685.

Nguyen, A.H., Thomsen, A.R.B., Cahill, T.J., 3rd, Huang, R., Huang, L.Y., Marcink, T., Clarke, O.B., Heissel, S., Masoudi, A., Ben-Hail, D., Samaan, F., Dandey, V.P., Tan, Y.Z., Hong, C., Mahoney, J.P., Triest, S., Little, J.t., Chen, X., Sunahara, R., Steyaert, J., Molina, H., Yu, Z., des Georges, A., Lefkowitz, R.J., 2019. Structure of an endosomal signaling GPCR-G protein-beta-arrestin megacomplex. Nat Struct Mol Biol 26, 1123-1131.

Niall, H.D., Keutmann, H., Sauer, R., Hogan, M., Dawson, B., Aurbach, G., Potts, J., Jr., 1970. The amino acid sequence of bovine parathyroid hormone I. Hoppe Seylers Z Physiol Chem 351, 1586-1588.

Nishimura, Y., Esaki, T., Isshiki, Y., Furuta, Y., Mizutani, A., Kotake, T., Emura, T., Watanabe, Y., Ohta, M., Nakagawa, T., Ogawa, K., Arai, S., Noda, H., Kitamura, H., Shimizu, M., Tamura, T., Sato, H., 2020. Lead Optimization and Avoidance of Reactive Metabolite Leading to PCO371, a Potent, Selective, and Orally Available Human Parathyroid Hormone Receptor 1 (hPTHR1) Agonist. J Med Chem 63, 5089-5099.

Nissenson, R.A., Diep, D., Strewler, G.J., 1988. Synthetic peptides comprising the amino-terminal sequence of a parathyroid hormone-like protein from human malignancies. Binding to parathyroid hormone receptors and activation of adenylate cyclase in bone cells and kidney. J Biol Chem 263, 12866-12871.

O'Brien, C.A., Plotkin, L.I., Galli, C., Goellner, J.J., Gortazar, A.R., Allen, M.R., Robling, A.G., Bouxsein, M., Schipani, E., Turner, C.H., Jilka, R.L., Weinstein, R.S., Manolagas, S.C., Bellido, T., 2008. Control of bone mass and remodeling by PTH receptor signaling in osteocytes. PLoS One 3, e2942.

Oden, A., McCloskey, E.V., Kanis, J.A., Harvey, N.C., Johansson, H., 2015. Burden of high fracture probability worldwide: secular increases 2010-2040. Osteoporos Int 26, 2243-2248.

Ohishi, M., Chiusaroli, R., Ominsky, M., Asuncion, F., Thomas, C., Khatri, R., Kostenuik, P., Schipani, E., 2009. Osteoprotegerin abrogated cortical porosity and bone marrow fibrosis in a mouse model of

constitutive activation of the PTH/PTHrP receptor. Am J Pathol 174, 2160-2171.

Ohishi, M., Ono, W., Ono, N., Khatri, R., Marzia, M., Baker, E.K., Root, S.H., Wilson, T.L., Iwamoto, Y., Kronenberg, H.M., Aguila, H.L., Purton, L.E., Schipani, E., 2012. A novel population of cells expressing both hematopoietic and mesenchymal markers is present in the normal adult bone marrow and is augmented in a murine model of marrow fibrosis. Am J Pathol 180, 811-818.

Okazaki, M., Ferrandon, S., Vilardaga, J.P., Bouxsein, M.L., Potts, J.T., Jr., Gardella, T.J., 2008. Prolonged signaling at the parathyroid hormone receptor by peptide ligands targeted to a specific receptor conformation. Proc Natl Acad Sci U S A 105, 16525-16530.

Onuchic, L., Ferraz-de-Souza, B., Mendonca, B.B., Correa, P.H., Martin, R.M., 2012. Potential effects of alendronate on fibroblast growth factor 23 levels and effective control of hypercalciuria in an adult with Jansen's metaphyseal chondrodysplasia. J Clin Endocrinol Metab 97, 1098-1103.

Papasani, M.R., Gensure, R.C., Yan, Y.L., Gunes, Y., Postlethwait, J.H., Ponugoti, B., John, M.R., Juppner, H., Rubin, D.A., 2004. Identification and characterization of the zebrafish and fugu genes encoding tuberoinfundibular peptide 39. Endocrinology 145, 5294-5304.

Parasuraman, S., 2011. Toxicological screening. J Pharmacol Pharmacother 2, 74-79.

Parfitt, A.M., Schipani, E., Rao, D.S., Kupin, W., Han, Z.H., Juppner, H., 1996. Hypercalcemia due to constitutive activity of the parathyroid hormone (PTH)/PTH-related peptide receptor: comparison with primary hyperparathyroidism. J Clin Endocrinol Metab 81, 3584-3588.

Picard, N., Capuano, P., Stange, G., Mihailova, M., Kaissling, B., Murer, H., Biber, J., Wagner, C.A., 2010. Acute parathyroid hormone differentially regulates renal brush border membrane phosphate cotransporters. Pflugers Arch 460, 677-687.

Pioszak, A.A., Parker, N.R., Gardella, T.J., Xu, H.E., 2009. Structural basis for parathyroid hormone-related protein binding to the parathyroid hormone receptor and design of conformation-selective peptides. J Biol Chem 284, 28382-28391.

Potts, J.T., 2005. Parathyroid hormone: past and present. J Endocrinol 187, 311-325.

Potts, J.T., Jr., Tregear, G.W., Keutmann, H.T., Niall, H.D., Sauer, R., Deftos, L.J., Dawson, B.F., Hogan, M.L., Aurbach, G.D., 1971. Synthesis of a biologically active N-terminal tetratriacontapeptide of parathyroid hormone. Proc Natl Acad Sci U S A 68, 63-67.

Power, D.M., Ingleton, P.M., Flanagan, J., Canario, A.V., Danks, J., Elgar, G., Clark, M.S., 2000.

Genomic structure and expression of parathyroid hormone-related protein gene (PTHrP) in a teleost, Fugu rubripes. Gene 250, 67-76.

Powers, J., Joy, K., Ruscio, A., Lagast, H., 2013. Prevalence and incidence of hypoparathyroidism in the United States using a large claims database. J Bone Miner Res 28, 2570-2576.

Qian, F., Leung, A., Abou-Samra, A., 1998. Agonist-dependent phosphorylation of the parathyroid hormone/parathyroid hormone-related peptide receptor. Biochemistry 37, 6240-6246.

Reginster, J.Y., Burlet, N., 2006. Osteoporosis: a still increasing prevalence. Bone 38, S4-9.

Reid, I.R., 2020. A broader strategy for osteoporosis interventions. Nat Rev Endocrinol 16, 333-339.

Rhee, Y., Bivi, N., Farrow, E., Lezcano, V., Plotkin, L.I., White, K.E., Bellido, T., 2011. Parathyroid hormone receptor signaling in osteocytes increases the expression of fibroblast growth factor-23 in vitro and in vivo. Bone 49, 636-643.

Rosen, H.N., Lim, M., Garber, J., Moreau, S., Bhargava, H.N., Pallotta, J., Spark, R., Greenspan, S., Rosenblatt, M., Chorev, M., 1997. The effect of PTH antagonist BIM-44002 on serum calcium and PTH levels in hypercalcemic hyperparathyroid patients. Calcif Tissue Int 61, 455-459.

Rosen, H.N., Moses, A.C., Garber, J., Iloputaife, I.D., Ross, D.S., Lee, S.L., Greenspan, S.L., 2000. Serum CTX: a new marker of bone resorption that shows treatment effect more often than other markers because of low coefficient of variability and large changes with bisphosphonate therapy. Calcif Tissue Int 66, 100-103.

Rosenblatt, M., Callahan, E.N., Mahaffey, J.E., Pont, A., Potts, J.T., Jr., 1977. Parathyroid hormone inhibitors. Design, synthesis, and biologic evaluation of hormone analogues. J Biol Chem 252, 5847-5851.

Roth, H., Fritsche, L.G., Meier, C., Pilz, P., Eigenthaler, M., Meyer-Marcotty, P., Stellzig-Eisenhauer, A., Proff, P., Kanno, C.M., Weber, B.H., 2014. Expanding the spectrum of PTH1R mutations in patients with primary failure of tooth eruption. Clin Oral Investig 18, 377-384.

Rubin, M.R., Bilezikian, J.P., 2003. The anabolic effects of parathyroid hormone therapy. Clin Geriatr Med 19, 415-432.

Saag, K.G., Petersen, J., Brandi, M.L., Karaplis, A.C., Lorentzon, M., Thomas, T., Maddox, J., Fan, M., Meisner, P.D., Grauer, A., 2017. Romosozumab or Alendronate for Fracture Prevention in Women with Osteoporosis. N Engl J Med 377, 1417-1427.

Saini, V., Marengi, D.A., Barry, K.J., Fulzele, K.S., Heiden, E., Liu, X., Dedic, C., Maeda, A., Lotinun, S., Baron, R., Pajevic, P.D., 2013. Parathyroid hormone (PTH)/PTH-related peptide type 1 receptor (PPR) signaling in osteocytes regulates anabolic and catabolic skeletal responses to PTH. J Biol Chem 288, 20122-20134.

Saito, H., Maeda, A., Ohtomo, S., Hirata, M., Kusano, K., Kato, S., Ogata, E., Segawa, H., Miyamoto, K., Fukushima, N., 2005. Circulating FGF-23 is regulated by 1alpha,25-dihydroxyvitamin D3 and phosphorus in vivo. J Biol Chem 280, 2543-2549.

Saito, H., Noda, H., Gatault, P., Bockenhauer, D., Loke, K.Y., Hiort, O., Silve, C., Sharwood, E., Martin, R.M., Dillon, M.J., Gillis, D., Harris, M., Rao, S.D., Pauli, R.M., Gardella, T.J., Juppner, H., 2018. Progression of Mineral Ion Abnormalities in Patients With Jansen Metaphyseal Chondrodysplasia. J Clin Endocrinol Metab 103, 2660-2669.

Schipani, E., Kruse, K., Juppner, H., 1995. A constitutively active mutant PTH-PTHrP receptor in Jansen-type metaphyseal chondrodysplasia. Science 268, 98-100.

Schipani, E., Langman, C., Hunzelman, J., Le Merrer, M., Loke, K.Y., Dillon, M.J., Silve, C., Juppner, H., 1999. A novel parathyroid hormone (PTH)/PTH-related peptide receptor mutation in Jansen's metaphyseal chondrodysplasia. J Clin Endocrinol Metab 84, 3052-3057.

Schipani, E., Langman, C.B., Parfitt, A.M., Jensen, G.S., Kikuchi, S., Kooh, S.W., Cole, W.G., Juppner, H., 1996. Constitutively activated receptors for parathyroid hormone and parathyroid hormone-related peptide in Jansen's metaphyseal chondrodysplasia. N Engl J Med 335, 708-714.

Schipani, E., Lanske, B., Hunzelman, J., Luz, A., Kovacs, C.S., Lee, K., Pirro, A., Kronenberg, H.M., Juppner, H., 1997. Targeted expression of constitutively active receptors for parathyroid hormone and parathyroid hormone-related peptide delays endochondral bone formation and rescues mice that lack parathyroid hormone-related peptide. Proc Natl Acad Sci U S A 94, 13689-13694.

Shimada, T., Hasegawa, H., Yamazaki, Y., Muto, T., Hino, R., Takeuchi, Y., Fujita, T., Nakahara, K., Fukumoto, S., Yamashita, T., 2004. FGF-23 is a potent regulator of vitamin D metabolism and phosphate homeostasis. J Bone Miner Res 19, 429-435.

Shimada, T., Mizutani, S., Muto, T., Yoneya, T., Hino, R., Takeda, S., Takeuchi, Y., Fujita, T., Fukumoto, S., Yamashita, T., 2001. Cloning and characterization of FGF23 as a causative factor of tumor-induced osteomalacia. Proc Natl Acad Sci U S A 98, 6500-6505.

Shimizu, M., Carter, P.H., Gardella, T.J., 2000a. Autoactivation of type-1 parathyroid hormone

receptors containing a tethered ligand. J Biol Chem 275, 19456-19460.

Shimizu, M., Carter, P.H., Khatri, A., Potts, J.T., Jr., Gardella, T.J., 2001a. Enhanced activity in parathyroid hormone-(1-14) and -(1-11): novel peptides for probing ligand-receptor interactions. Endocrinology 142, 3068-3074.

Shimizu, M., Joyashiki, E., Noda, H., Watanabe, T., Okazaki, M., Nagayasu, M., Adachi, K., Tamura, T., Potts, J.T., Jr., Gardella, T.J., Kawabe, Y., 2016a. Pharmacodynamic Actions of a Long-Acting PTH Analog (LA-PTH) in Thyroparathyroidectomized (TPTX) Rats and Normal Monkeys. J Bone Miner Res 31, 1405-1412.

Shimizu, M., Noda, H., Joyashiki, E., Nakagawa, C., Asanuma, K., Hayasaka, A., Kato, M., Nanami, M., Inada, M., Miyaura, C., Tamura, T., 2016b. The Optimal Duration of PTH(1-34) Infusion Is One Hour per Day to Increase Bone Mass in Rats. Biol Pharm Bull 39, 625-630.

Shimizu, M., Potts, J.T., Jr., Gardella, T.J., 2000b. Minimization of parathyroid hormone. Novel amino-terminal parathyroid hormone fragments with enhanced potency in activating the type-1 parathyroid hormone receptor. J Biol Chem 275, 21836-21843.

Shimizu, N., Guo, J., Gardella, T.J., 2001b. Parathyroid hormone (PTH)-(1-14) and -(1-11) analogs conformationally constrained by alpha-aminoisobutyric acid mediate full agonist responses via the juxtamembrane region of the PTH-1 receptor. J Biol Chem 276, 49003-49012.

Shoback, D., 2008. Clinical practice. Hypoparathyroidism. N Engl J Med 359, 391-403.

Shoback, D., Thatcher, J., Leombruno, R., Brown, E., 1983. Effects of extracellular Ca++ and Mg++ on cytosolic Ca++ and PTH release in dispersed bovine parathyroid cells. Endocrinology 113, 424-426.

Silva, B.C., Costa, A.G., Cusano, N.E., Kousteni, S., Bilezikian, J.P., 2011. Catabolic and anabolic actions of parathyroid hormone on the skeleton. J Endocrinol Invest 34, 801-810.

Silverthorn, K.G., Houston, C.S., Duncan, B.P., 1987. Murk Jansen's metaphyseal chondrodysplasia with long-term followup. Pediatr Radiol 17, 119-123.

Singh, A.T., Gilchrist, A., Voyno-Yasenetskaya, T., Radeff-Huang, J.M., Stern, P.H., 2005. G alpha12/G alpha13 subunits of heterotrimeric G proteins mediate parathyroid hormone activation of phospholipase D in UMR-106 osteoblastic cells. Endocrinology 146, 2171-2175.

Strewler, G.J., 2000. The physiology of parathyroid hormone-related protein. N Engl J Med 342, 177-

185.

Sutkeviciute, I., Vilardaga, J.P., 2020. Structural insights into emergent signaling modes of G protein-coupled receptors. J Biol Chem 295, 11626-11642.

Suva, L.J., Winslow, G.A., Wettenhall, R.E., Hammonds, R.G., Moseley, J.M., Diefenbach-Jagger, H., Rodda, C.P., Kemp, B.E., Rodriguez, H., Chen, E.Y., et al., 1987. A parathyroid hormone-related protein implicated in malignant hypercalcemia: cloning and expression. Science 237, 893-896.

Syme, C.A., Friedman, P.A., Bisello, A., 2005. Parathyroid hormone receptor trafficking contributes to the activation of extracellular signal-regulated kinases but is not required for regulation of cAMP signaling. J Biol Chem 280, 11281-11288.

Tamura, T., Noda, H., Joyashiki, E., Hoshino, M., Watanabe, T., Kinosaki, M., Nishimura, Y., Esaki, T., Ogawa, K., Miyake, T., Arai, S., Shimizu, M., Kitamura, H., Sato, H., Kawabe, Y., 2016. Identification of an orally active small-molecule PTHR1 agonist for the treatment of hypoparathyroidism. Nat Commun 7, 13384.

Tawfeek, H.A., Qian, F., Abou-Samra, A.B., 2002. Phosphorylation of the receptor for PTH and PTHrP is required for internalization and regulates receptor signaling. Mol Endocrinol 16, 1-13.

Thomsen, A.R.B., Plouffe, B., Cahill, T.J., 3rd, Shukla, A.K., Tarrasch, J.T., Dosey, A.M., Kahsai, A.W., Strachan, R.T., Pani, B., Mahoney, J.P., Huang, L., Breton, B., Heydenreich, F.M., Sunahara, R.K., Skiniotis, G., Bouvier, M., Lefkowitz, R.J., 2016. GPCR-G Protein-beta-Arrestin Super-Complex Mediates Sustained G Protein Signaling. Cell 166, 907-919.

Trivett, M.K., Potter, I.C., Power, G., Zhou, H., Macmillan, D.L., Martin, T.J., Danks, J.A., 2005. Parathyroid hormone-related protein production in the lamprey Geotria australis: developmental and evolutionary perspectives. Dev Genes Evol 215, 553-563.

Udagawa, N., Takahashi, N., Yasuda, H., Mizuno, A., Itoh, K., Ueno, Y., Shinki, T., Gillespie, M.T., Martin, T.J., Higashio, K., Suda, T., 2000. Osteoprotegerin produced by osteoblasts is an important regulator in osteoclast development and function. Endocrinology 141, 3478-3484.

Underbjerg, L., Sikjaer, T., Mosekilde, L., Rejnmark, L., 2013. Cardiovascular and renal complications to postsurgical hypoparathyroidism: a Danish nationwide controlled historic follow-up study. J Bone Miner Res 28, 2277-2285.

Unnanuntana, A., Gladnick, B.P., Donnelly, E., Lane, J.M., 2010. The assessment of fracture risk. J Bone Joint Surg Am 92, 743-753.

van Abel, M., Hoenderop, J.G., van der Kemp, A.W., Friedlaender, M.M., van Leeuwen, J.P., Bindels, R.J., 2005. Coordinated control of renal Ca(2+) transport proteins by parathyroid hormone. Kidney Int 68, 1708-1721.

Vestergaard, P., Rejnmark, L., Mosekilde, L., 2007. Increased mortality in patients with a hip fracture-effect of pre-morbid conditions and post-fracture complications. Osteoporos Int 18, 1583-1593.

Vilardaga, J.P., Krasel, C., Chauvin, S., Bambino, T., Lohse, M.J., Nissenson, R.A., 2002. Internalization determinants of the parathyroid hormone receptor differentially regulate beta-arrestin/receptor association. J Biol Chem 277, 8121-8129.

Weber, G., Cazzuffi, M.A., Frisone, F., de Angelis, M., Pasolini, D., Tomaselli, V., Chiumello, G., 1988. Nephrocalcinosis in children and adolescents: sonographic evaluation during long-term treatment with 1,25-dihydroxycholecalciferol. Child Nephrol Urol 9, 273-276.

Wehbi, V.L., Stevenson, H.P., Feinstein, T.N., Calero, G., Romero, G., Vilardaga, J.P., 2013. Noncanonical GPCR signaling arising from a PTH receptor-arrestin-Gbetagamma complex. Proc Natl Acad Sci U S A 110, 1530-1535.

Weir, E.C., Philbrick, W.M., Amling, M., Neff, L.A., Baron, R., Broadus, A.E., 1996. Targeted overexpression of parathyroid hormone-related peptide in chondrocytes causes chondrodysplasia and delayed endochondral bone formation. Proc Natl Acad Sci U S A 93, 10240-10245.

Yin, Y., de Waal, P.W., He, Y., Zhao, L.H., Yang, D., Cai, X., Jiang, Y., Melcher, K., Wang, M.W., Xu, H.E., 2017. Rearrangement of a polar core provides a conserved mechanism for constitutive activation of class B G protein-coupled receptors. J Biol Chem 292, 9865-9881.

Zhang, H., Qiao, A., Yang, D., Yang, L., Dai, A., de Graaf, C., Reedtz-Runge, S., Dharmarajan, V., Zhang, H., Han, G.W., Grant, T.D., Sierra, R.G., Weierstall, U., Nelson, G., Liu, W., Wu, Y., Ma, L., Cai, X., Lin, G., Wu, X., Geng, Z., Dong, Y., Song, G., Griffin, P.R., Lau, J., Cherezov, V., Yang, H., Hanson, M.A., Stevens, R.C., Zhao, Q., Jiang, H., Wang, M.W., Wu, B., 2017a. Structure of the full-length glucagon class B G-protein-coupled receptor. Nature 546, 259-264.

Zhang, H., Qiao, A., Yang, L., Van Eps, N., Frederiksen, K.S., Yang, D., Dai, A., Cai, X., Zhang, H., Yi, C., Cao, C., He, L., Yang, H., Lau, J., Ernst, O.P., Hanson, M.A., Stevens, R.C., Wang, M.W., Reedtz-Runge, S., Jiang, H., Zhao, Q., Wu, B., 2018. Structure of the glucagon receptor in complex with a glucagon analogue. Nature 553, 106-110.

Zhang, P., Jobert, A.S., Couvineau, A., Silve, C., 1998. A homozygous inactivating mutation in the

parathyroid hormone/parathyroid hormone-related peptide receptor causing Blomstrand chondrodysplasia. J Clin Endocrinol Metab 83, 3365-3368.

Zhang, Y., Sun, B., Feng, D., Hu, H., Chu, M., Qu, Q., Tarrasch, J.T., Li, S., Sun Kobilka, T., Kobilka, B.K., Skiniotis, G., 2017b. Cryo-EM structure of the activated GLP-1 receptor in complex with a G protein. Nature 546, 248-253.

Zhao, L.H., Ma, S., Sutkeviciute, I., Shen, D.D., Zhou, X.E., de Waal, P.W., Li, C.Y., Kang, Y., Clark, L.J., Jean-Alphonse, F.G., White, A.D., Yang, D., Dai, A., Cai, X., Chen, J., Li, C., Jiang, Y., Watanabe, T., Gardella, T.J., Melcher, K., Wang, M.W., Vilardaga, J.P., Xu, H.E., Zhang, Y., 2019. Structure and dynamics of the active human parathyroid hormone receptor-1. Science 364, 148-153.

和文要旨

I型副甲状腺ホルモン受容体（PTHR1）は Family B の G タンパク質共役型受容体（GPCR）に属し、2 つの異なるペプチドである副甲状腺ホルモン（PTH）と副甲状腺ホルモン関連タンパク質（PTHrP）を内因性のリガンドとして持つ。PTHR1 を介したこれら 2 つのリガンドの作用により、生体内でのカルシウムとリンの恒常性維持に加え、骨組織の成長と代謝制御が行われる。そのため、PTHR1 は骨粗鬆症、副甲状腺機能低下症および Jansen 型骨幹端異形成症（JMC）を含む骨代謝関連疾患の重要な創薬ターゲットとして位置づけられる。PTHR1 を含めて Family B の GPCR のいくつかは、近年の技術革新により、これまで難しかったタンパク質の立体構造が解かれ、創薬研究の手掛かりが提供され始めている。一方で各リガンドと受容体の相互作用が、受容体下流の各種シグナル伝達応答をどのように制御するかについては、未だ不明な点も多い。また、PTHR1 を標的とした臨床的に利用可能な薬剤は、いずれもペプチドリガンドのアゴニストであり、適応症も骨粗鬆症と副甲状腺機能低下症のみである。また、ペプチドの持つ特徴である短い生体内半減期が、幅広い PTHR1 関連疾患に対しての臨床応用の実質的な障壁となっている。従って、PTHR1 関連疾患のための各種ペプチドリガンドによる治療可能性を追求することは、各疾患への新たな治療選択肢を提供するだけでなく、骨代謝関連疾患それぞれへの理解を促進するとともに、PTHR1 を含む Family B GPCR に対する創薬機会を広げる知見を得ることが期待できる。

そこで本研究では、まず JMC の病態モデルマウスを用いて、PTHR1 に対する inverse agonist ペプチド（[Leu^{11},dTrp^{12},Trp^{23},Tyr^{36}]-PTHrP(7–36)NH_2）の治療薬としての適用可能性を検討した。JMC は PTHR1 の恒常活性化型変異により引き起こされる常染色体優性遺伝性疾患として知られ、低身長症、長管骨の骨幹端部の骨異形成症、高カルシウム血症および高カルシウム尿症といった症状を呈する。有効な治療法は存在しない。

JMC 変異の一つである 223 番目のアミノ酸がヒスチジンからアルギニンへ変異した

PTHR1（PTHR1-H223R）を *Collagen 1a1* プロモーター制御下で骨芽細胞特異的に過剰発現させたマウス（C1HR マウス）は、四肢の短縮を伴う長管骨の骨幹端部の骨異形成、骨髄腔を埋める程の海綿骨量の増加と皮質骨の菲薄化、高骨代謝回転に伴う骨髄の繊維化や骨代謝マーカーの増加を呈する。この C1HR マウスへ inverse agonist を 1 回の投与当たり 500 nmol/kg の用量で生後 7 日目から 17 日間 1 日 2 回連日皮下投与したところ、C1HR マウスの病態の一部、すなわち過剰な骨量増加、高骨代謝回転に伴う骨髄の繊維化や骨代謝マーカーの増加が有意に改善された。この検討結果は、PTHR1 に対する inverse agonist が JMC の治療法として有効な選択肢となり得るというコンセプトを、初めて *in vivo* において実証したものであり、今後の JMC に対する治療薬の開発に対して有用な知見を提供したと考えられる。ただし、この検討で用いたトランスジェニックマウスの病態は、骨芽細胞のみでのシグナル異常を反映しているため、特に JMC の病態で問題となる低身長症を最も正確に再現する軟骨細胞特異的 PTHR1-H223R 過剰発現マウスでの検討も今後の重要な研究課題として挙げられる。また、500 nmol/kg という高投与量での頻回投与をもってしても部分的な病態改善効果であったことから、実臨床への応用に向けては、inverse agonist 自体の活性向上だけでなく、薬物動態の改善やシグナル制御レベルでの作用の延長を図る取り組みが必要と考えられる。

次に本研究では、PTH と PTHrP とのハイブリッドペプチドを創成・改変することで、リガンドの血中濃度非依存的に作用が持続するアゴニストペプチド（LA-PTH）を創成し、副甲状腺機能低下症に対する適用可能性を検討した。副甲状腺機能低下症は PTH の分泌低下もしくは欠損によって起こり、低カルシウム血症とそれに伴う痙攣、テタニー、不整脈等の症状を呈する疾患である。これまで標準療法としてカルシウム製剤とビタミン D 製剤の投薬が用いられてきたが、尿中カルシウム排泄の上昇を伴うことから、血中カルシウムを十分正常化できないこと、また長期的には腎結石や石灰沈着による腎機能の低下が課題となっていた。近年 PTH(1–84)の 1 日 1 回の皮下投与が、あるべきホルモンを補充する療法である

本疾患の新たな治療選択肢として米国と EU で承認されたが、その血中半減期の短さから血中カルシウムと尿中カルシウム排泄両面のコントロールにおいて、十分な効果が示されていない。

受容体への結合様式とシグナル持続性を比較した近年の研究により、PTHR1 の 2 つの構造のうち、G タンパク質結合型活性化構造（R^G）への選択的リガンドと比べて、G タンパク質非結合型構造（R^0）への選択的リガンドは、アゴニスト活性シグナルの持続性が長く、マウスにおける血中カルシウム上昇作用も持続することが明らかとなった。その後、PTH と PTHrP との間にも R^G/R^0 選択性やシグナル持続性の違いが明らかとなったことから、本検討では様々な PTH/PTHrP ハイブリッドアナログを合成し、その結合様式を評価することで R^0 選択性の強い PTH/PTHrP ハイブリッドアナログである [$Ala^{1,3,12}$,Gln^{10},Arg^{11},Trp^{14}]-PTH(1–14)/PTHrP(15–36) （以下、M-PTH/PTHrP）が見出された。R^0 選択性の強い M-PTH/PTHrP は正常ラットへの 5 nmol/kg 静脈内投与において、PTH(1–34)や PTHrP(1–36)と比べて明らかに長い血中カルシウム上昇作用を示し、副甲状腺機能低下症の病態モデルである甲状腺・副甲状腺摘出（TPTX）ラットにおいて、PTH(1–34)が一過性の血中カルシウム上昇作用を示すのに対して、M-PTH/PTHrP は 24 時間以上の持続的な血中カルシウム上昇作用を示した。興味深いことに、正常ラットへの静脈内投与後の血中濃度推移の評価から、M-PTH/PTHrP は PTH(1–34)と同様に投与後 1 時間以内に速やかに血中から消失し、その血中カルシウム上昇作用の持続性は、血中濃度非依存的なものであることが示された。TPTX ラットへの 11 日間の連日投与による検討では、活性型ビタミン D 製剤であるアルファカルシドールの経口投与が尿中カルシウム排泄を有意に上昇させながら血中カルシウムを正常化する一方で、M-PTH/PTHrP の皮下投与は、尿中カルシウム排泄を亢進せずに血中カルシウムを正常化した。さらに、TPTX ラットと正常サルにおいて M-PTH/PTHrP と同等レベルの血中カルシウム上昇作用を維持しながら、皮下注射剤として製剤化に重要である中性付近での溶解性を高めるアミノ酸配列改変を加えたアナログペプチド[$Ala^{1,3,12,18,22}$,Gln^{10},Arg^{11},Trp^{14},Lys^{26}]-

PTH(1–14)/PTHrP(15–36)（以下、LA-PTH）を創成することに成功した。

本研究において、JMC には inverse agonist の適用可能性を、また副甲状腺機能低下症にはシグナル持続性の強い LA-PTH の適用可能性を示したことで、それぞれの疾患への新たな治療選択肢が提示されると共に、PTHR1 の持つ薬剤標的としての幅広い可能性が改めて示された。さらに、ペプチド薬が持つ短半減期という薬物動態的課題に対し、R^G/R^0 選択性という結合様式に基づいたシグナル持続性の強いペプチドリガンドの選別により、作用の持続する薬剤を創出できる可能性が示された。近年の研究からこのコンセプトは PTHR1 以外の GPCR へも共有される可能性が高く、本研究での知見は PTHR1 関連疾患のみならず、広く他の GPCR 関連疾患に対する薬剤開発に有用と考えられ、今後の発展が期待される。